

博 士 論 文

**Characterization of flow behaviors
during compression molding of
chopped carbon fiber tape reinforced thermoplastics
(炭素繊維テープ強化熱可塑性樹脂
圧縮成形時の流動挙動)**

李 漢哲

本書の内容の一部あるいは全部を無断で複製すると、
著作権および出版権侵害となることがありますので御注意下さい。

— 2017年6月1日 —

Doctoral dissertation 2017

June 2017

Department of Systems Innovation

School of Engineering

The University of Tokyo

Lee Hanchul

論文要旨

論文題目 Characterization of flow behaviors during compression molding of chopped carbon fiber tape reinforced thermoplastics

(炭素繊維テープ強化熱可塑性樹脂圧縮成形時の流動挙動)

氏名 李 漢哲

Carbon fiber reinforced thermoplastics (CFRTP) have been the subject of various studies in the aerospace and automotive technologies for recent years because of their high mechanical performance and possibility for a mass production process. Although the actual mass production of the composite system are achievable when those are linked to the automated, continuous and rapid processing, there have been particular advances and challenges. Chopped carbon fiber tape reinforced thermoplastics (CTT) describes the thermoplastic composite system, prepared by preform sheets consisting of chopped pre-impregnated tapes, and molding technologies. The thermoplastic composite has the potential for achieving the features of cost effective process because the composite can be classified as randomly oriented strands (ROS) composites with multi-axial discontinuous strands. Therefore, the formed CTT parts (>50%) exhibit balanced properties in terms of both reliable mechanical performance and ease of forming.

Much of recent efforts has been investigated in experimental evaluations of mechanical properties and internal geometry analysis using final molded CTT samples in a range of minimizing the possible defects. On the other hand, even though the forming of the material generally does not require impractical forming conditions, flow behaviors of the material have not been clarified under current circumstances. Thus, it is valuable to characterize flow behaviors such as forming characteristics and relevant flow mechanisms in forming of CTT components. The efforts aim to investigate influential factors on forming behaviors and build the related governing equations using purposeful and systematic approaches.

This study aims to encompass various aspects of flow and rheology, which significantly are related to the processing efficiency and cost effective use of materials. In order to specifically discuss the objective, this study is divided into three main parts for characterizing flow behaviors of CTT composites. In Chapter 1, the recent achievements of comparable composite systems are introduced, mainly related to fiber filled thermoplastic composites. The forming techniques for highly filled

composite systems at the temperature above the melting point are dissimilar to the typical polymer processing techniques with the low volume fraction of fillers (diluted suspension). In the case of former, forming techniques are not easy to align filler directions, whereas the flow of polymer melt and its velocity field highly affect filler orientation in the latter case. It leads the constraints of the former case when approaching to the methods from a fluid mechanics perspective. It is necessary to embrace an alternative methodology compared to the conventional ways of analyzing polymer melts.

Chapter 2 and 3 involve to experimentally demonstrate the relations between forming parameters and forming behaviors in the given cases in various forming conditions. Chapter 2 focuses on identifying formability of CTT parts in various forming conditions in the given geometry with complex features. Chapter 3 is devoted to an experimental observation of flow progression and validation of defect formation, which are closely related to forming complex parts. It is possible to observe the flow front during compression molding of CTT suspensions in particular forming conditions using a unique mold configuration. Several squeeze flow tests are designed to discuss forming conditions and mold filling behaviors to create a valid comparing group for numerical simulation.

Chapter 4 presents a characterization of rheological properties adapted from valid theoretical approaches for shear viscosity of fiber filled suspensions. With the approaches, shear viscosity of CTT suspensions is expressed in the form of the Herschel-Bulkley fluid model with yield stress. In particular, preform preparation and deformation mode are dominant issues because the assumptions applied in the methodology are closely connected with an internal geometry such as fiber orientation and sample consistency.

Chapter 5 contains the results of thermo-mechanical behaviors by employing a thermo-mechanical analyzer. This study aims to obtain coefficients of thermal expansion (CTE) and deduce corresponding volumetric thermal expansions, which are significant aspects of process modeling for thermoplastic composites. The measured results clearly deliver anisotropic properties of materials, and the results are analyzed by defining CTE in principal directions, and suggest a valid interpretation for fiber reinforced composites.

Eventually, most of the essential issues for applying numerical approaches are assessed and characterized; formability, squeeze flow behaviors, defect formation in manufacturing, rheological properties, and thermo-mechanical properties. Much of efforts has been primarily focused on establishing the baseline for process modeling in CTT manufacturing. Therefore, the efforts possibly guide one to achieve the design of mold frames, drawing a processing window for newly developing products with a geometric feature, the deduction of optimal processing conditions, and finally the cost-effective usage of materials. It is expected to promote commercial applications of the material in an industrial field by offering systematic and practical solutions in cases when utilizing the materials.

ACKNOWLEDGMENTS

The work presented in this dissertation led to the suggestion of experimental characterization methods, models and guidelines to characterize flow behaviors of chopped carbon fiber tape reinforced thermoplastics composites processed by compression molding. A part of this study has been conducted within the framework of the project “The Future Pioneering Projects/Innovative Structural Materials Project” funded by the Ministry of Economy, Trade, and Industry of Japan since 2013FY. All the work presented in this dissertation was conducted by the author, with the aid of cooperation from the following institutes:

In the entire thesis, Industrial Technology Center of Fukui Prefecture provided its specially developed materials. Part of contributions in this thesis is considered as its products with high level of quality control.

Chapter 2 - Sanko Gosei Ltd. contributed for the installation and operation of the experimental apparatus used in this study. And it allowed the author to utilize the apparatus with a supportive environment for the experimental procedures.

Chapter 4 - Innovative Composite Materials Research and Development Center allowed the author to utilize a rheology apparatus in the institute. And the institute provided a supportive environment for the experimental procedures.

Chapter 5 – Hokkaido Research Organization/Industrial Research Institute provided experimental data by ‘request experiments’. The accumulated experimental experience of the institute allowed it to perform the tests in accordance with appropriate standards and provided reliable data.

The authors would like to sincerely express appreciation to every institute and everyone involved in this study.

TABLE OF CONTENTS

Chapter 1 Introduction	15
1.1 Research background.....	15
1.1.1 Thermoplastic composites.....	16
1.1.2 Carbon fiber reinforced thermoplastics.....	19
1.1.3 Forming techniques in fiber reinforced plastics manufacturing.....	23
1.2 Overview of doctoral dissertation.....	25
Chapter 2 Experimental Validation of Forming Complex Part	28
2.1 Introduction.....	28
2.2 Background.....	28
2.3 Materials	29
2.3.1 Overall procedures	29
2.3.2 Preliminary procedures	31
2.3.3 Preform preparation	32
2.4 Experimental procedures	33
2.4.1 Instrument	33
2.4.2 Experimental design.....	33
2.4.3 Relevant test: optical microscopy	36
2.4.4 Consideration of heating phase	36
2.5 Results and discussion	36
2.5.1 Theoretical analysis.....	36
2.5.2 Mold filling behaviors.....	38
2.6 Concluding remarks.....	42
Chapter 3 Experimental Validation of Squeeze Flow Behaviors	43
3.1 Introduction.....	43
3.2 Background.....	43
3.3 Materials	44
3.4 Experimental Procedures	44
3.4.1 Instrument and charge preparation.....	44
3.4.2 Sample pre-consolidation.....	49
3.4.3 Experimental design.....	51
3.4.4 Consideration of heating phase	56

3.4.5 Relevant tests.....	57
3.5 Results and discussion.....	60
3.6 Concluding remarks	70
Chapter 4 Characterization of Rheological Properties.....	71
4.1 Introduction.....	71
4.2 Theory	72
4.2.1 Polymer melt rheology	72
4.2.2 Suspension rheology: micro-mechanical model for highly filled fiber suspensions	74
4.2.3 Model development.....	77
4.3 Experimental procedures.....	78
4.3.1 Materials.....	78
4.3.2 Melt rheology measurement	82
4.3.3 Yield stress measurement	83
4.3.4 Suspension rheology measurement	84
4.4 Results and discussion.....	85
4.4.1 Polymer matrix shear viscosity	85
4.4.2 Suspension yield stress.....	87
4.4.3 Suspension shear viscosity	91
4.5 Concluding remarks	95
Chapter 5 Characterization of Thermal Expansion Behaviors	97
5.1 Introduction	97
5.1 Experimental procedures.....	98
5.1.1 Specimen preparation.....	98
5.1.2 Apparatus	100
5.2 Results and discussion.....	101
5.2.1 Influences of thermal and mechanical history	101
5.2.2 Anisotropic thermal expansion coefficients	103
5.3 Concluding remarks	106
Chapter 6 Conclusions of Dissertation	107
6.1 Scientific contributions	107
6.2 Expansion of this dissertation	110
References	112

Appendix A – Nomenclature	117
A.1. List of acronyms	117
A.2. List of symbols.....	118
 Appendix B – List of Publications.....	 121

LIST OF TABLES

Table 1 - 1. Comparison between thermoset and thermoplastic composites (adapted from [9]).....	19
Table 2 - 1. Experimental design matrix for matched die forming of chopped carbon fiber tape reinforced thermoplastics.	34
Table 3 - 1. Prepared preform dimensions for each case of the experiment.....	49
Table 3 - 2. Experimental design matrix for squeeze flow tests.	52
Table 3 - 3. Summary of applied effective pressure in squeeze flow tests.	66
Table 3 - 4. Summary of fiber, resin, void content and the final strain.	67
Table 3 - 5. Mechanical properties of squeeze flow and typical flat panel samples.....	69
Table 4 - 1. Fundamental parameters of two types of CTT samples.	81
Table 4 - 2. Summary of geometric parameters for modeling two types of CTT.	82
Table 4 - 3. Rheological parameters for three generalized Newtonian fluids (GNF) models.	86
Table 5 - 1. Initial length measured at ambient temperature.	102
Table 5 - 2. Comparison of in-plane CTE and through thickness CTE of CTT specimens.....	105

LIST OF FIGURES

Chapter 1

Figure 1. 1. Components of commercial automobile that are made from carbon fiber SMC using compression molding [7].	16
Figure 1. 2. Comparison of thermoset and thermoplastic polymer structures: (a) thermoset polymer, (b) thermoplastic polymer (adapted from [9]).	17
Figure 1. 3. Comparison of carbon fiber manufacturing: (a) Polyacrylonitrile (PAN), (b) pitch-based (adapted from [9]).	20
Figure 1. 4. Relative performance and processability of various materials forms (adapted from [16]).	21
Figure 1. 5. Comparison of various carbon fiber reinforced thermoplastics (CFRTP) composite forms.	22
Figure 1. 6. Schematic of sheet molding compound (SMC) production [12].	23
Figure 1. 7. Schematic of automated compression molding of glass mat thermoplastics (GMT) sheets [12].	24
Figure 1. 8. Schematic of the targeted process of chopped carbon fiber tape reinforced thermoplastics (CTT) parts production: rapid, mass, automated and continuous [23].	25
Figure 1. 9. Flowchart of an overview of the doctoral dissertation.	27

Chapter 2

Figure 2. 1. Overview of the processing steps for forming chopped carbon fiber tape reinforced thermoplastics component. (Adapted from [23]).	30
Figure 2. 2. Flow diagram of pre-impregnated sheets cutting in fiber direction [23].	31
Figure 2. 3. Schematic representation and summary of wet dispersion procedure.	32
Figure 2. 4. Schematics diagrams of the ribbed tray samples molded in this study. (a) 3-dimensional view, (b) top view and (c) dimensions of ribbed section.	34
Figure 2. 5. Nominal molding cycles used during the production of the ribbed trays formed using a matched die.	35
Figure 2. 6. Photographs of ribbed sections formed at an effective pressure of 10 MPa for 3 min for strand lengths of (a) 12 mm, (b) 18 mm, (c) 24 mm and (d) 30 mm.	38
Figure 2. 7. Photographs of filled ribbed sections for strand lengths of 18 mm and pressures of (a) 5 MPa, (b) 10 MPa, (c) 15 MPa and (d) an example of a localized defect at the corner.	39

Figure 2. 8. Optical micrographs of cross-sections of CTT samples cut along the length direction of the taller rib for samples prepared with a strand length of 18 mm and pressures of (a) 5 MPa, (b) 10 MPa, and (c) 15 MPa.....	40
Figure 2. 9. Effect of effective pressure and strand length on the complete filling.....	41
Figure 2. 10. Effect of consolidation time and strand length on the complete filling.	41

Chapter 3

Figure 3. 1. Schematic representation of components configuration equipped with a laboratory press. .	45
Figure 3. 2. Schematics of thermocouples embedded in mold configuration.	45
Figure 3. 3. Temperature monitoring panels showing temperatures of upper and lower molds.....	46
Figure 3. 4. Mold configuration and preform dimensions for squeeze flow tests using an open mold: (a) sectional view, (b) top view and (c) 3-dimensional view.	47
Figure 3. 5. Schematic representation of operation system during compression molding cycles: (a) initial stage of the cycle without contact and (b) actual contact and mold filling stage.	48
Figure 3. 6. Recorded molding cycles for producing a pre-consolidated charge using a closed mold.....	50
Figure 3. 7. Photographs of prepared charges: (a) preform charge for case A and B and (b) pre-consolidated charge for case C.....	51
Figure 3. 8. Initial setups of the preform charge and lower mold geometry for case A and B.	52
Figure 3. 9. Temperature and applied force profiles of open mold cases.	53
Figure 3. 10. Processing conditions for case D: (a) force profile and (b) temperature profile.	55
Figure 3. 11. Initial setups of the preform charge and lower mold geometry for case D.	55
Figure 3. 12. Temperature profile during the heating phase of squeeze flow test C.	57
Figure 3. 13. Photograph of molded sample from a top view, a schematic representation of flow (yellow arrows) and cutting edges in case D (green solid lines and white dotted line).....	58
Figure 3. 14. A burning off device with the nitrogen gas provider.....	59
Figure 3. 15. Images taken from the video footage showing the progression of the flow fronts through the open mold over time in phase 2: (a) case A and (b) case B.....	61
Figure 3. 16. Images taken from the video footage showing the progression of the flow fronts through the open mold over time in phase 2 for case C.	62
Figure 3. 17. Applied force and corresponding relative position in open mold cases: (a) case A, (b) case B and (c) case C.	64
Figure 3. 18. Mold filling by squeeze flow tests using CTT: (a) case A, (b) case B and (c) case C.	65
Figure 3. 19. Representative cross-sectional micrographs of CTT samples (the plane of symmetry along the flow front) formed under different conditions showing void formation: (a) case A, (b) case B and (c) case D.	68

Chapter 4

Figure 4. 1. Fiber distribution in CTT observed by X-ray computed tomography: (a) in-plane orientation and (b) out-of-plane orientation (adapted from [49]).	76
Figure 4. 2. Schematic representation of relevant surfaces forces at contact points (Adapted from [43]).	76
Figure 4. 3. Overview of production of flat panel samples using CTT.	78
Figure 4. 4. Schematic representation of shearing gap in a cubic unit volume.	81
Figure 4. 5. Complex shear viscosity of PA6 and functional fitting to three Newtonian fluids (GNF) models.	86
Figure 4. 6. Representative plots showing shear stress and strain over time in stress ramp test: CTT55 sample.	87
Figure 4. 7. Yield stress evaluation for CTT44 suspensions by complex viscosity peak: (a) sample 1, (b) sample 2, (c) sample 3 and (d) sample 4.	89
Figure 4. 8. Yield stress evaluation for CTT55 suspensions by complex viscosity peak: (a) sample 1, (b) sample 2, (c) sample 3 and (d) sample 4.	91
Figure 4. 9. Complex viscosity as a function of the effective shear rate at various strain amplitudes: (a) CTT44 and (b) CTT55.	92
Figure 4. 10. Loss tangent with varying angular frequencies and strain amplitudes for CTT55 suspensions.	94
Figure 4. 11. Filler effects of CTT suspensions on viscosity plots.	94

Chapter 5

Figure 5. 1. Evaluation of the mean (ΔT) and differential αT coefficients of linear thermal expansion [13].	98
Figure 5. 2. Schematic representation of fibers aligned in uni-directional system [54].	100
Figure 5. 3. Schematic diagram of thermo-mechanical analysis (TMA) apparatus [13].	101
Figure 5. 4. Change of length of CTT specimen during controlled 1 st and 2 nd heating and cooling; normal probe, $l_o = 4.0$ mm, specimen cross-section approx. 4×4 mm, applied load 0.038N, heating or cooling rate 5 °C/min.	102
Figure 5. 5. Reproducibility plots of change of length for through thickness expansion specimens; normal probe, $l_o = 4.0$ mm, specimen cross-section approx. 4×4 mm, applied load 0.038N, heating rate 5 °C/min.	103
Figure 5. 6. Through thickness CTE of three CTT specimens during 2 nd heating; normal probe, $l_o = 4.0$ mm, specimen cross-section approx. 4×4 mm, applied load 0.038N, heating or cooling rate 5 °C/min.	104

Figure 5. 7. Comparison of in-plane CTE α_{ci} and through thickness CTE α_{ct} ; $l_o = 4.0$ mm, specimen cross-section approx. 4×4 mm, applied load 0.038N, heating or cooling rate 5 °C/min.....105

lists of acronyms and symbols can be found in Appendix A.

Chapter 1

Introduction

1.1 Research background

In the mid-1990s, the United States government with the nation's major automotive manufacturers set up a program to enhance fuel efficient vehicles.¹ Such policy directions are not only limited to the nation and get expanding all over the world because of the issues on greenhouse gas (GHG) emission including carbon dioxide (CO₂), and relevant global warming effects.^{2,3} In addition to the environmental issues, the market uncertainty of crude oil price⁴ and the necessity for electric vehicles in an automotive industry⁵ have accelerated the efforts on developing automobiles with light weight for several decades. For achieving the objective, the use of plastic would significantly minimize the weight of vehicles by replacing metal alloy components and would reduce power demands of the engine system. This possibility would be contributed by the long-lasting and accessible research in polymer processing field.⁶ Beyond the possibility, the use of composite materials has been studied from diverse perspectives of material, mechanical, process, automation engineering fields and a lot of involved industries.

Fig. 1.1 shows the first mass produced automobile to apply compression molded carbon fiber sheet molding compound (SMC).⁷ Carbon fiber was used to facilitate both structural performance and weight savings. Nine components were produced from the material in the entire components of the vehicle. Although SMC typically involves the use of matrix as thermoset plastics, compression molding is a frequently used process in both thermoset and thermoplastic composites manufacturing.⁸ Large panels and various geometries with a complex feature are used in diverse industrial applications. In cases when a manufacturer uses forming techniques with a particular mold cavity to form complex shaped parts, the material properties, and performance of the final molded components are highly influenced by processing techniques used and flow behaviors of the material.

Based on potentials and the recent applications, the ultimate objective of this study is to contribute to the mass production of carbon fiber reinforced thermoplastics (CFRTP) and to amplify the current level of applications of the material. In particular, the CFRTP has proven its advantages in the

feasibility of commercial products in the particular industrial sectors. Therefore, the material shift from steel alloys to CFRTP would be inevitable and environmentally beneficial. By specifying the scope of discussion and reviewing possible techniques, the more clear description would be available in terms of the practical applications when selecting the CFRTP as structural components for the commercial usage. The boundaries of consideration imply how and why the material is invaluable for cost effective usage, has resulted in a new possibility of material selection for automotive industries. From the next section, the overview of thermoplastic composites by comparing with thermoset composites would be placed. Also, the classification of relevant materials and technological terms, and feasible techniques would convey a more clear understanding of the present study “Characterization of flow behaviors during compression molding of chopped carbon fiber tape reinforced thermoplastics (CTT)”.

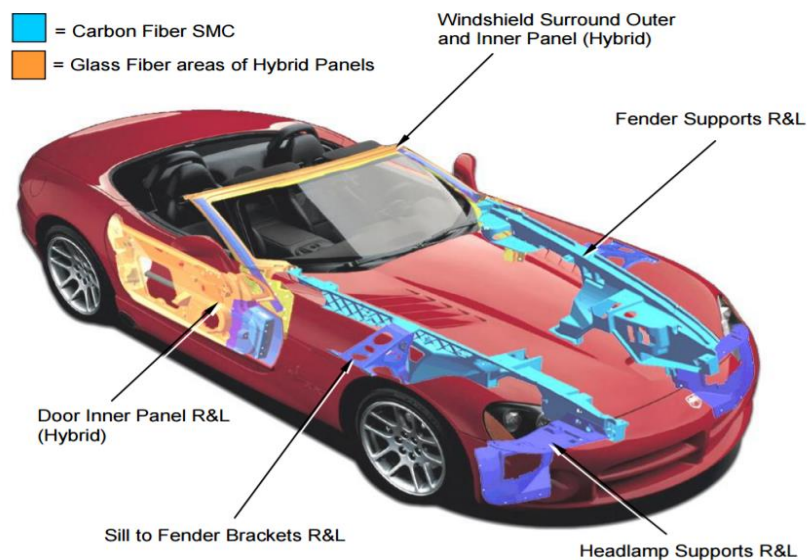


Figure 1. 1. Components of commercial automobile that are made from carbon fiber SMC using compression molding [7].

1.1.1 Thermoplastic composites

Composite materials consist of two different materials that can be combined. During the 1980s and early 1990s, agencies of United States government, aerospace manufacturers, and material providers invested hundreds of millions of dollars in developing thermoplastic composites to replace conventional thermosetting composites. Despite the partial achievements of full replacement, the potential advantages of thermoplastics and essential knowledge have been discovered. As a general class of polymers, thermoplastics are more widely used than thermosets, taking a share approximately 80% of all polymer products.⁹

The primary consideration in this section is the difference of matrix properties between

thermoplastics and thermosets. By controlling process conditions, CFRTMP manufacturing can be accomplished by rapid heating, forming, and cooling without degradation of the material's mechanical properties.¹⁰ The difference leads additional pros and cons when applying the materials for industrial purposes. It is necessary to discuss focusing on comparison of two composites systems to obtain further development of characterization methodology.

The thermoset polymer requires crosslinking reactions during the curing process. Relatively low molecular weight M_w builds its internal structure as the molecular weight increases as shown in Fig. 1.2(a). The chemical reactions keep maintaining until the molecular obtain gelation and strong covalent bonding during cure. Through this curing process, tight network of molecules are created. In contrast, thermoplastics have to be fully reacted and formed with high molecular weight in the form of pellet, fibers, even film prior to the forming steps. They can be melted and flow during forming steps without crosslinking reactions as shown in Fig. 1.2(b). The main chains of them are held together by weak secondary bonds during processing.

The absence of cross-linking is connected with environmental benefits for the worker, who deals with the materials because of the absence of unreacted resin components during the manufacturing process. The lack of unreacted resin is also related to low storage cost of thermoplastic composites compared to that of thermoset composites because the unreacted resin in thermoset pre-impregnated materials requires refrigeration facility to store them prior to the actual processing depending on the plan on using the material.

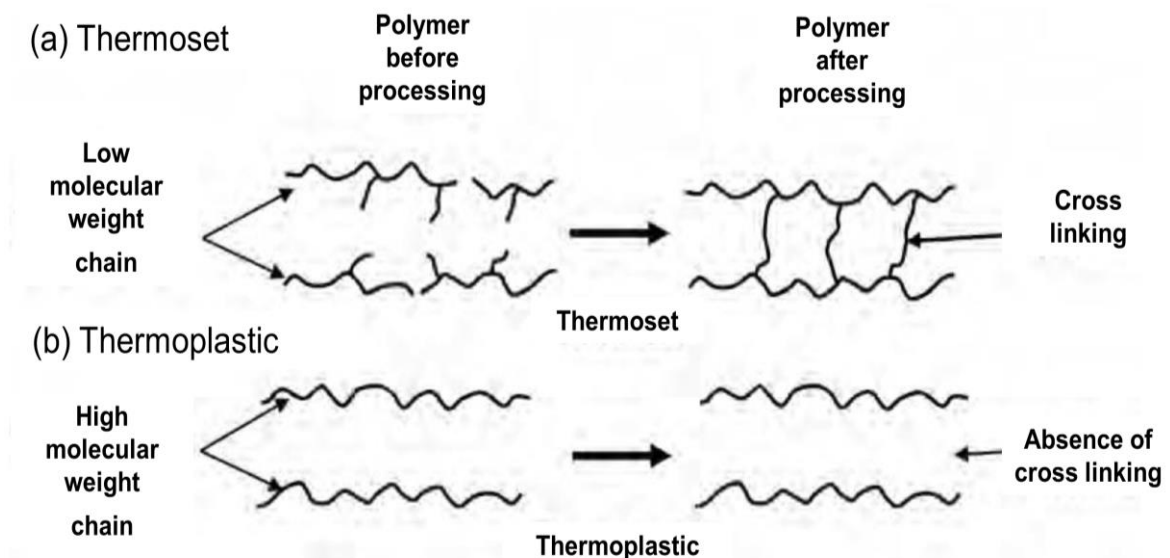


Figure 1. 2. Comparison of thermoset and thermoplastic polymer structures: (a) thermoset polymer, (b) thermoplastic polymer (adapted from [9]).

Another potential advantage of thermoplastic composites is the processing efficiency. The processing of thermoplastic composites is ideally simpler than that for thermoset composites. Theoretically, thermoplastics are thermos-formed and consolidated in minutes, while thermosets need relatively long curing process for achieving the cross-linkings. However, the high temperature in the range of 260 to 425 °C is required during the forming process.⁹ Therefore, the time consumption for heating and cooling of forming tools is a drawback in thermoplastic composites processing. Therefore, the importance of cooling phase is considered as a significant aspect because the crystallization behavior of thermoplastic matrix influences the mechanical performance of finally formed parts.¹¹

One of the compensating this factor when forming thermoplastic material involves to second processing above their melting temperatures. Thus, it is possible to design sequential processing steps. For example, large and flat sheets are consolidated by the press, and then cut into smaller pieces and thermoformed into complex shapes. Although this technique possesses difficulty in forming processes in cases when using inextensible characteristics of the continuous fiber composites,⁹ it can be overcome by using discontinuous fiber systems. Reprocessing can be used for parts with defects (such as unbond regions) and offer one of the joining options. The former allows manufacturers to repairs the defects without the distortion of reinforcing materials. The latter, joining the application, provides design flexibility when designing a new type of structural geometries. Multiple possibilities including melt fusion, resistance welding, ultrasonic welding, and induction welding facilitate the manufacturers to consider thermoplastic composites as alternatives for steel or thermoset composites. Those can be combined with conventional bonding, such as adhesive sealing, mechanical fastening by using bolts, nuts, screws and another type of fasteners.

Viscosity during processing, related to the molecular weight M_w , causes the different consideration of establishing manufacturing process from a fluid mechanic's viewpoint. For instance, in the case of pultrusion process for combining two phases of materials (fluid and solid), one uses Darcy's law to appropriately reflect the resin impregnation and the heat transfer related to curing kinetics. In contrast, Darcy's law is not the proper approach to model the relationship between flow rate and pressure drop due to the high viscosity of the material.¹² Moreover, the variation of viscosity during manufacturing process have to be dealt because of shear thinning natures of thermoplastics.

Table 1-1 summarizes the comparison between thermoset composites and thermoplastic composites. The last statement involves to moisture absorption and chemical resistance. Thermoplastic composites generally absorb very little moisture compared to thermoset composites.⁹ Cured thermoset composites absorb moisture from the atmosphere and are susceptible to resulting thermal degradation. Several amorphous thermoplastics are vulnerable to solvents and possible to dissolve, whereas semi-crystalline thermoplastics are highly resistant to chemical interaction.

Although this section describes an overview of advantages of thermoplastic composites from a

positive perspective, it is true that utilization of thermoplastic composites has not been fully developed in cases of carbon fiber reinforced plastics. For instance, polyether ether ketone (PEEK) polyether ketone ketone (PEKK), polyphenylene sulfide (PPS) are widely used thermoplastic polymers for continuous fiber reinforced thermoplastic composites. Polypropylene (PP) is polymer matrix for mat structure reinforced thermoplastics with glass fibers. PEEK, PEKK, PPS, and PEI can be classified as high-performance thermoplastics, which are expensive in general. Those are usually aromatic thermoplastic with phenylene ring group. The present study concerns Polyamide 6 (PA6) semi-crystalline thermoplastic polymers as a matrix, which has a reasonable cost.¹³ The cost range varies depending on a product type, grade, and additional characteristics.

Table 1 - 1. Comparison between thermoset and thermoplastic composites (adapted from [9]).

Classification by polymer matrix	Thermoset composites	Thermoplastic composites
Cross linking reactions	Necessary	Dispensable
Processing	Complicating	Simple
Reprocessing	Infeasible	Feasible
Storage cost	Require refrigeration	Lower
Viscosity during processing	Low viscosity	High viscosity
Danger to the worker	Unreacted resin component	Less danger
Joining options	Mechanical fastening, adhesive bonding	Welding techniques, mechanical fastening, adhesive bonding

In this section, a brief comparison between thermoplastic and thermoset composites caused from matrix type has been discussed. From this starting point, the scope of discussion would concentrate on carbon fiber reinforced thermoplastics (CFRTP) in next section.

1.1.2 Carbon fiber reinforced thermoplastics

Carbon fiber reinforced plastics (CFRP) have attracted a wide range of industrial applications because of their good mechanical performance and a wide range of uses to which they can be applied. In recent years, many industrial sectors have adopted CFRPs to achieve mechanical properties and weight savings of different products. The widespread application of CFRP is found not only in the aerospace and automotive technologies but also in sports and leisure fields. According to the reliable market report, the total demand for CFRP in automotive industries is expected to maintain sustained

growth until the mid-2020s.¹⁴

CFRP is classified into two types of composites in terms of the polymer matrix used: carbon fiber reinforced thermosets (CFRTS), and carbon fiber reinforced thermoplastics (CFRTP). CFRTS have been studied by a lot of researchers for decades, and the relevant fabrication and manufacturing technologies have been sufficiently developed, frequently used in aerospace industries.¹⁵ The difference of polymer matrix and the forming application has been discussed in the previous section: the manufacture of CFRTS components requires a curing stage for the cross-linking of molecular chains, whereas the manufacture of CFRTP components does not require this process. CFRTP components offer additional advantages in joining and forming applications because thermoplastic polymers allow reversible transitions between solid and fluid phases.⁹

Carbon fiber can be made from rayon, Polyacrylonitrile (PAN) and petroleum pitch precursors. Despite the high cost of PAN, PAN is widely used precursor because the carbon yield is higher than that of rayon-based carbon fibers.⁹ The simplified manufacturing processes for PAN and pitch-based carbon fiber is illustrated in Fig. 1.3(a) and (b), respectively. The PAN based carbon fiber possess a high degree of orientation in the raw precursor and undergo several steps of the production process. The importance of surface treatment is about improving adhesion properties of them, and the objective of sizing is to make fiber easier to handle and protect the surface of the material.

(a) PAN Process

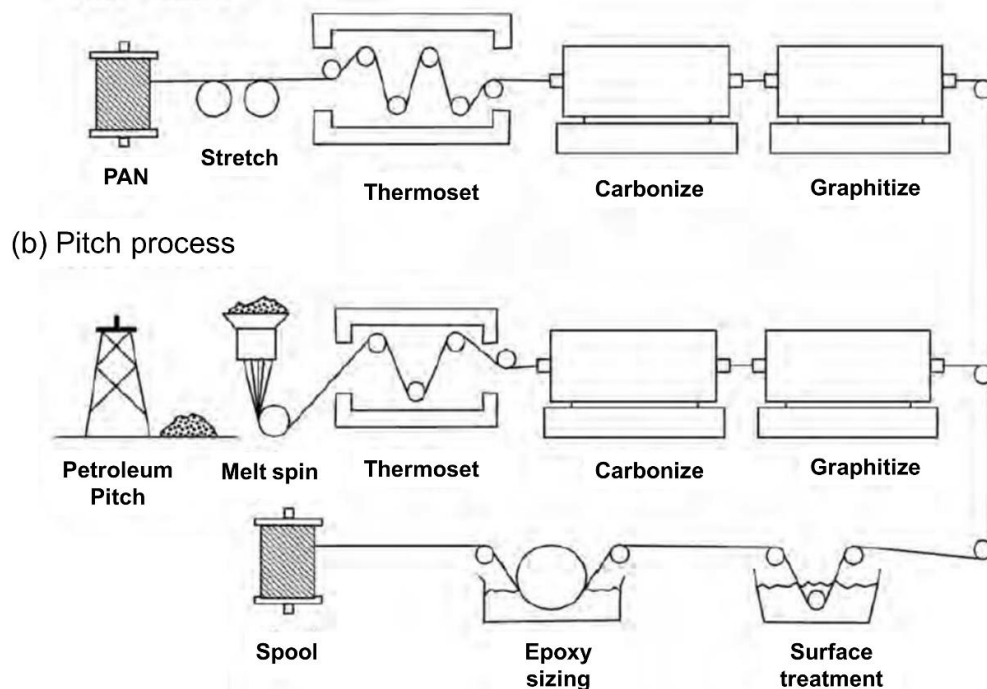


Figure 1. 3. Comparison of carbon fiber manufacturing: (a) Polyacrylonitrile (PAN), (b) pitch-based (adapted from [9]).

1.1.2.1 Overview [1]

One of the attractive properties of carbon fiber is its lower specific gravity, approximately 30% lower than glass fibers. The material has good thermal and electrical conductivity and lower linear expansion coefficient. However, carbon fibers are generally expensive than another type of fibers. Fundamentally, the quality of performance of carbon fibers depends on the composition of precursor fibers, such as PAN or petroleum pitch. Because the carbon fiber manufacturing processes include carbonization and graphitization, the heating conditions also influence the properties of carbon fibers.

1.1.2.2 Chopped carbon fiber reinforced thermoplastics

Chopped carbon fiber tape reinforced thermoplastics (CTT) is considered as one type of randomly oriented strands (ROS) because morphological characteristics observations have shown that the material consists of discontinuous long fibers and exhibits random orientation of fibers in-plane. Although producing details depend on the adequate application purposes, CTT molded components present balanced characteristics in terms of both mechanical performance and ease of processing as illustrated in Fig 1.4.¹⁶ The mechanical performance of molded components made with CTT has been evaluated by various methodologies, including experimental, theoretical, and numerical approaches.¹⁷⁻¹⁹ One prior research demonstrated the ease of forming despite a relatively longer fiber length compared to the geometric complexity of the mold cavity in a moderate range of process conditions typical of practical applications.²⁰ Also, various approaches have been investigated to increase the commercial availability of the ROS, such as the analytical models that have been proposed for predicting mechanical performance, defect formation caused by process conditions, and squeeze flow behavior during compression molding.²¹⁻²²

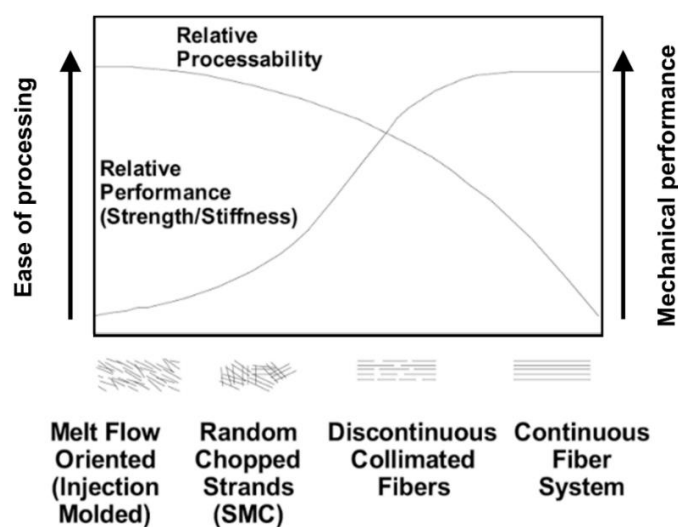


Figure 1. 4. Relative performance and processability of various materials forms (adapted from [16]).

Although the primary focus of this study is to investigate several properties related to forming behaviors of CTT, multiple options are available when using carbon fiber reinforced thermoplastics as structural components as shown in Fig. 1.5. Continuous laminate composites are a conventional type of carbon fiber reinforced plastics. Thermoplastic matrix based prepreg sheets are also can be used to fabricate instead of thermosetting matrix based prepregs, which are the main stream in the carbon fiber reinforced plastic applications. Continuous fiber composites have inextensibility in the fiber direction, and it leads difficulties in manufacturing complex components.

Regarding the constraints of application range, CTT offer extensibility in the fiber direction and design flexibility can be obtained by employing breaks along the fiber length. CTT composites consist of pre-impregnated chopped with planar random orientation. The initial form of pre-impregnated and uni-directional sheets and the sheets are cut in two directions (prepregs length and width) to create a tape like dimension. Each strand in one unit of tape is nearly parallel to each strand. Chopped tapes are generally undergone the process for fabricating preform sheets prior to the forming application. The chopped tapes are aligned in the plane with multi-axial and randomly distributed to fabricate the preform sheets. By arranging the sheets being up to the circumstances, final formed geometry have statistically homogeneity of fibers and polymer matrix when preparing well-defined preform fabrication and applying appropriate forming techniques.

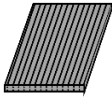
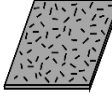


Type of composite system	Continuous laminates 	Injection molded 	Mat structure thermoplastics 	Chopped carbon fiber tape reinforced thermoplastics 
Fiber volume fraction V_f	High (>50%)	Relatively low	Middle (20–30%)	High (>50%)
Aspect ratio L/D	Highest	Low (variation)	Middle (hundreds)	High (hundreds-thousands)
Formability	Directional dependent	Superior	General	Superior
In-plane isotropy	Designable	Process dependent	Feasible	Feasible

Figure 1. 5. Comparison of various carbon fiber reinforced thermoplastics (CFRTP) composite forms.

Although mat structure CFRTP have advantages in utilizing recycled fibers or light weight contribution when applying the material, forming behaviors, have not been fully developed under current circumstances. Injection molded CFRTP parts have been used in specific areas in the engineering field, but have difficulties in a wider range of applications because of the mechanical performance of parts. There are particular constraints in having high volume fraction and fiber

breakage related to the use of complex manufacturing process including extrusion and injection molding. Clarifying forming properties of CTT has been thought as an urgent issue compared to another type of CFRTP forms in large scale manufacturing because parts made from CTT is one of the strong candidates for its potential for structural components produced by rapid manufacturing. Among diverse types of thermoplastic matrix, PA6 is employed in the present study and current ongoing innovation in CFRTP applications. For a more demanding application, such as higher temperatures and loads, PA6 is more suitable than widely used thermoplastic, for example, PP. In addition, PA6 possess higher strength than that of PP in general grade of commercial products.¹ Interfacial shear strength between carbon fibers and polymeric matrix is an important consideration when determining polymer matrix consisting the composite system.

1.1.3 Forming techniques in fiber reinforced plastics manufacturing

1.1.3.1 Comparable forming techniques

The compound (or compounded material) is the product that is placed in the compression molding tool. The compound can be produced by combining the polymer matrix with additives, fillers, and reinforcements. Based on the type of matrix, thermoplastic or thermosetting, the compound can be classified as four main types: SMC (Sheet molding compound), BMC (Bulk molding compound) for thermosetting matrix and LFT (Long fiber thermoplastic) and GMT (Glass mat thermoplastic) for thermoplastic matrix under current level of commercial applications.¹

Fig. 1.6 illustrates two sequential steps involved in the manufacturing of SMC: compounding of the resin and additives, and the fabrication of the SMC sheet. Continuous production of SMC is obtainable by equipping chopping section, combination line, and compaction belt. In the early stage of the process, the resin ingredients are pre-mixed in batches. Subsequently, the compounding of the resin is carried out by a simultaneous process of applying resin ingredient to a carrier film and

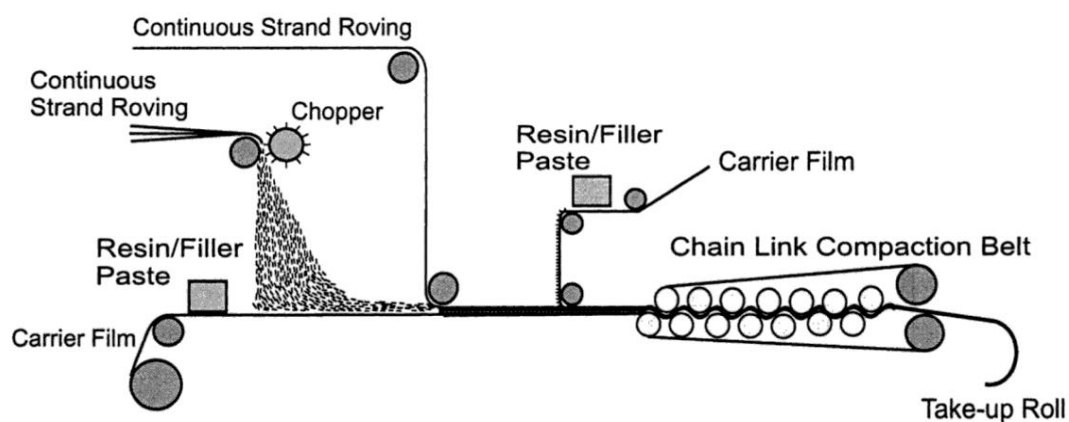


Figure 1. 6. Schematic of sheet molding compound (SMC) production [12].

chopping fibers, generally glass fibers, is performed. After this process, compression between two carrier films to form SMC sheet in the combination line where the SMC sheet is formed. Impregnation of the fiber is required in the compaction step. The SMC sheet includes all the ingredients for molding the final part in a sheet form. Depending on the alignment of chopped strands, planar random orientated sheets is achievable. BMC involves to mixing process of resin paste and short fibers and extrusion without formation of sheets unlike SMC.

Glass mat thermoplastics are semi-finished sheets manufactured by combining thermoplastic resin with mat type of fibers. The most common combination is PP as the polymer matrix and glass fibers. GMT's are tough and light weight compression molded example. Final produced GMT lacks the excellent high temperature mechanical performance that thermosetting compounds yields. GMT sheets are formed by using glass fiber mat and extruded resin for achieving impregnation of fiber mat prior to the compression molding process. Fig 1.7 illustrates sequential steps in a continuous cycle including preheating, stacking of desired mold charge and final compression molding.

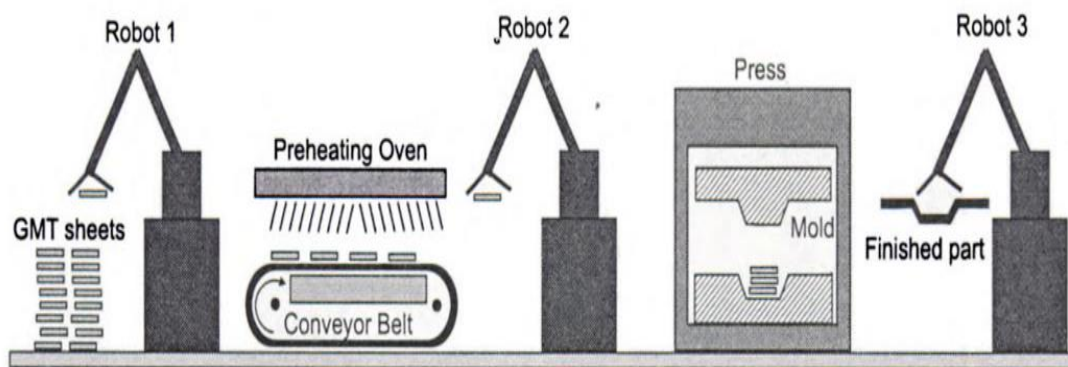


Figure 1. 7. Schematic of automated compression molding of glass mat thermoplastics (GMT) sheets [12].

1.1.3.2 Targeted production process for CTT mass production

Fig. 1.8 illustrates the ultimate goal of production process, which aims at rapid, mass, continuous and automated cycle. The process has been designed to take advantages of part of SMC and GMT manufacturing without a decrease of mechanical performance. To provide continuous and controllable materials prior to the specific heating and compression with reliable quality, wide sheet type of preforms of CTT are prepared. In this process, impregnation of initial form of fibers is required by compaction tools, such as compaction roller or belt. With the preforms, a preferable dimension of preforms is cut and heated by automated and continuous systems. Heated preforms undergo rapid compression processes, such as stamp forming or compression molding in short cycle time. In the sequential process, each part of steps can replaceable or modifiable depending on the required final products. Various efforts have been

placed by networks of the current Japanese national project on exploring this challenging initiative, taking specific part partially or entirely.

Because of the existence of the preform preparation to achieve this continuous process from the long term perspective, material preparation process prior to the compression process commonly involves the preform fabrication in this study. Although the specific details of the initiative have not been completely established yet, this study aims to contribute to this goal by using the current level of forming techniques, such as compression molding in longer cycle time or matched die forming of small molded sample in shorter time, and so forth. Essentially, the primary focus of this study is to suggest several experimental methods, establishing a baseline of forming perspectives of the material.

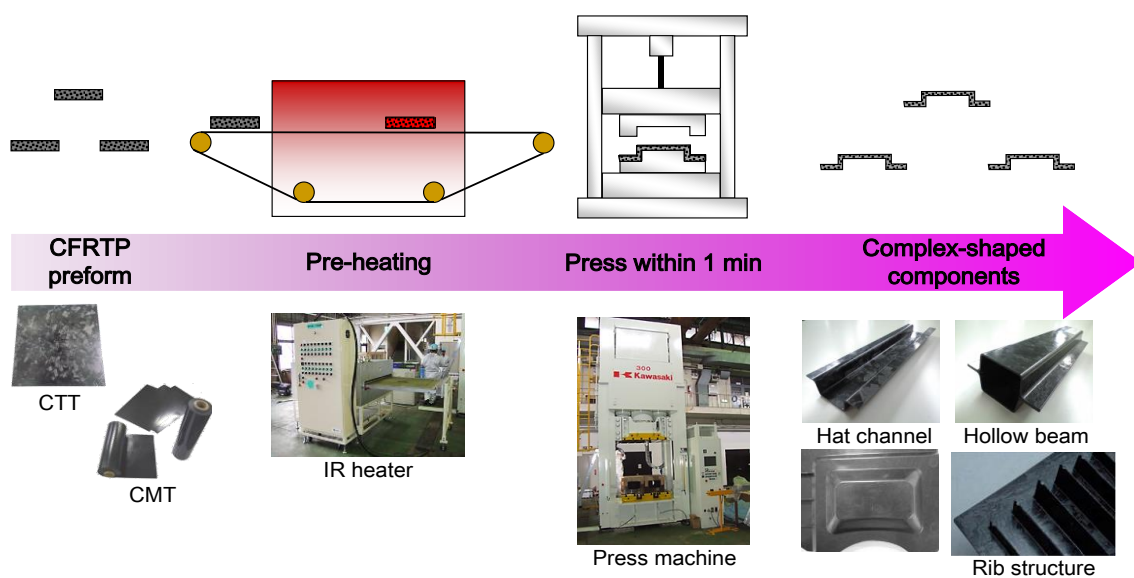


Figure 1. 8. Schematic of the targeted process of chopped carbon fiber tape reinforced thermoplastics (CTT) parts production: rapid, mass, automated and continuous [23].

1.2 Overview of doctoral dissertation

Fig. 1.9 summarizes a brief overview of this dissertation. Chapter 1 describes basic research background related to the forming process of fiber reinforced plastics and the targeted continuous forming process using CTT. Chapter 2 and 3 of this dissertation concentrate on an efficient way of validating forming characteristics employing experimental methodologies. Chapter 2 aims at drawing processing window when forming the complex part, especially having two sharp ribs. The molded sample is one of the solid evidence of formability using CTT preform sheets. The possibility of direct use of the preforms is confirmed, and it ensures forming applications of the material. In addition to the confirmation, the relationship between forming parameters and formability is

investigated in a practical range assigned.

Chapter 3 employs several squeeze flow cases to observe the progression of flow front and evaluate the mold filling time during compression molding. The simplified approach, which presents flow behaviors during compression molding process, allows one to understand important perspectives in the process. In addition, involved properties, such as void formation, mechanical properties are assessed using reliable experimental methods. Those case studies contribute to suggest one possible candidate for setting comparing a group to process modeling in fiber reinforced thermoplastics manufacturing.

Chapter 4 characterizes rheological properties of CTT samples using valid theoretical considerations for shear viscosity for fiber concentrated suspensions. This study aims at establishing out-of-plane shear viscosity models for CTT suspensions during the forming process, which are treated as dominant deformation mode in cases of complex flow during compression molding. Various experimental setups are designed to construct the models: materials of two kinds of volume fraction, three sequential steps (viscosity of polymer matrix without fiber filler, the yield stress of CTT suspensions, viscosity models for CTT suspensions) and various strain amplitudes to convert angular frequency condition to effective shear rates by multiple plots. From the procedure, the rheological equation is achievable if the approach and theoretical simplification are effective.

Chapter 5 delivers thermo-mechanical behaviors of CTT composites using a thermo-mechanical analyzer. This study characterizes coefficients of thermal expansion (CTE) in principal directions and guarantees reproducibility of experimental results, which are related to sample homogeneity and quality assurance of the material. Anisotropic CTE will represent directional dependent expansion due to the internal structure of the composite samples: dispersion of fibers in the polymer matrix and their networking structure.

Chapter 6 describes achievements of the present study and challenges under current circumstances of development. The chapter emphasizes the contribution of this research to toe engineering applications. Based on results of this study, anyone can access to characterize important properties, which are involved to flow behaviors of carbon fiber reinforced thermoplastics during compression molding process; rheological properties, thermal expansion properties, mold filling behaviors and even defect evaluation of molded part from the molding process.

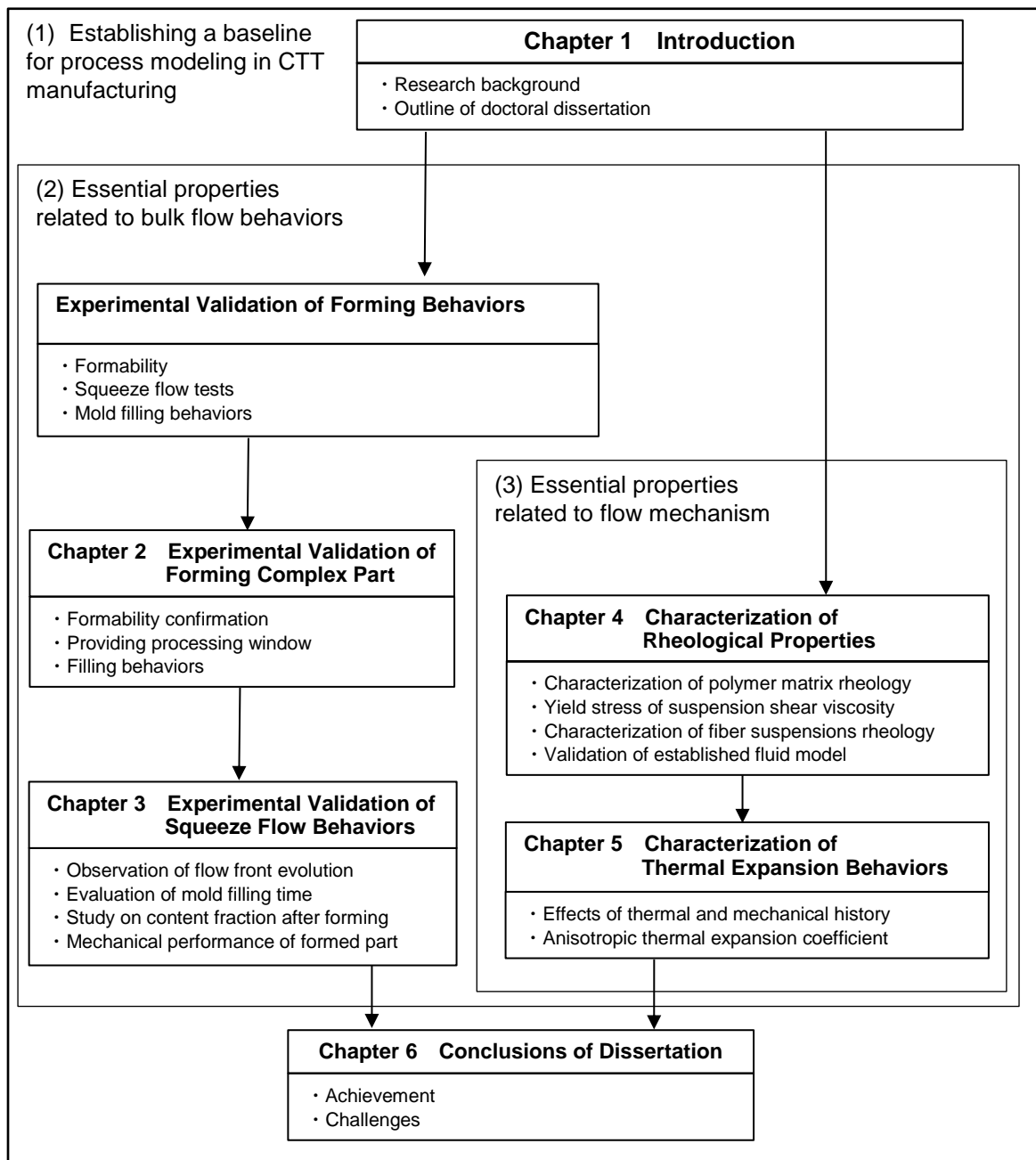


Figure 1. 9. Flowchart of an overview of the doctoral dissertation.

Chapter 2

Experimental Validation of Forming Complex Part

2.1 Introduction

Clarifying the relationship between the forming parameters and mold filling characteristics of highly concentrated fiber suspensions contributes to an extension of practical applications. Here we investigated the pivotal parameters of strand size and effective pressure and validated filling a complex mold cavity under practical processing conditions. The findings of this study are expected to contribute to ongoing innovations in the development of CTT applications. This section investigates the use of prepregs (PA6 as an impregnated resin) based CTT, and the objective of the present section is to experimentally investigate the relationship between the forming parameters and mold filling behaviors using a forming sample with a very complex geometry. This case study facilitates to recommend optimized processing conditions for the material by applying various forming parameters. As CTT materials with a high fiber content (>50%) and random orientation of cut strands were used, the type of filler, filler geometry (length, radius, aspect ratio), and geometry of the forming die are dependent variables in forming applications. The forming parameters, initial charge dimensions, and placement in forming tools and charge properties during sample molding were experimentally investigated. Among those variables, we hypothesized that the global flow might be highly dependent on the forming conditions, especially the effective pressure and forming time.

2.2 Background

Randomly oriented strand (ROS) composites consist of pre-impregnated chopped strands cut in the longitudinal direction. Unlike continuous laminate composites which have inextensibility in the longitudinal direction, discontinuity of randomly oriented strands in ROS composites makes it possible to produce complex parts by preparing the desired strand dimension when forming the composites.¹⁶ CTT can be categorized as ROS composites based on analysis of their morphology and

fiber orientation. A unique characteristic in manufacturing this composite is the use of the preform as sheets, which is similar to the manufacturing of SMC. CTT molded parts possess the combined benefits of good mechanical performance and ease of forming in general. In recent years, the mechanical properties of ROS composites have been studied using advanced characterization techniques,^{17, 18, 24-26} while few existing studies have compared the process complexity and pivotal factors of formability.

The forming characteristics of thermoplastic ROS composites have also been investigated in terms of defect formation induced by varying the processing conditions.²⁷ Squeeze flow tests for reproducing compression molding process is one of the most frequently used approaches for characterizing key aspects of the molding process. Many previous studies have investigated the flow behavior of PEEK as the polymer matrix.^{21, 22, 27} In comparison, little detailed information exists regarding the use of PA6 matrix (widely used engineering plastics) for CTT materials, enabling lower temperature forming than that of using PEEK as matrix polymer matrix.

2.3 Materials

2.3.1 Overall procedures

Fig. 2.1 shows an overall processing steps for forming complex-shaped components using CTT materials. Industrial Technology Center of Fukui Prefecture provided uni-directional pre-impregnated sheets with an average thickness of 44 μm . The prepreg sheets are semi-impregnated by tow spreading technique and resin impregnation process, which was specifically investigated in the previous study.²⁸ The prepregs consist of PA6 films (Diamiron™ C, Mitsubishi Plastics, Inc.) and carbon fiber tows (TR 50S; Mitsubishi Rayon Co., Ltd.). The importance of using the prepregs is that molded parts have structurally stable properties and ease of processing. The overall procedures contain cutting the desired strand sizes; wet dispersion process to achieve the formation of sheets, evaporating absorbed water and in-plane random orientation; preparing for required dimensions of the preform; applying optimized the forming technique. Selecting an appropriate and efficient forming technique is a pivotal factor to obtain defect-free parts with a good quality because before forming a step, most of the preparation works are well defined and strictly controlled. There would be a more specific description of each step to introduce well-defined manufacturing procedures for CTT parts in next section.

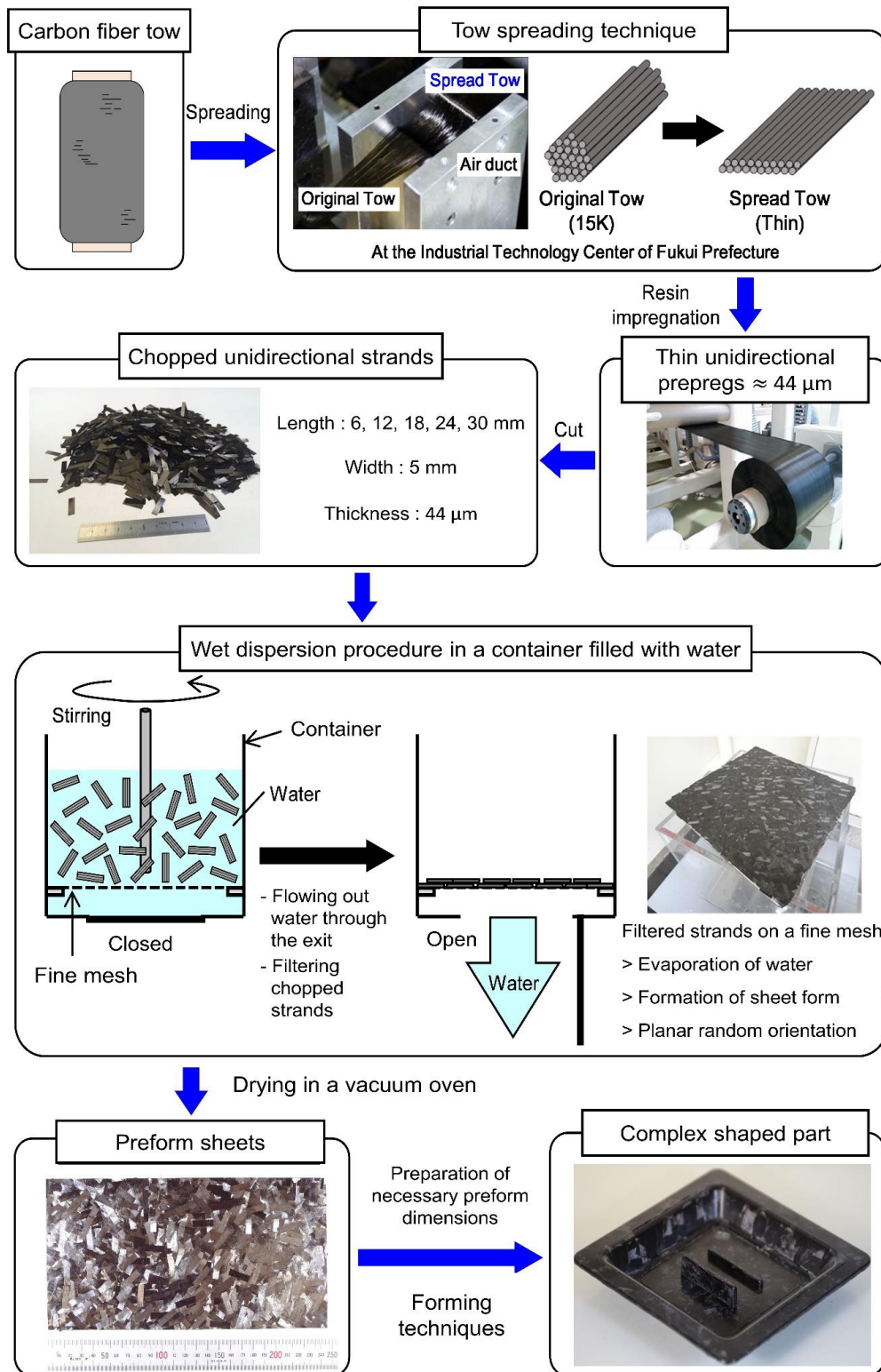


Figure 2. 1. Overview of the processing steps for forming chopped carbon fiber tape reinforced thermoplastics component. (Adapted from [23]).

2.3.2 Preliminary procedures

The first step of preparation works is to attain desired strand sizes of 6, 12, 18, 24 and 30 mm long with a constant width of 5 mm by chopping the prepregs. Prior to cut in a perpendicular direction to the aligned fibers, prepregs are precisely cut with 5 mm wide along longitudinal direction using a digital cutting machine (Zund), also known as prepreg cutter, with a maximum deviation of ± 0.02 mm. One unit of the longitudinal direction is 250 mm in general. Using one of computer-aided design (CAD) software, Solid Works (Dassault Systemes) in the present case, it is possible to generate dxf type file as illustrated in Fig. 2.2. Importing the design file to operation system connected with the cutting machine is the second step. By utilizing the operation system and control console, the accurate control of cutting sequence, speed and areas are accessible. Also, vacuuming the lower side of prepregs can achieve dimensional conformance when cutting such thin sheets with particular dimensions. In order to reduce the possibility of misalignment, and low impregnation degree at each edge, both edges of cut prepregs are eliminated at the end of this procedure. Therefore, unidirectional prepreg sheets with slits are the final form of the procedure.

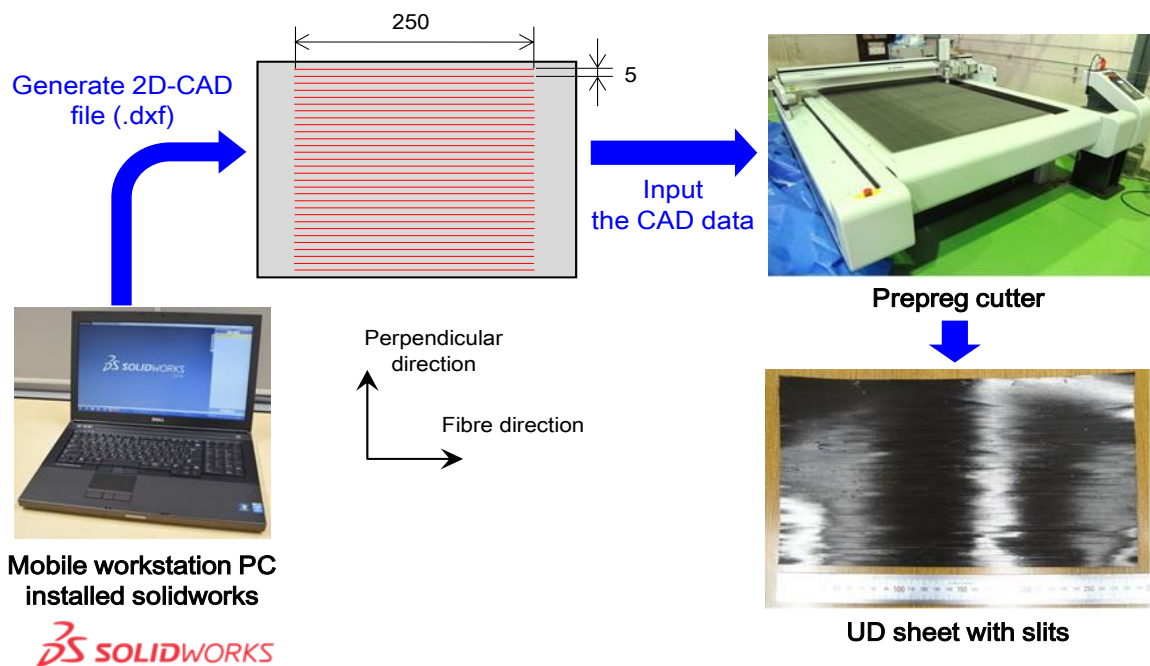


Figure 2. 2. Flow diagram of pre-impregnated sheets cutting in fiber direction [23].

Cutting in the perpendicular direction is required using a customized cutter. Selecting length of the strand (6, 12, 18, 24 and 30 mm) is easily achievable because various types of the cutter were designed to have a diversity of preform types for various experimental cases and purposes. Using the customized cutter and compression instrument allows one to fabricate accurate dimensions of chopped strands with negligible deviation.

2.3.3 Preform preparation

The preparation of preform sheets has been introduced in CTT fabrication. The aim of preparation is to improve the controllability of the molding process and to facilitate the planar random orientation of fibers. Such structural considerations aim at minimizing the out-of-plane misalignment of the carbon fibers because the out-of-plane misalignment may degrade the mechanical performance of molded specimens. Also, manufacturing ROS composites does not engage this procedure in cases of other research groups, this process is considered as important because the ultimate goal of applying this material is the mass and continuous production using a conveyer belt with a form of sheets.

Five types of preform sheets were prepared by using various chopped strand size: 6 mm, 12 mm, 18 mm, 24 mm, 30 mm long and 5 mm wide in the following steps as shown in Fig. 2.3. First of all, a certain amount (20-23g) of chopped strands are inserted in a container filled with water to achieve planar random orientation by stirring the filled water with centrifugal force. Subsequently, the bottom of the water container is opened to flow out filled water, while the chopped strands are filtered through a mesh frame (28 × 28 cm); one unit of the mesh is a square shape (4 × 4 mm). Water absorbed in the strands is evaporated for 3 min, and then the filtered strands are heated and pressed at 260°C, above the melting point of PA6 \approx 220°C,⁶ for 1 min to make a final form of sheets with a square dimension (25 × 25 cm). The preform sheets are approximately 0.4 ± 0.1 mm thick including internal free spaces existed. The sheets are not fully compressed and consolidated and contain internal free spaces. Therefore, imposing sufficient consolidation by compression and heating is significant during forming procedures. The preform sheets are dried (90°C for 12 h) using a vacuum oven, minimizing deterioration of material properties by water absorption of PA6 matrix in prepreg sheets. Those preform sheets are cut into particular dimensions (86 × 86 mm), which fit the matched die without a ribbed section of forming instrument used in this chapter.

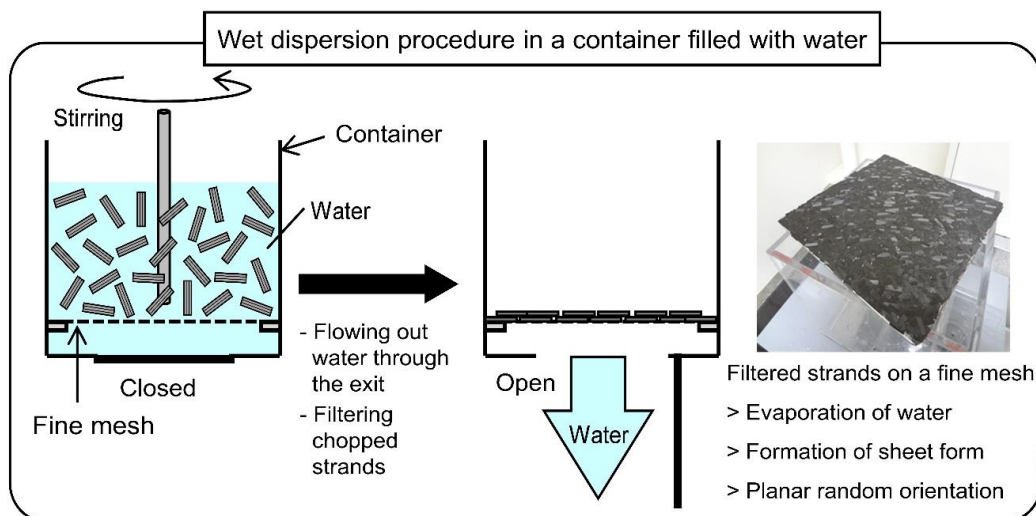


Figure 2. 3. Schematic representation and summary of wet dispersion procedure.

2.4 Experimental procedures

2.4.1 Instrument

The hot press used in this chapter was a simple instrument designed for manufacturing commercial products (Sanko Gosei Ltd.) with geometric complexity. The matched die forming technique involves the composite sheet is formed using two tools of the die surfaces, generally to achieve one step forming step when forming complex shaped parts compared to using sequential forming steps.¹⁰ The geometry has very complex geometry including double curvature and two sharp ribs, and therefore, it is possible to confirm validity of complex forming using CTT materials. The mold filling phase of the compression molding cycle begins when the upper mold contacts with the charge of material lying on the lower mold surface. As soon as contact is made, pressure from the downward movement of the upper mold forces material to flow. The piston pressure of the hydraulic pump equipped in the instrument was monitored recorded during molding cycles, and this value was converted to the applied force of the entire instrument. From the force value, an effective pressure ($p_{eff} = F/LW$) could be approximately calculated by considering the preform dimension used (86 × 86 mm). The upper and lower platens, different from forming die, were heated by embedded heating cartridges and there was an inherent temperature difference between the platens and the die. Therefore, the temperature of the upper and lower surfaces of the die using a thermometer was measured prior to the insertion of the preform sheets into the die in order to confirm this temperature deviation. A cooling system consisting of water and air circuits was also embedded in the upper and lower platens.

2.4.2 Experimental design

The matched die used in this research was specially designed to form the complex ribbed plate samples, as shown in Fig. 2(a), with upper and lower flat sections and a double curvature at each corner of the lower flat section. In addition, these molded samples were designed to include two tapered ribs, with dimensions as shown in Fig. 2(b) and (c). The lower die contained the geometry to form the ribs and thus Fig. 2(c) represents the opposite direction of compressive forming.

The preform sheets used in this study were composed of strands with nominally identical dimensions, where each preform type was classified by the strand length. Table 2-1 summarizes design matrix for matched die forming of CTT. The thickness of the final molded component corresponded to an initial charge weight of 22 g with a maximum deviation of ± 1.0 g. An experimental test matrix was designed to evaluate the influences of forming parameters including the strand size, effective pressure calculated, and consolidation time on the filling the molding die using CTT preforms. Identifying the relationship between the forming parameters and complete filling in the given dimension of the die would provide a processing window for the forming of

relevant samples for practical applications.

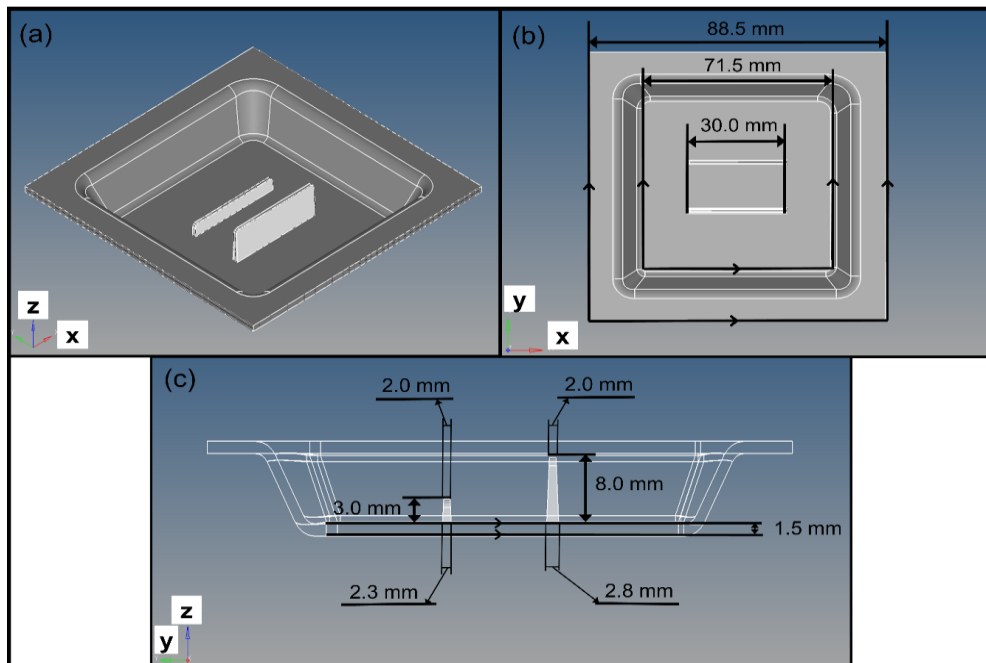


Figure 2. 4. Schematics diagrams of the ribbed tray samples molded in this study. (a) 3-dimensional view, (b) top view and (c) dimensions of ribbed section.

Table 2 - 1. Experimental design matrix for matched die forming of chopped carbon fiber tape reinforced thermoplastics.

Length (mm)	Strand size		Effective pressure (MPa)
	Width (mm)	Thickness (μm)	
6	5	44	5, 10, 15, 20
12			5, 10
18			5, 10, 15, 20
24			5, 10
30			5, 10, 15, 20

Fig. 2.5 shows nominal molding cycles at various effective pressures during the forming process of a ribbed tray. The upper and lower dies were heated to the required temperature for effective forming (260°C) in all designed cases. After a stable temperature of the die surfaces was reached, the following four steps were performed for all samples in the experimental matrix. First of all, ten plies

of the square preform charges were placed on the lower die and then the upper mold half comes in contact with the charge of material moved downward for nominal contact, marked as point (1) in Fig. 2.5. Subsequently, a constant temperature was imposed for 3 min to melt the polymer matrix, heating phase, indicated by the region between points (1) and (2) in Fig. 2.5. Simultaneous forming and consolidation were then applied, indicated by the region between points (2) and (3) in the figure. In the phase, intimate contact and adhesion of adjacent plies, eliminating internal free spaces of the preforms and allowing resin percolation were achievable. Also, the step involved the formation of squeeze flow to fill the mold geometry and fill the ribbed and flat sections. As shown in Fig. 2.5 by the dashed and dotted lines, several samples were prepared with various p_{eff} values ranging from 5 to 20 MPa (the operating range of the equipment) in 3 min. In order to investigate the effects of consolidation time for all five strand length cases, times of 3 and 10 min were used at a p_{eff} of 10 MPa. During the cooling (solidification) phase, the applied load was maintained and the platens were cooled down to 90°C by the water cooling system and 80°C by the air cooler, which is slightly above the glass transition temperature of the polymer matrix (70°C).⁶ The identical cooling conditions were applied to all samples to induce an equivalent thermal history and crystallization degree by the cooling phase. After finishing the sequential molding cycles, the molded samples were ejected from the molding die.

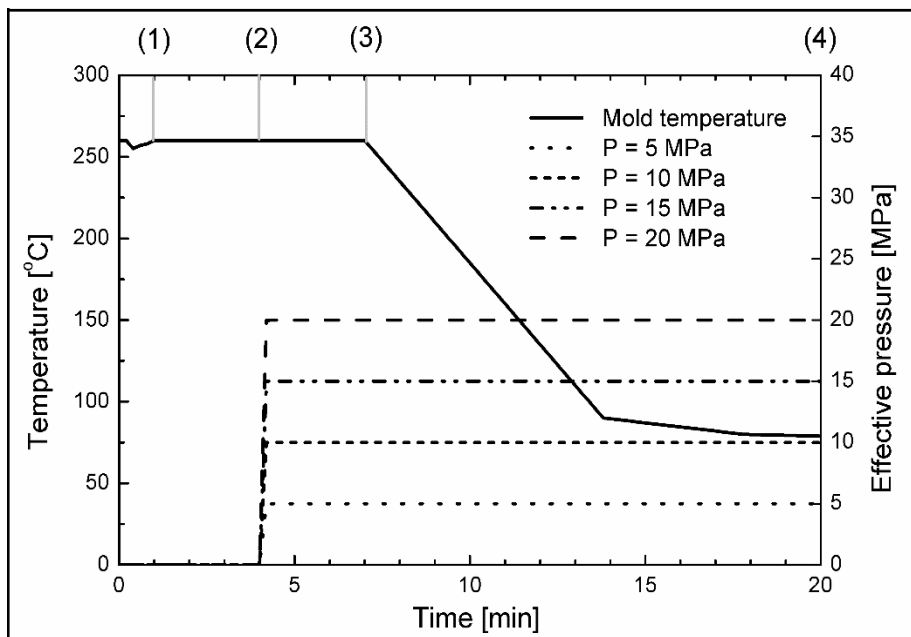


Figure 2.5. Nominal molding cycles used during the production of the ribbed trays formed using a matched die.

2.4.3 Relevant test: optical microscopy

Cross-sectional samples after the molding process were observed using optical microscopy. The micrographs of ribbed sections were taken from the plane of symmetry at the middle of rib length. The molded samples were polished with a finer finish using a sequential procedure using sandpapers in 400, 600, 800, and 2000 on a rotating disk device followed by 3.0 μm , 1.0 μm , and 0.25 μm polycrystalline diamond suspensions to achieve a finer finish.

2.4.4 Consideration of heating phase

A common step in the forming trials studied here is a heating step before beginning the actual filling and consolidation phase. This step is fundamental for validating the rheology and heat transport through the height of composite samples. An essential requirement for the experimental rheological analysis of suspensions is the complete melting of the polymer composition. The existence of unmelted polymer or porosity leads that the flow domain during the filling step cannot be treated as a two-phase system and this complicates the valid analysis; assuming the polymer matrix is melted and considered as a liquid phase, the material can be treated as a continuum of two phase system.

The heating step was also used to achieve isothermal conditions in the samples during the heating step, where thermal diffusivity through the thickness direction is the main factor. It is necessary to consider a heating time for thermal diffusion through the thickness. In the present cases, the density of the composite ρ was 1510 kg/m^3 , its heat capacity C_p was 1430 $\text{J kg}^{-1} \text{K}^{-1}$ and the thermal conductivity of the system K was 0.93 $\text{W m}^{-1} \text{K}^{-1}$ as inferred from its volume fraction and literatures.^{6, 12, 29} The sample thickness h was approximately 2 mm, and a 3 min heating step was undertaken for the forming of the ribbed tray samples. Therefore, the associated heating step was 78 times longer than the characteristic time t_c of 2.3 sec, where t_c can be defined by Eq. 2-1. This evaluation suggest that steady-state isothermal condition is reached after 3 min, which is 78 times t_c .

$$t_c = \frac{\rho C_p}{K} \left(\frac{h}{2}\right)^2 \quad \text{Eq. 2-1}$$

2.5 Results and discussion

2.5.1 Theoretical analysis

The molded samples by the matched die forming showed dimensional conformance with the mold geometry and defects such as surface buckling could not be observed in produced samples. For the experimental conditions used here, the squeeze flow mechanism was essential for forming the complex geometries. However, flow into the ribs followed a unique mechanism as these sections were perpendicular to the flat section, which had multi-axial fibers in an in-plane orientation. In-

plane orientation of preform plies close to the ribbed section may be highly deformed to fill ribs. After flow into the ribbed section had begun, the melted suspensions underwent a flow mechanism similar to that in a thin channel with the corresponding p_{eff} at the rib entrance.

Despite the geometric limits of flow at the narrow entrances for entering the ribbed sections (2.3 and 2.8 mm) compared to the strand length (6, 12, 18, 24 and 30 mm), the suspensions of carbon fiber and melted polymers were able to form sharp ribs depending on processing conditions. This forming achievement was possible by the agglomerating and bending of the initial fiber structure without a remarkable phase separation. The geometry of the mold cavity was fixed variable in this study to make a valid comparison of flow behavior in various cases. Two major issues regarding the strand size and flow properties were the influences of strand length on the effective viscosity and yield stress of materials. Assuming complete melting of the polymer matrix during the heating phase, CTT suspensions can be included as highly concentrated fiber suspensions; hyper-concentrated regime by the following equations:¹⁶

$$\pi/4 > f > \pi/16 \text{ (square array) Eq. 2-2}$$

$$\pi/2\sqrt{3} > f > \pi/8\sqrt{3} \text{ (hexagonal array) Eq. 2-3}$$

$$(L/D) > 100 \text{ Eq. 2-4}$$

where f represents the fiber volume fraction of composite system, which is within possibility of Eq. 2-2 and 2-3 for CTT sample, L is the length of rod-like particle, and D is the diameter of the particle. L/D ranges from 857 to 4290 (>100) regarding all length because the average D of fibers is known as 7 μm . Hence, it is clear that CTT suspensions are within the hyper-concentrated regime and it is possible to adopt an analysis to interpret flow behaviors. The effective viscosity in this regime increases with increasing L/D even when packing geometry of fibers are neglected. Therefore, overcoming the flow resistance when forming the materials is difficult even though there is a high driving force from the applied pressure.

Fig. 2.6 represents figures taken from photographs of ribbed sections produced at the equivalent p_{eff} of 10 MPa for 3 min with various strand lengths, where the effect of the strand length is clear; longer strand length is relatively hard to achieve filling the ribs. In addition, the dependence of the yield stress on strand size is widely known properties for highly filled thermoplastic ROS composites, where the materials start flowing over a critical stress level. In the studies, combined experimental and modeling studies showed that longer strand lengths showed higher yield stresses during squeeze flow.^{22, 30} Larger contact areas between each strand with increasing L/D increase in friction effects, growing the yield stress level of the system.

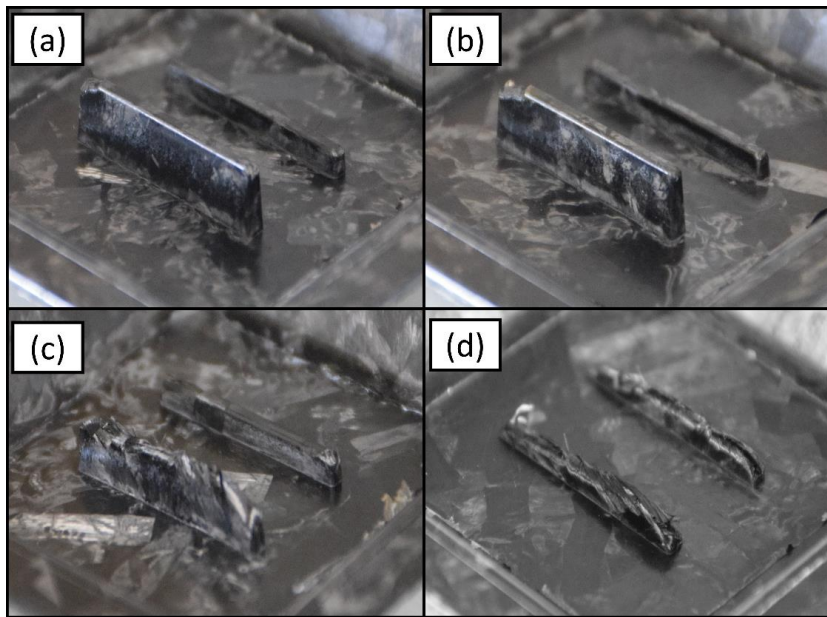


Figure 2. 6. Photographs of ribbed sections formed at an effective pressure of 10 MPa for 3 min for strand lengths of (a) 12 mm, (b) 18 mm, (c) 24 mm and (d) 30 mm.

2.5.2 Mold filling behaviors

Defining the mold filling behaviors by adopting a quantitative way in a given conditions and mold cavity is a kind of challenging task. In this section, the analysis concentrates on mold filling into the four corners of the flat section and the two narrow ribs in order to limit the scope of discussion; these sections were determined as we expected them to be the most difficult to fill due to geometric constraints, which hinder flow at the narrow entrances of the ribs (2.3 and 2.8 mm) compared to the shortest strand length (6 mm). It is clear that longer strand cases had difficulties in forming such geometry. Photographs of several typical morphologies of formed rib sections for various cases are shown in Fig. 2.7(a), (b) and (c). Higher pressure allowed to fill ribbed sections in cases for an identical strand length. A localized defect at the corner of a rib is presented in Fig. 2.7(d), which is taken account of ‘complete filling’. Three optical micrographs in Fig. 2.8 show cross-sections of the taller rib for a strand length of 18 mm at different pressures (5, 10, and 15 MPa for (a), (b), and (c), respectively). The lower pressure condition in Fig. 2.7(a) resulted in an unfilled area in the taller rib, while the higher pressures shown in Fig. 2.7(b) and (c) showed full filling of taller ribs. By considering the observation of each case, it is possible to define the filling behaviors by adopting a dimensionless value associated with ‘complete filling’ of the mold cavity, defined as follows:

1. Complete filling of each corner gained one point; thus if all four corners of the flat section were filled, the sample earned four points in total.
2. If the ribbed sections were fully filled, the sample was assigned a value proportional to the height of each rib: $h_s = 3$ points if the shorter rib is filled, $h_t = 8$ points, if the taller rib is filled.
3. If the filled suspensions reached the end of the rib (2.0×30 mm at the top of the rib) and there was a localized defect in the ribs (as shown in Fig. 2.7(d)), the sample obtained $(h_s - 1)$ and $(h_t - 1)$.

Hence, if the molded sample satisfies all these criteria described here, a value of 15 is assigned for complete filling in the total score.

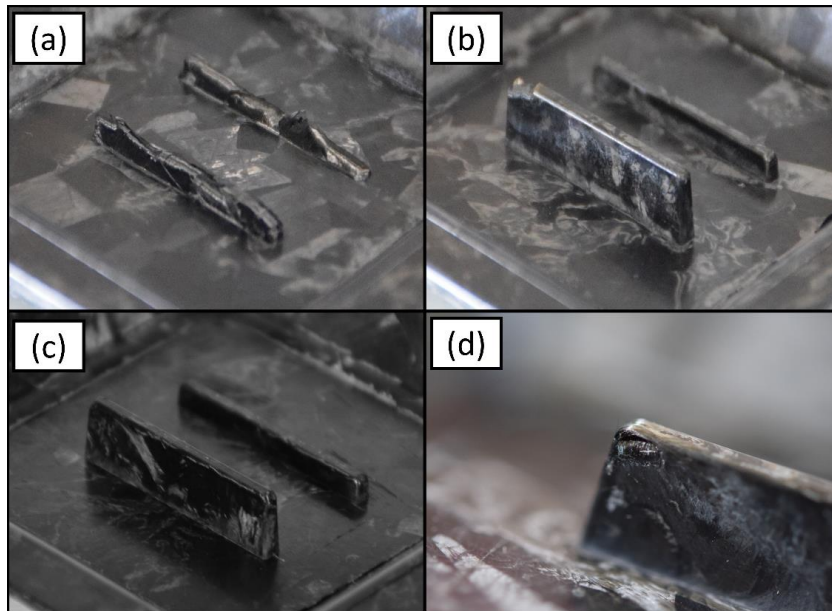


Figure 2. 7. Photographs of filled ribbed sections for strand lengths of 18 mm and pressures of (a) 5 MPa, (b) 10 MPa, (c) 15 MPa and (d) an example of a localized defect at the corner.

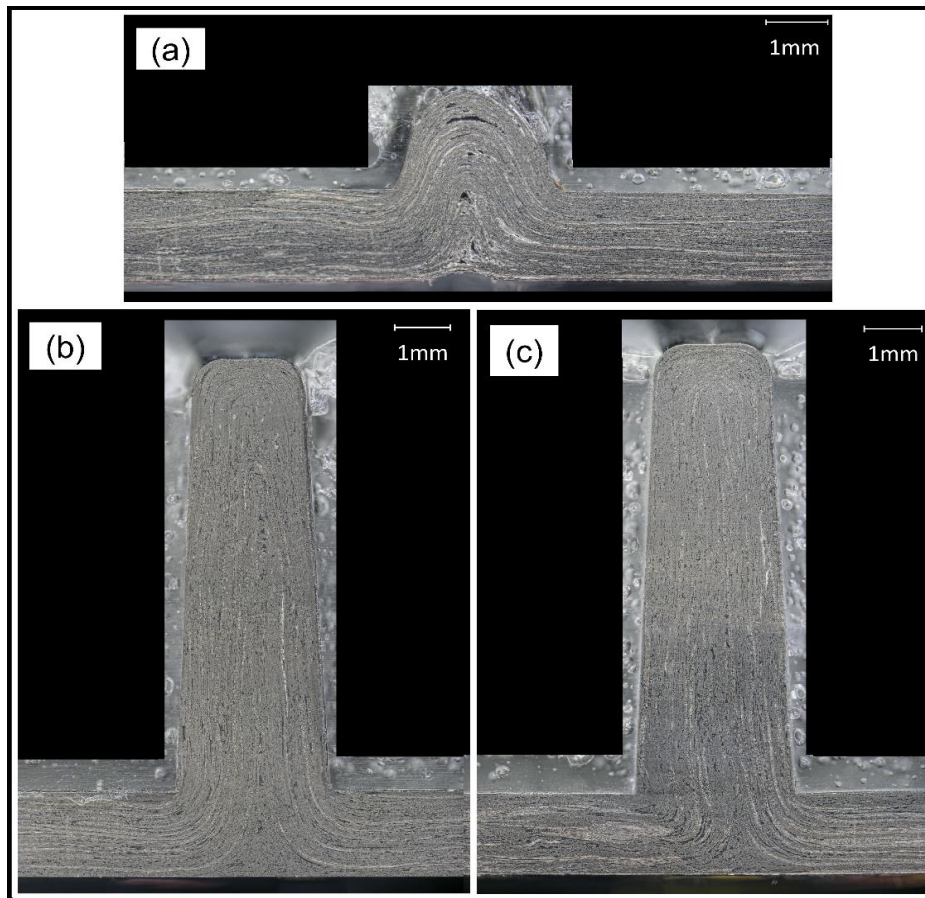


Figure 2. 8. Optical micrographs of cross-sections of CTT samples cut along the length direction of the taller rib for samples prepared with a strand length of 18 mm and pressures of (a) 5 MPa, (b) 10 MPa, and (c) 15 MPa.

Three forming parameters effects are summarized in Fig. 2.9 and 2.10, employing the dimensionless ‘complete filling’ value; effective pressure, consolidation time, and strand length. Fig. 2.9 represents the general tendency of CTT formability in diverse strand lengths and pressures cases. The complete filling value generally increases with the effective pressure, whereas 3 min of heating at 5 MPa is not sufficient to form ribbed sections. The ratio of rib height to width of rib entrance is 1.3 for the shorter rib and 2.9 for the taller rib. Even at a pressure of 10 MPa, it is hard to attain full filling with the longer strand sizes in the given mold cavity. The consolidation time seems to be less influential than the influences of pressure and strand size. The complete filling value of 15 is only achievable for the shorter strand lengths of 6 and 12 mm for 10 min of forming. Fig. 2.9 contains the results that the strand length highly affects the formability of this material. It is apparent that the flow behavior of the CTT using 24 and 30 mm strand lengths is not sufficient for complete filling a die under these test conditions.

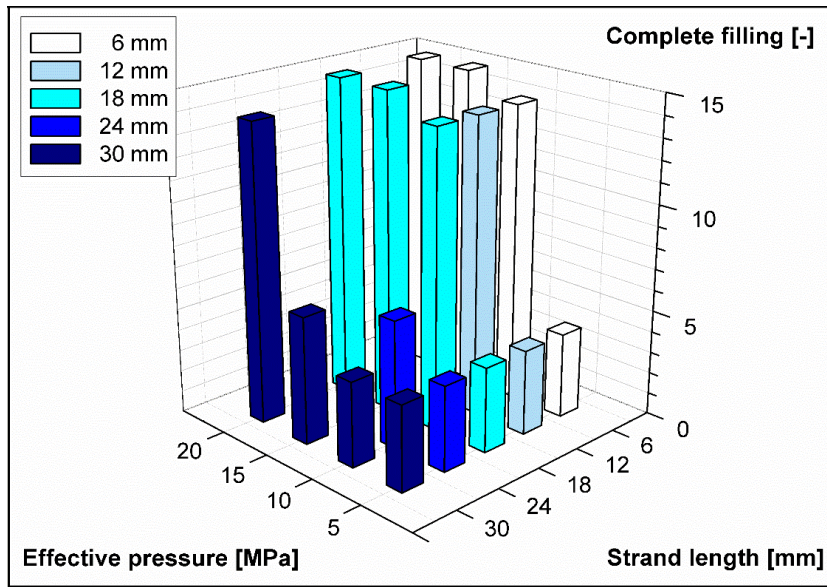


Figure 2. 9. Effect of effective pressure and strand length on the complete filling.

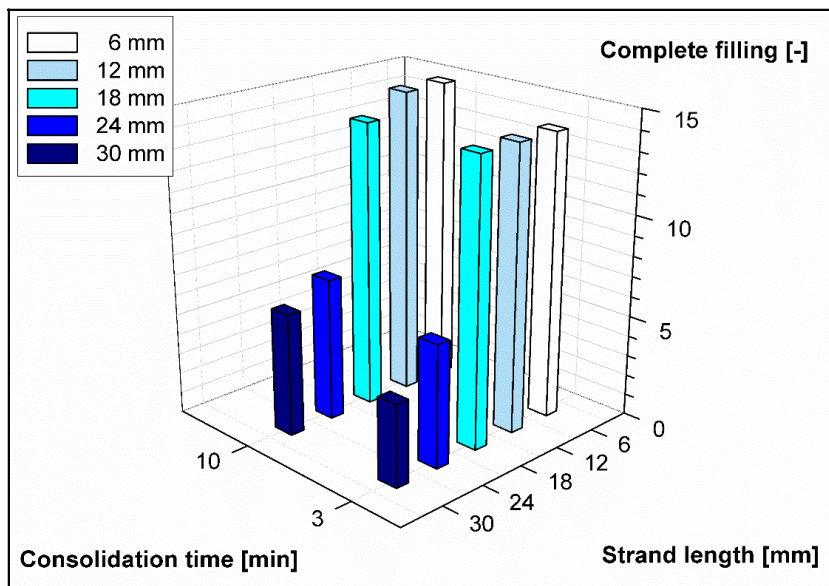


Figure 2. 10. Effect of consolidation time and strand length on the complete filling.

2.6 Concluding remarks

This chapter illustrates a rough sketch of processing window of CTT materials, applying to the ribbed plate geometry. This study is expected to contribute to the practical application when forming complex shaped components. Unlike the cases of continuous fiber laminates, which have inextensibility along the fiber direction, the forming characteristics of CTT suspensions are greatly dependent on strand size and the effective pressure. The solid advantage of using CTT materials from this study is that simplified forming processes can be achievable compared to the complex procedures for continuous laminate composites when producing complex shaped part using joining techniques.

The relationship between formability and processing parameters was studied by filling a mold with complex features in short time (10 min), and the influential factors were discussed. Critical defects, e.g. surface buckling or phase separation were not observable in the formed ribbed tray samples because of the use of preforms with multi-axial discontinuous fiber fillers from impregnated prepregs. In regards to filling the complex-shaped mold, in general cases, strands longer (6–30 mm) than the rib entrance width (2.3 and 2.8 mm) seems to be difficult to fill the ribbed sections. However, the use of 10 MPa of effective pressure achieved full filling of the ribs with shorter strands of 6 and 12 mm.

Because effective viscosities and yield stress are known as influential factors on forming behaviors of highly concentrated suspensions, including CTT in melt state of polymer, process simplification is required to advance the analysis beyond this empirical forming trials in the direction of reducing the geometric complexity of molded part. It was found that shorter strands resulted in better filling of small, complex molding die. Therefore, in the next chapter, in order to simplify the analysis, the strand size is fixed to 5 mm wide and 6 mm long so that we can concentrate on investigating one type of composite system clearly. It is hard to assume similar flows occur when using different strand length in terms of the yield stress and suspension rheology. The use of commercial software for numerical simulations of processing technology, such as injection molding or compression molding, is constrained by the aspect ratio of fibers when calculating fiber orientation. This is because long fibers are not easily rotated and aligned by the effects of velocity field generated. Therefore, the use of preforms consisted of shorter strands (lower aspect ratio) is the most reasonable way for this purpose.

The importance of rheological and thermo-mechanical studies has been suggested, although this chapter did not fully concern the effects of those by simply assigning process conditions to compensate the influences. This is because those properties suggest the possibility of establishing constitutive equation during forming processes. Also, those would contribute to understanding practical constraints when applying the materials to the manufacturing process. Those properties will be studied in Chapter 4 and 5, respectively.

Chapter 3

Experimental Validation of Squeeze Flow Behaviors

3.1 Introduction

Squeeze flow are commonly used methodology when characterizing flow behaviors of various polymer melts or suspensions. Investigating the progression of flow front during compression molding is essential aspect when characterizing forming behaviors. Here we investigated influences of several forming conditions on properties of formed parts and demonstrated squeeze flow behaviors under practical processing conditions. In addition, a simplified method for observing the evolution the flow front using a video camera is proposed, where the dependence of the processing conditions on the mold filling time could be observed. The importance of the consolidation process is emphasized the porosity, and mechanical properties of samples prepared under squeeze flow are quantified. The findings of this study are expected to contribute to ongoing innovations in the development of CTT applications.

3.2 Background

Diverse studies have been introduced regarding the flow behavior of fiber-reinforced composites, such as permeability measurement, filling, and molding behaviors, which were prepared using several different forming techniques.³¹⁻³³ Squeeze flow tests for reproducing compression molding process is one of the most widely used approaches for discovering key aspects of the molding process, such as progression of flow front and sample height changes at applied normal force.⁵⁶ The present section is devoted to an important discussion of the formed components adopting the squeeze flow experiments, which aims to provide valuable advice for the practical manufacturing of CTT materials. The effects of the forming parameters are expected to be applicable to a wide range of forming applications. This section introduces a method for experimentally observing the progression of the flow front using a video camera and analyzes the mold filling time with a squeeze flow test. Sample defects, in particular voids, produced during the squeeze flow test were quantified by comparing

several squeeze flow cases. In addition, alternative processing conditions are suggested in terms of void formation and mechanical properties for cases showing sufficient consolidation.

3.3 Materials

Uni-directional pre-impregnated sheets with an average thickness of 44 μm provided by the Industrial Technology Center of Fukui Prefecture were used to fabricate preform sheets. The preform sheets were prepared by identical procedures described in Chapter 2 except the size of chopped strands (6 mm long and 5 mm wide) in the following steps. First of all, the chopped strands are dispersed in a container filled with water to achieve planar random orientation by stirring the filled water with centrifugal force. Subsequently, the bottom of the water container is opened to flow out filled water, while the chopped strands are filtered through a mesh frame (28 \times 28 cm); one unit of the mesh is a square shape (4 \times 4 mm). The water absorbed in the strands is evaporated, and then the filtered strands are heated and pressed at 260°C, above the melting point of PA6 \approx 220°C for 1 min to make a final form of sheets with a square dimension (25 \times 25 cm). The preform sheets are approximately 0.4 ± 0.1 mm thick with internal free spaces because the sheets are not fully consolidated. The preform sheets are dried (90°C for 12 h) using a vacuum oven prior to squeezing flow tests or pre-consolidation process. Those preform sheets are cut into particular dimensions depending on each experimental design.

3.4 Experimental Procedures

3.4.1 Instrument and charge preparation

A Laboratory Press 30T (Pinette Emidecau Industries, the maximum force of 30 ton) was employed to perform squeeze flow tests. The instrument facilitates to precisely control and captures the processing conditions (platen temperature, applied force, and relative positions between two platens). Each platen (upper and lower) as illustrated in Fig. 3.1 contains nine heating areas with their proportional-integral (PI) controllers. The basic type of molds (upper and lower) were separately assembled with the each platen in cases of producing cuboid samples with dimensions of 125 mm wide and 250 mm long. In this case, the upper mold precisely fitted with the lower mold. The height of produced samples corresponds to processing conditions (applied load, cooling condition) and the weight of charged preforms. In addition, cooling processes were controlled by water and air solenoid valves embedded in each platen. The temperature is controlled by combining the heating and cooling systems. The applied force is dominated by hydraulic load controller at designated set points. In addition to the systems, monitoring the internal mold temperature in real time is possible due to thermocouple probes directly contacted at one of the surfaces of upper and lower molds as shown in

Fig. 3.2. Fig. 3.3 represents temperature monitors connected with the thermocouples. Therefore, the temperature of upper and lower mold temperature can be observed during molding cycles. Hence, the inefficiency of thermal conduction and resulting discrepancy between platen and mold temperature are observable in a real time. Such accurate measuring systems make it possible to set equivalent processing conditions in all tests.

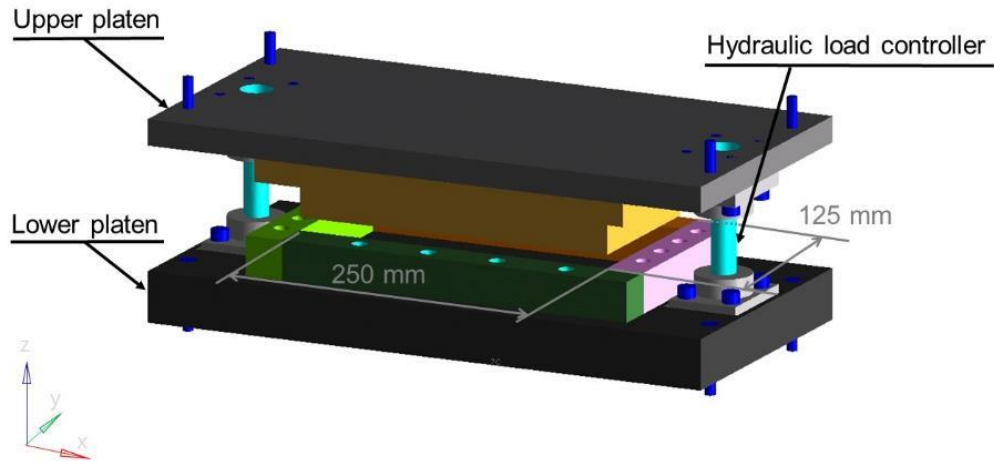


Figure 3. 1. Schematic representation of components configuration equipped with a laboratory press.

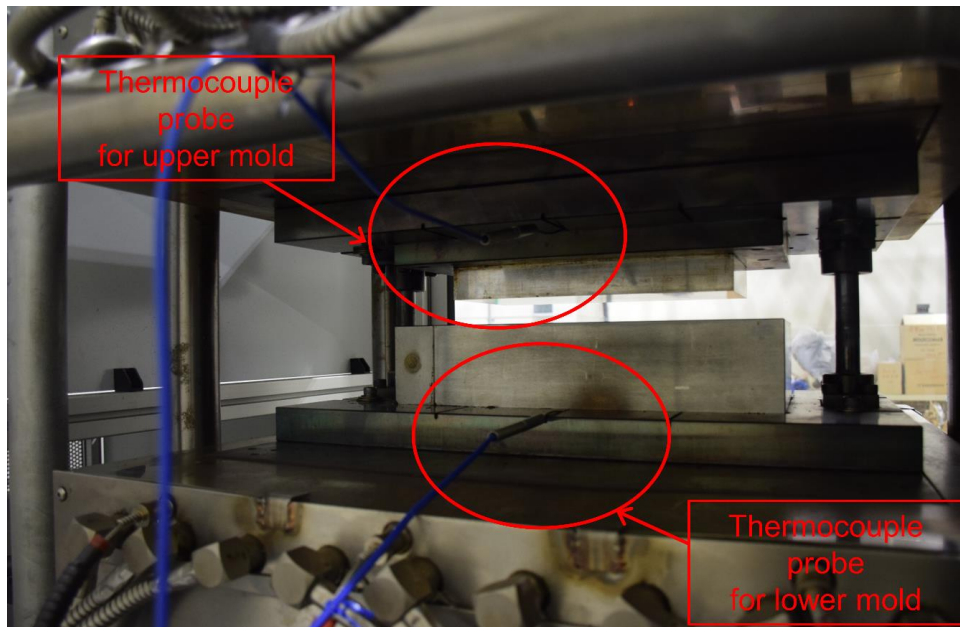


Figure 3. 2. Schematics of thermocouples embedded in mold configuration.

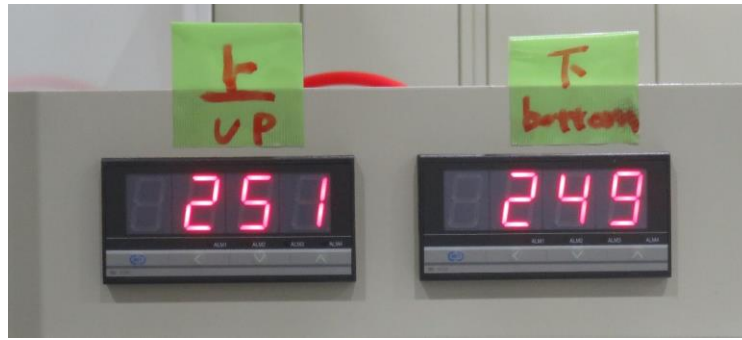


Figure 3. 3. Temperature monitoring panels showing temperatures of upper and lower molds.

There are two types of mold configuration used in this section. One of them is the closed mold configuration previously described and shown in Fig. 3.1. The configuration is a closed system, and thus makes prepared materials possible to simply experience constant thermal history. Another is an open mold configuration, which was specially designed to have two open areas to observe the progression of global flow during squeeze flow tests using a video recorder, as depicted in Fig. 3.4(c). Such macroscopic observation provides invaluable insight into the mold filling behavior and initial deformation of the sample during the heating phase without requiring transparent molds. The design aimed to let a charge undergo symmetric deformation at the center plane when locating the charge at the center of the mold cavity. A squeeze flow test is a simplified method for analyzing the forming process with a complex geometry and has been shown to be suitable for cases validating shear flow, for examples, L shapes, S shapes, and those with various type of cross-sections.¹⁰ Although limits of the instrument and thermal instability introduce certain experimental constraints, it is an efficient way for estimating mold filling behavior and assessing mold filling time.

When using an open mold system, most of controlling and measuring systems are feasible because the entire instrument of laboratory press, even for upper and lower platens, is not changed except the lower mold design. The areas indicated by the white dotted line in Fig. 3.4(b) show the eliminated areas from the closed mold, which is the primary difference between the closed and open mold configuration. The upper mold dimension of open mold configuration is identical with the closed mold configuration. In open mold cases, the preform charge is squeezed by direct contacts between molds (upper and lower) and an inserted charge as shown in Fig. 3.4(a). Therefore, the driving force of squeeze flow is a pressure difference between the contact surfaces and free surfaces of the charge. The red arrows in Fig. 3.4(a) and (c) indicate directions of applied force. Therefore, the resulting contact areas are the two contact surfaces between molds and charges. Fig. 3.4 (b) shows dimensions of charges in case A and B, open mold cases with the direct insertion of charges in the form of preform sheets.

The mold filling phase of the compression molding cycle begins when the upper mold contacts with the charge of material lying on the lower mold surface. As soon as contact is made, pressure from

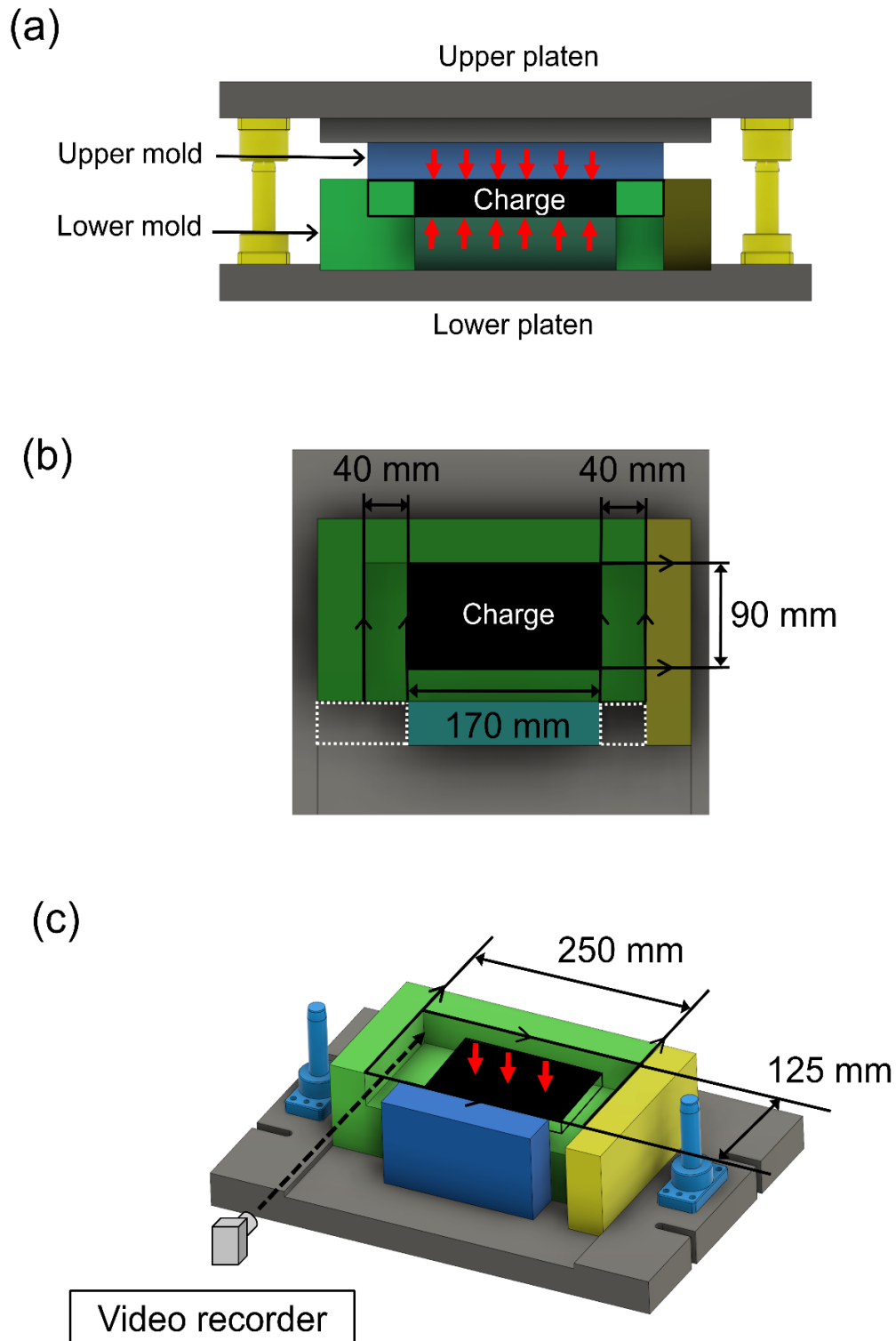


Figure 3. 4. Mold configuration and preform dimensions for squeeze flow tests using an open mold: (a) sectional view, (b) top view and (c) 3-dimensional view.

the upward movement of the lower mold forces material to flow, as shown in Fig. 3.5(a) and (b), after a heating phase. After making inserted charges as an isothermal state (discussed in 3.4.4), getting actual contact between charges and two molds initiates a compression stage and a resulting squeeze flow. The closing speed is slowed down to the maximum speed before the contact moment to avoid overshooting of force. Fig. 3.5(a) and (b) also denote the viewpoint of the video recorder when observing the evolution of the flow front. Fundamentally, the directions of applied force and operating method are equivalent in the closed mold system as well.

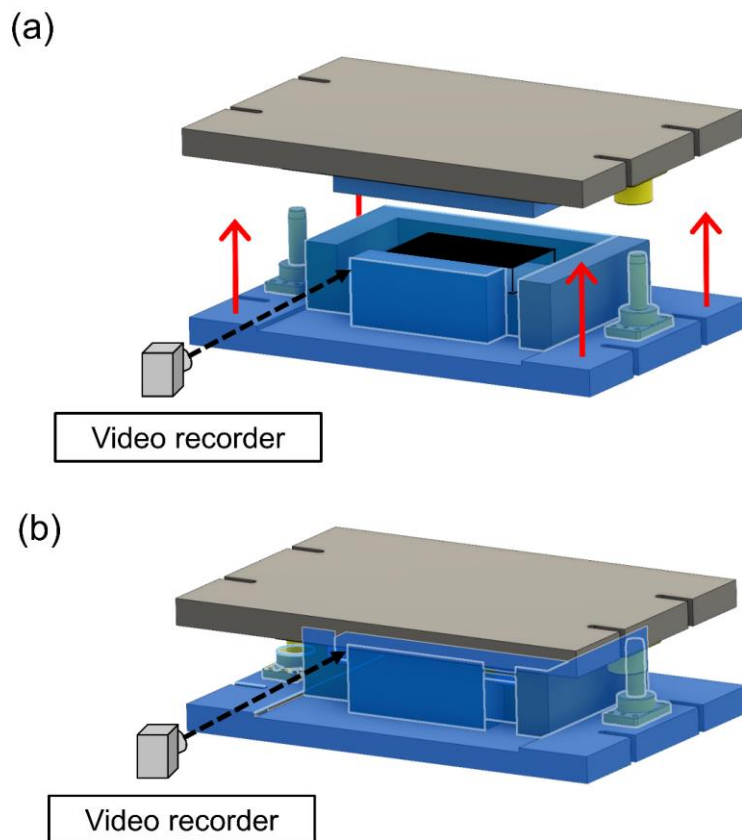


Figure 3. 5. Schematic representation of operation system during compression molding cycles: (a) initial stage of the cycle without contact and (b) actual contact and mold filling stage.

Four squeeze flow cases were designed to observe the evolution of the flow front, and discuss a difference of the open mold cases and closed mold case: case A (open mold at low applied force), case B (open mold at high applied force), case C (open mold with pre-consolidated charge) and case D (closed mold case). Preventing the melted material from flowing out of the open areas was considered when determining the initial charge dimensions of open mold cases and position of the

samples. Table 3-1 shows the dimensions of prepared preforms for each case, respectively; 90 mm wide and 170 mm long for case A and B; 120 mm wide and 245 mm long for case C; 120 mm wide and 170 mm long for case D. Charges for case C are pre-consolidated by the designated molding cycle to minimize a possibility of void formation, and is specified in the next section. All squeeze flow tests did not form knit-line due to single charge placement. Table 2-1 briefly summarizes essential information of prepared preform dimensions, ply numbers and the weight of materials for each case.

Table 3 - 1. Prepared preform dimensions for each case of the experiment.

Case	Mold type	Preform plies	Preform dimensions		
			Width (mm)	Length (mm)	Weight (g)
A	Open	54	90	170	212±1 g
B	Open	54	90	170	212±1 g
C	Open	58	120	245	456±1 g
D	Closed	18	120	170	94±1 g

3.4.2 Sample pre-consolidation

58 plies of preforms were consolidated by molding cycles as shown in Fig. 3.6. The weight of 58 preform plies (120 mm wide and 245 mm long) ranged in 456 g \pm 1 g in each molding cycle. The preform dimension was for producing flat panels (125 mm wide, 250 mm long and average thickness of 9.5 mm) pre-consolidated by compression molding on an industrial press without wrinkles and voids. The consolidated samples was used to observe the flow front during squeeze flow with low possibility of void formation. For the purpose, the panels were trimmed and samples (99 mm wide and 170 mm long, 9.5 mm thick and the weight of 242 g \pm 0.5 g) were cut using diamond blade saw. The samples were used as an initial charge for case C of squeeze flow tests. Thus, the length of cut samples conformed to that of invisible areas in the lower mold when positioning the samples at the center of the mold as shown. Also, one of the outer surfaces contacted with longer mold wall without open areas. Therefore, if there is a squeeze flow from the invisible areas, the observation of flow front would be possible through the open areas. The length of charge conforms to invisible areas in open mold configuration when positioning the charge at the center of mold cavity as described in the previous section.

The processing conditions were recorded by a data acquisition system equipped with the hot press used in the entire molding cycle as shown in Fig. 3.6. The black dashed line denotes the temperature

in a middle of upper platen, whereas the red dashed line represents the temperature in a middle of lower platen. The solid blue line represents the applied force adjusted by the setting of the user-defined recipe. The set temperature of both platens was 265°C and resulted in a corresponding mold temperature of $260^{\circ}\text{C} \pm 2^{\circ}\text{C}$ as observed by the embedded thermocouples in upper and lower molds. Regarding effective pressure p_{eff} during molding cycles, prepared preforms underwent sequential steps: 1 MPa and 5 MPa in the present force level and the dimension of contact areas of applied force.

The primary reason for preparing pre-consolidated samples is to produce void-free charges. In the previous study, inserted preforms are expected to experience sufficient heat and pressure for consolidation, enabling that consolidated samples have negligible voids. This could be deduced from thoughts that the set conditions for the present samples had longer consolidation time (20 min) than that of in cuboid samples with an average thickness of 2 mm producing (10 min) in equivalent processing conditions of previous literature.¹⁸ In order to assure full consolidation and reduce the possibility of void formation when producing such thick samples (9.5 mm thick approximately 5 times thicker than typical specimen). In cuboid sample manufacturing Compared to the case A and B, the direct use of preform sheets as a charge, pre-consolidated samples have a lower possibility of void formation and the high possibility of homogeneous properties.

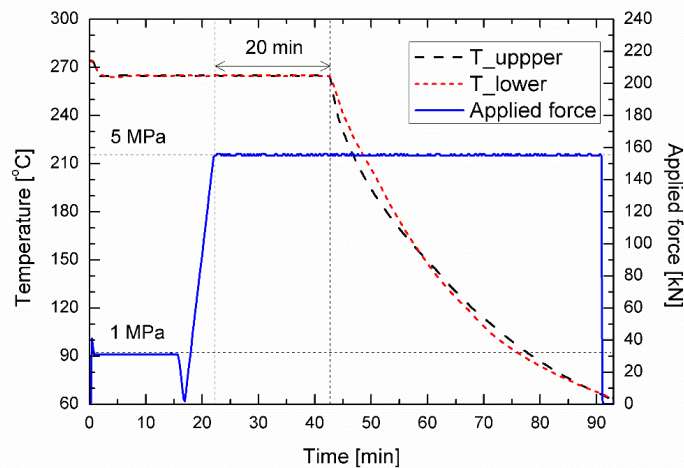


Figure 3. 6. Recorded molding cycles for producing a pre-consolidated charge using a closed mold.

Fig. 3.7 shows photographs of prepared charges: a preform charge for case A and B and a pre-consolidated charge for case C. When using preform sheets as a charge, water soluble white ink was marked at two edges of preform sheets to observe the progression of flow as shown in Fig. 3.7(a). When squeezing out from the initial state of sheets as shown. Meanwhile, one plane was marked using the same ink to track the progression of flow when the pre-consolidated charge flows as shown in Fig. 3.7(b).

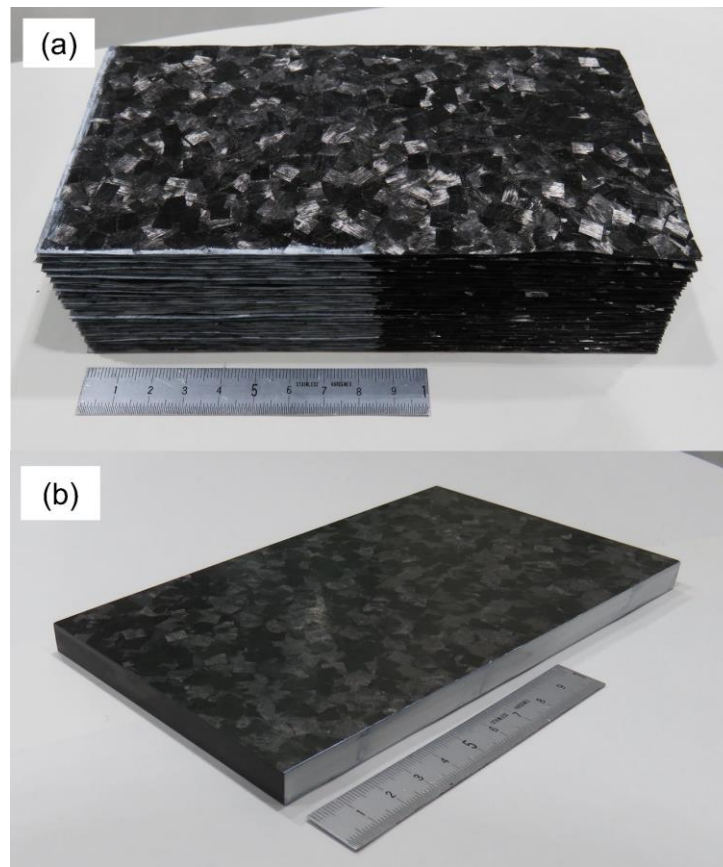


Figure 3. 7. Photographs of prepared charges: (a) preform charge for case A and B and (b) pre-consolidated charge for case C.

3.4.3 Experimental design

The dimensions of initial charges were empirically chosen to retain the visible areas from the viewpoint because the visible areas through the open area were limited by geometric constraints of mold configuration. Equivalent preform plies and dimensions were used in case A and B, whereas case C used pre-consolidated samples as an initial charge. Processing conditions, such as the applying force, its duration, gradient, temperature of platens, its duration and gradient could be controlled by the adjustable recipe file as shown in Table 3-2.

Fig. 3.8 shows initial setups of the preform charge (90 mm wide and 170 mm long) for case A and B in the given open mold cavity. The open mold case was designed to observe the progression of global flow during squeeze flow tests using a video recorder from the open area in the lower mold. The mold design aimed to let a charge undergo symmetric deformation at the center plane. The preform charge was initially placed at the center and attached to longer mold wall with no open areas. The heated charge after phase 1 flowed along the longer mold wall direction. The visible area from the video recorder was 40 mm in each squeezing side because the total length of mold was 250 mm and initial charge length was 170 mm. Three surfaces except contact surfaces with the upper and

lower mold of the sample were free surfaces, and the empty space was the C shape in the initial stage of the experiments. Case C test was conducted using pre-consolidated charge in the same length with the length of preform sheets in case A and B. Therefore, the total length of visible area is identical in case A, B, and C.

Table 3 - 2. Experimental design matrix for squeeze flow tests.

Case	Mold type	Preform plies	Phase 1		Phase 2		Cooling phase		
			Force (kN)	Duration (min)	Force (kN)	Duration (min)	Force (kN)	Duration (min)	
A	Open	54	1)	0	5	15	24	0	10
			2)	1	10				
B	Open	54	1)	0	5	30	14	0	10
			2)	1	10				
C	Open	58	0	30	30	-	15	10	
D	Closed	18	31	15	156	10	156	10	
Reference [18]	Closed	12	31	15	156	10	156	10	



Figure 3. 8. Initial setups of the preform charge and lower mold geometry for case A and B.

The experimental design matrix for squeeze flow tests focusing on the applied force conditions is specifically described in Table 3-2. The tolerance of force and temperature was set to minimum values in order to validate the settings. Fig. 3.9 contains plots of applied force profile on the initial charges during the entire cycle of all open mold cases. In phase 1, the contacting force was low (0–1 kN) compared to the applied force during the filling stage (15–30 kN). After finishing phase 1, heating phase for open mold cases, force increased manually up to 15 kN for case A (minimum force setpoint), 30 kN for case B and C, respectively to achieve full filling of mold cavity without flowing out from open areas. Phase 2 in the cases A, B and C included both initial compression and flow initiation. Force control allowed for a compensation of thermal expansion of prepared charges. Polytetrafluoroethylene (PTFE) film was used to prevent the reflection of charge movement on the steel mold wall (at filling end position) in case C. If there is no such consideration, it would be hard to define the termination of mold filling.

Fig. 3.9 shows recorded temperature at the center of the upper platen in all open mold cases. All three cases represent constant temperature during phase 1, heating phase. In the case A, the temperature reached to 270°C during phase 2 (filling stage) slightly higher than the temperature of case B and C (255°C), in order to compensate for heat losses by natural convection through the open areas for a longer time. These set temperatures of case B and C resulted in a corresponding mold temperature of $250^{\circ}\text{C} \pm 2^{\circ}\text{C}$ as measured by the thermocouples in the molds. The thermal stabilization of the inserted charge for case C was assessed during the heating phase in 30 min. Cooling process was carried out using both the water and air circuits at a cooling rate ($20^{\circ}\text{C}/\text{min}$) in manual mode, and then samples were ejected from mold cavity at 70°C , glass transition temperature T_g of PA6 matrix.⁶

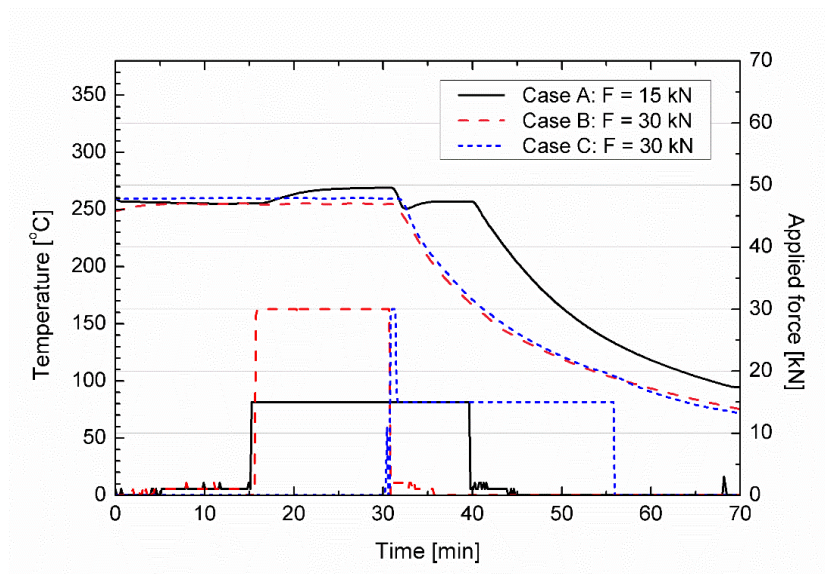


Figure 3. 9. Temperature and applied force profiles of open mold cases.

The primary difference between the open mold cases (case A and B) and the closed mold case (case D) was the insufficient chances to consolidate (both force and time in heating and filling stages) during squeeze flow tests. In regards, samples for case C were pre-consolidated using open mold configuration. The applied closing force during the cooling phase in case A and B was 0 kN, and it was nominal contact not actual consolidation to prevent void formation. Therefore, the open mold cases include two possible defects theoretically. The first defect is a high void content due to the low closing force in phase 1 for eliminating existed free spaces in the preform sheets by compression compared to the case C, D and manufacturing of flat panel samples without flow as described as 'reference' in Table 3-2. The second defect would be the localized loss of contact between the mold walls and the material and resulting surface voids, originating from the thermal and crystallization shrinkage during cooling.²⁷ In the case of producing ribbed trays, such defects could affect the forming of complex features because the compression force is indirectly applied to the section.

Fig. 3.10 represents plots of applied force and temperature recorded by data acquisition system (set value of temperature was 255°C). The heating conditions, sequential load levels, and heating at a constant temperature, showing $250^{\circ}\text{C} \pm 2^{\circ}\text{C}$ at temperature monitors of upper and lower molds, during phase 1 and 2 and cooling conditions for case D were equivalent to those of typical manufacturing of flat panel samples without flow. The only difference is force gradient (0.2 kN/s instead of 0.5 kN/s) to reach the set closing force of 156 kN, and the corresponding longer time to reach the value (13 min) during phase 2 than that of typical manufacturing. The longer time aimed at minimizing the distortion of fiber orientation from sudden application of closing force. Similar to the pre-consolidation process, 156 kN corresponds to 5 MPa of effective pressure p_{eff} on molded samples after terminating the filling process. The closed mold case was designed to undergo unidirectional squeeze flow toward each of the shorter mold walls. The preform charge initially covered 70% of the cavity and was centered in the middle of the mold to ensure symmetric molding and final properties of the samples. Two surfaces except contact surfaces with the upper and lower mold of the sample were free surfaces, and the two empty spaces were located on each side of the mold cavity in the initial stage of the experiments.

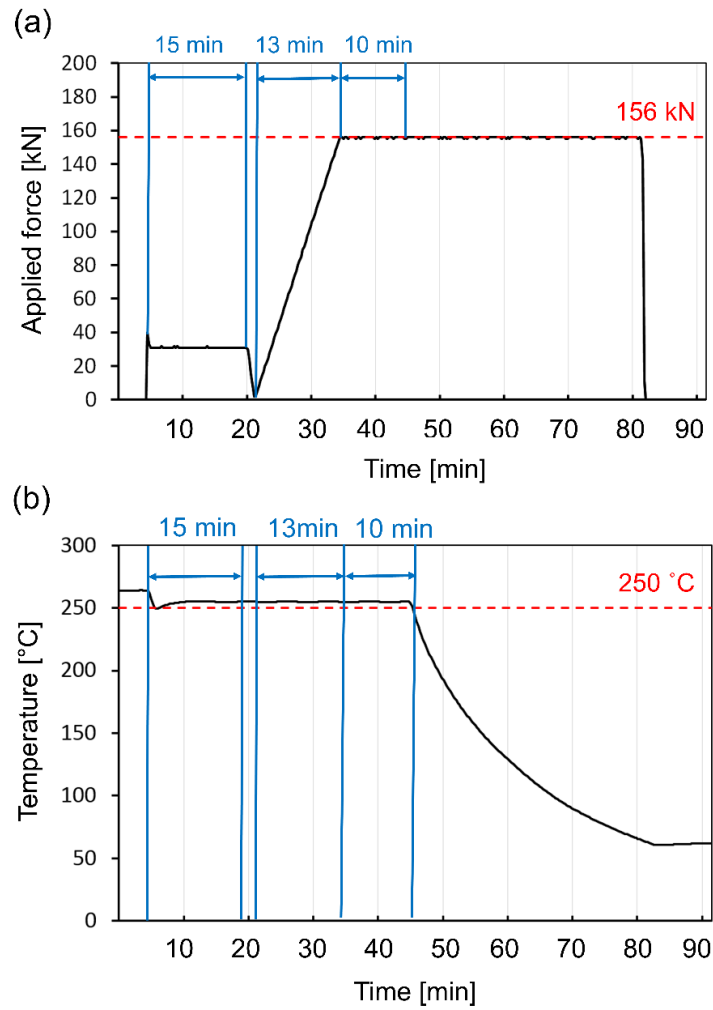


Figure 3. 10. Processing conditions for case D: (a) force profile and (b) temperature profile.

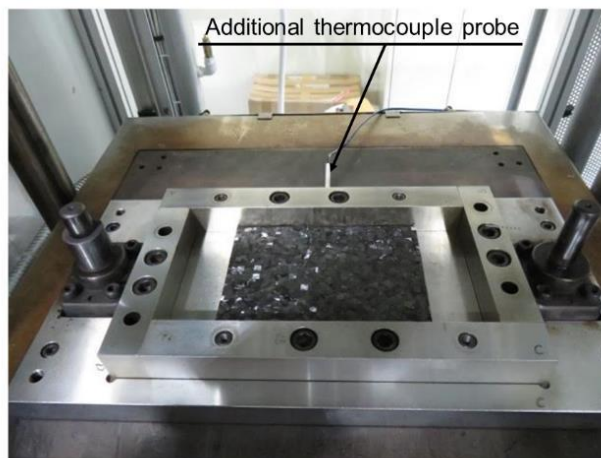


Figure 3. 11. Initial setups of the preform charge and lower mold geometry for case D.

3.4.4 Consideration of heating phase

A common step in the squeeze flow tests studied here is a heating step before beginning the squeeze flow. This step is essential for validating the rheology and thermal diffusion of the composite samples. A fundamental requirement for the rheological analysis of suspensions is the complete melting of the polymer matrix. If unmelted polymer or many pores are present, the flow domain cannot be treated as a two-phase system of melted polymer and fiber reinforcement, and this complicates the analysis.

The heating step was also used to achieve isothermal conditions in the samples during compression molding, where thermal diffusivity through the thickness direction is the significant factor. Therefore, it is necessary to estimate a heating time for thermal stabilization; in the present cases, the density of the composite ρ was 1510 kg/m^3 , its heat capacity C_p was $1430 \text{ J kg}^{-1} \text{ K}^{-1}$ and the thermal conductivity of the system K was $0.93 \text{ W m}^{-1} \text{ K}^{-1}$ as inferred from its volume fraction and literatures.^{6, 12, 29} The sample thickness h was 13 mm, and a 15 min heating step was undertaken for the squeeze flow cases of case A and B, whereas the sample thickness for case C was 19 mm and the heating step took 30 min when considering heating was only applied on the lower surface of charge. Therefore, the associated heating step was nine times longer than the characteristic time t_c of 97.4 s in the former case and 8.7 times longer than the t_c of 208 s for the latter case, where t_c is defined by Eq. 3-1.

$$t_c = \frac{\rho C_p}{K} \left(\frac{h}{2}\right)^2 \text{ Eq. 3-1}$$

In the case C, thermal stabilization test was performed because the evaluated t_c is quite long because of thick sample height and it is hard to ensure isothermal condition of heated charges. In the case C, force control as 0 kN with nominal contact or 1 kN, similar to the case of A and B, was impossible in used instrumented press because the pre-consolidated sample had high stiffness. The pre-consolidated sample was quite stiff and it led high contact force despite low closing speed compared to preform sheets, which allows closing force as 0 or 1 kN, in case A and B. Thus, the control sensor could not reach the force setpoint by the recipe setting. Although the closing speed could be set as slowest closing speed of 0.5 mm/s (maximum closing speed = 5 mm/s), the contact between the upper surface of sample and the upper mold by automatic cycle led the overshooting of force and stopped the cycle. Therefore, the sample was firstly heated until the isothermal condition without contacts of the sample and upper mold and compression was carried out by manual setting instead of using automatic cycle set by recipe setting. That means the heating was mainly applied by thermal conduction from the heat source at lower platen.

A thermocouple was placed on the upper surface of the pre-consolidated charge for case C. The thermocouple was attached to the center of upper surface by polyimide (PI) tape (0.055 mm thick), which has high heat resistance and adhesion property even at high temperature. Fig. 3.12 shows the temperature after insertion of pre-consolidated sample in the thermocouple on the sample and platen

temperatures measured at upper and lower platens at the constant temperature of 255°C). Monitoring panels connected with thermocouples in the upper and lower molds represented $250^{\circ}\text{C} \pm 2^{\circ}\text{C}$ during the heating process. The plots suggest that a stabilization time of 30 min to ensure steady state isothermal condition after the heating phase.

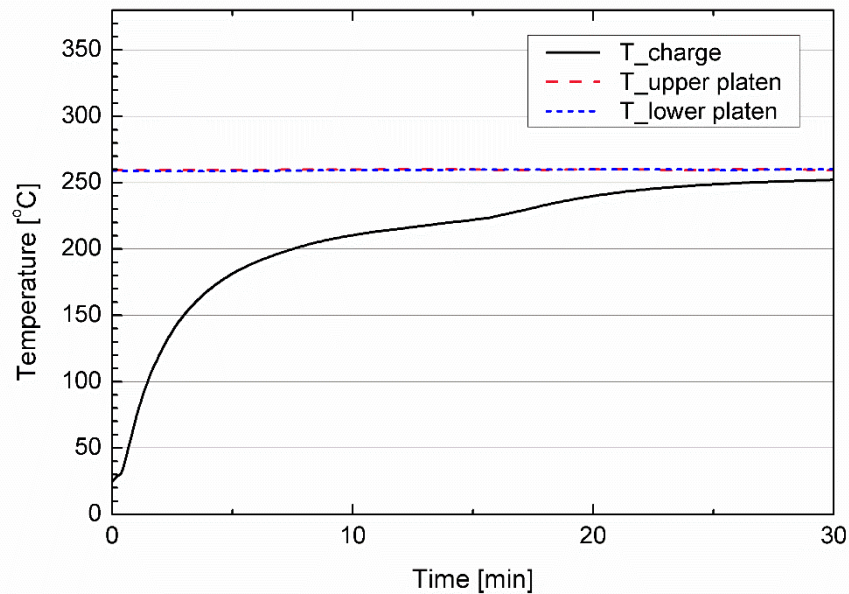


Figure 3.12. Temperature profile during the heating phase of squeeze flow test C.

3.4.5 Relevant tests

3.4.5.1 Fiber volume fraction and void content

The burn-off technique was applied to evaluate the volume fraction of fibers V_f and void fraction V_v for five samples from each experimental case except case C. In the case D, closed mold, three 25 mm long, 20 mm wide and 1.97 mm thick samples were cut from the filling ends adjacent to the shorter mold walls using a diamond blade saw. Fig. 3.13 shows the photograph of molded sample in the case D and cut areas for the test as white dotted line. The case was designed to have uni-directional flow from the center symmetric plane. In the open mold cases, case A and B, samples 30 mm long, 25 mm wide and 5.3 mm thick for case A and 5.0 mm thick for case B were cut from the filling ends, although the initial charge dimension was smaller than the case D. As the open mold cases and case B experienced a different thermal history, specimens adjacent to the open areas were excluded in this evaluation.

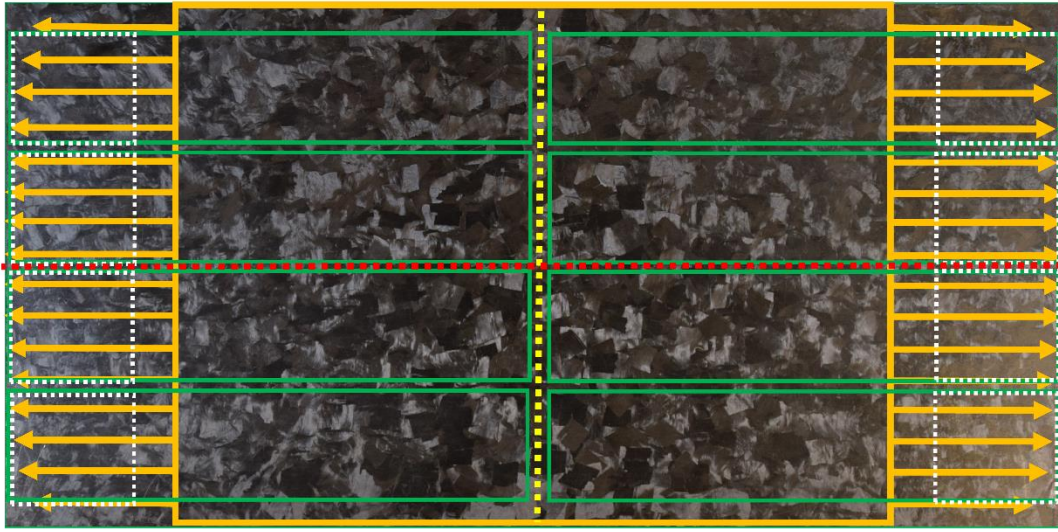


Figure 3.13. Photograph of molded sample from a top view, a schematic representation of flow (yellow arrows) and cutting edges in case D (green solid lines and white dotted line).

The density and weight of each sample were measured using a density meter (MDS-300, Alfa Mirage Co., Ltd.) and a digital scale with a precision of four decimal places, respectively. The relative fraction of the polymer matrix and the fibers were estimated by measuring the weight change after thermal decomposition in a nitrogen atmosphere for two h at a constant temperature of 500°C. Fig. 3.14 shows a burning off device equipped with a closed container filled with nitrogen gas. To make sure that the thermal decomposition process was terminated and the weight change did not occur as time went by, the weight was measured at 1 h and 2 h in the entire process. The weight of fibers was also estimated by comparing the weight of remained fibers in the container after terminating the burning off process and a container. Therefore, the void fraction V_v of each sample could be calculated in accordance with Eq. 3-2 using the measured variables and the densities provided by material manufacturer $\rho_m=1.14 \text{ g/cm}^3$ and $\rho_f=1.82 \text{ g/cm}^3$, where W is weight, V indicates volume, and the subscripts f , m , c , and v denote the fiber, matrix, composite, and voids respectively.

$$V_v = 1 - \frac{(W_f/\rho_f + W_m/\rho_m)\rho_c}{W_c} \quad \text{Eq. 3-2}$$



Figure 3. 14. A burning off device with the nitrogen gas provider.

3.4.5.2 Mechanical testing

In order to compare the mechanical performance of case D with that of the referred properties in the case of flat panels without flow, tensile tests were performed following the ASTM D3039 standard.³⁴ The molded sample by one molding cycle for case D was 250 mm long, 125 mm wide and approximately 2 mm thick. Specimens 124 mm long, 25 mm wide and 1.97 mm thick were taken from the symmetric plane in the middle of molded sample length towards the filling end along the filling direction marked as a green solid line in Fig. 3.13. Therefore, at least eight specimens could be used in one molded sample in consideration of loss by the thickness of cutting blade. Results of 5 specimens were collected and averaged for equivalent comparison with the previous study.¹⁸ Each specimen was expected to represent the influence of the squeeze flow along the flow direction. Each specimen width and thickness were measured using digital calipers and a thickness gauge at least four regions along the specimen length to ensure dimensional conformance of each sample. During the tensile tests of all five specimens, the stroke speed was set as 1 mm/min, the grip length was approximately 35 mm, and strain values were measured in 0.5 s time intervals between two measuring points using a single axis extensometer, which possessed a 30 mm gauge length.

3.4.5.3 Optical microscopy

Cross-sections of molded samples were experimentally observed using an optical microscopy (VHX-1000, Keyence Corporation). The micrograph of case D was taken from the plane of symmetry along the flow front path (the middle of the molded sample along the length direction) marked as the red dotted line in Fig. 3.14. Open mold samples were cut along the flow direction close to the longer mold wall to minimize the negative influence of natural convection on thermal stability from the open areas. Cross-sections of the samples were located approximately 5 mm from the mold wall, which contacted with the initial charge position because there was no plane of symmetry along the flow front path in the open mold cases unlike the case D with the uni-directional flow. The samples were polished using sequential processes by rubbing sandpapers in 400, 600, 800, and 2000 grit on the cut surfaces using a rotating disk. And then there was following additional polishing by 3.0 μm , 1.0 μm , and 0.25 μm polycrystalline diamond suspensions to attain a finer finish on the surfaces.

3.5 Results and discussion

Fig. 3.15(a), (b) and Fig. 16 represent images from a video of the progression of the flow fronts over time from the open end for test cases A, B and C in the filling phase (phase 2), where the numbers in parentheses means the measured relative position of the lower mold; if the lower and upper mold completely contact, the relative position would be zero because calibration was conducted before starting the test cycle 'initialization'. The hot press was a force controlled instrument, and the assigned load setting determined the rate at which the molds moved together. The images captured from the video recorder were not enlarged in height since the height corresponded to the compressive deformation rate. The samples filled under cases A, B and C showed different flow progression, mold filling time and final flow positions, described as the mold filling ratio. The entire mold was nearly filled in both cases; only a small unfilled area was observed for case B and C, whereas case A had a larger unfilled area. Stabilization of the final position of the flow front occurred at 16 min 45 sec for case A and at 2 min 17 sec in case B. The mold filling time was the shortest in Case C; 35 sec. Higher closing force decreased mold filling time after the equivalent heating phase (phase 1) in the given experimental set-ups. It is obvious that the high level of closing force with equivalent fiber content caused to rapid mold filling when observing video-graphed results.

As shown in Fig. 3.15, the corner of lower mold was shown up as a black line, and reflection of melted charge hindered the accurate evaluation of mold filling time because video recording was performed three dimensional viewpoint. In order to overcome the phenomenon, the PTFE film was adhered to prevent the reflection for case C. Fig. 3.16 shows images from video footage as at various

time intervals. The blue square area represents shorter mold wall (125 mm) from the viewpoint, and red line marks flow front during the phase 2, filling phase. The heart of the compression molding process is mold filling.¹ By using several setting experimental skills, such as minimizing the reflection and marking the edges of pre-consolidated charge, it was possible to validate more accurate evaluation of the mold filling in case of C compared to the case A and B. The mold filling is quite rapid, shorter than 1 min, facilitates rapid manufacturing cycles in forming applications of the material.

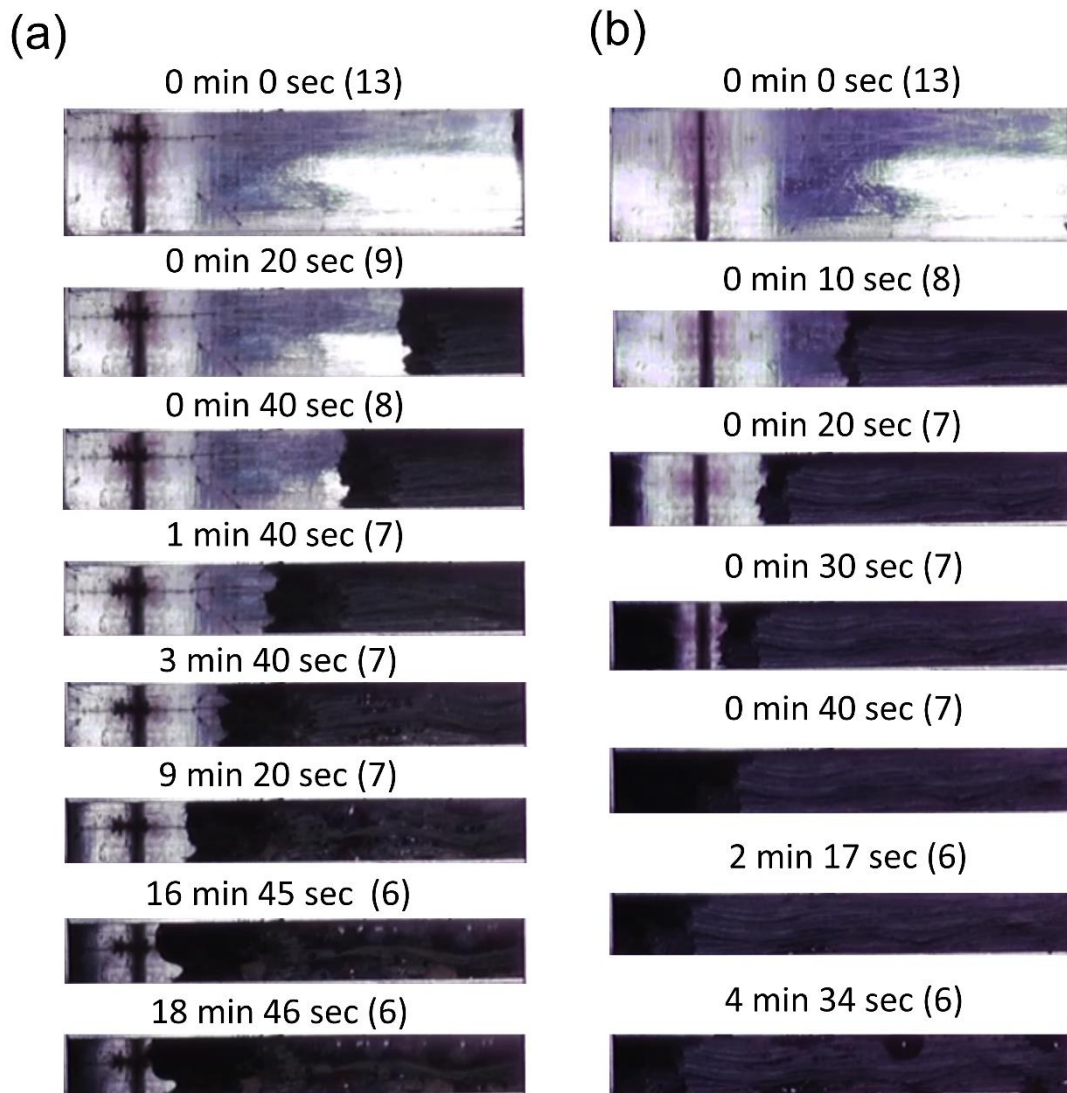


Figure 3.15. Images taken from the video footage showing the progression of the flow fronts through the open mold over time in phase 2: (a) case A and (b) case B.

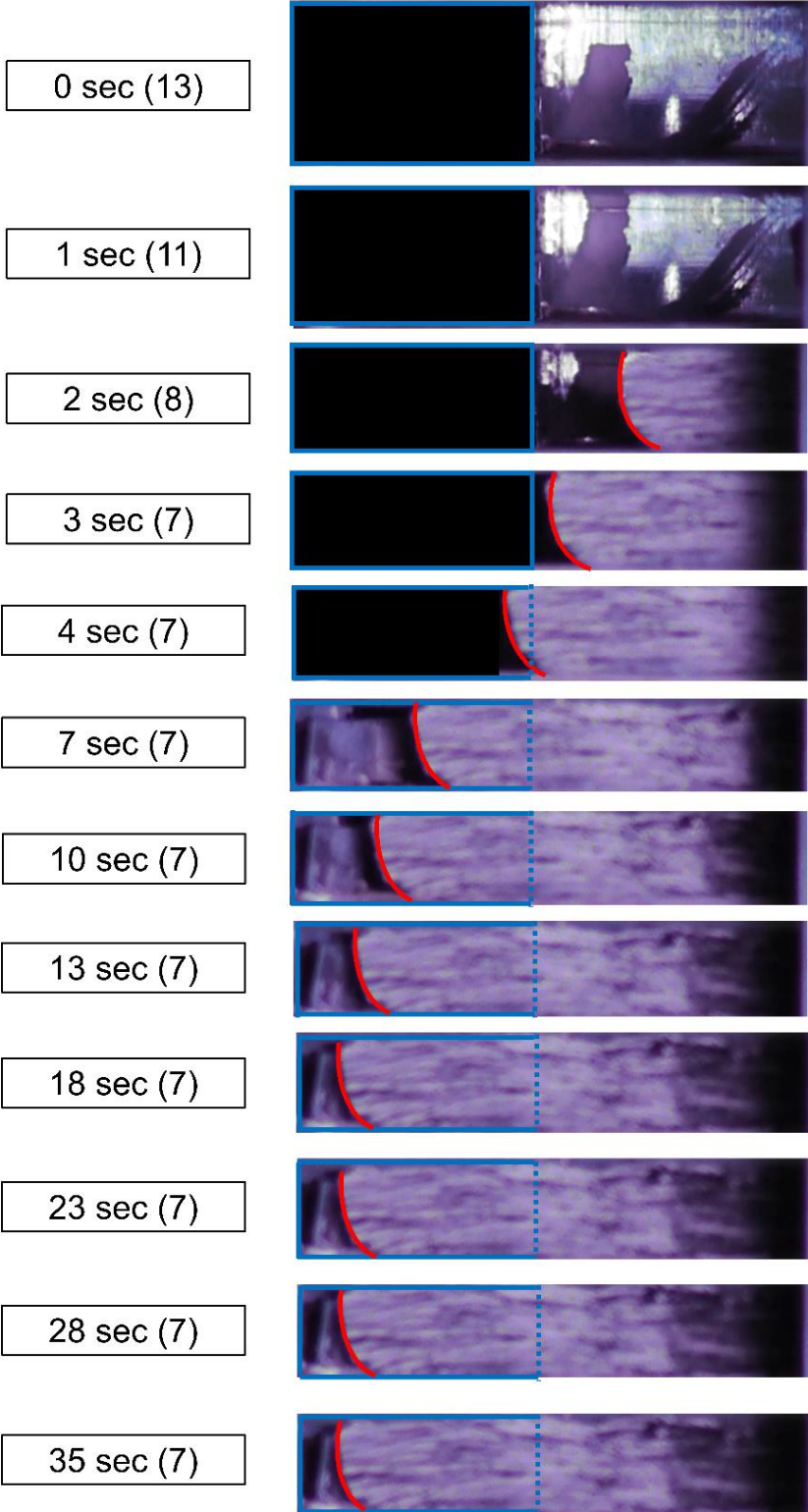
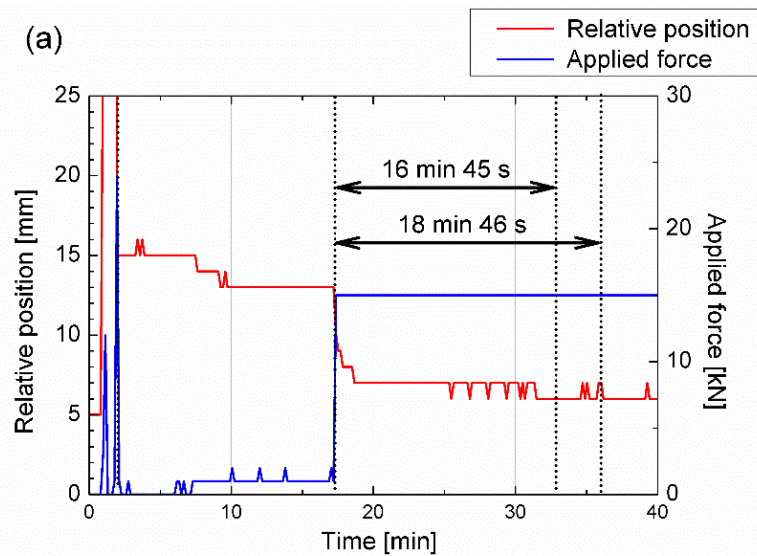


Figure 3. 16. Images taken from the video footage showing the progression of the flow fronts through the open mold over time in phase 2 for case C.

Fig. 3.17(a), (b) and (c) show the recorded applied force and corresponding relative position for three types of open mold cases. The relative position means the gap between the upper mold and lower mold set from the initialization process. Hence, the value delivers information of sample height in the case of A and B between two molds and is plotted as the red line in the Fig. 3.17(a) and (b). The arrows with two directions represent the evaluated mold filling time in three open mold cases. In the case of A and B, there are two ways of evaluating mold filling time. The shorter one is evaluated by stabilization time of relative position (16 min 45 sec in case A and 2 min 17 min in case B). Another way is to analyze the video footage and observing the flow movement. It is possible to approximate the video records and resulting mold filling time is 18 min 46 sec in case A and 4 min 34 sec in case B as shown in Fig. 3.17(a) and (b). Although the latter implied constraints of recording, the overall tendency of each condition clearly shows high applied force induces rapid mold filling. In the case of C, the result is more interesting in terms of filling speed. The phase 1 is not included in the Fig. 17(c) because there was no contacting force in phase 1 for heating, and the relative position does not mean the height of charge in the phase unlike the case A and B. Hence, the mold filling time is evaluated by the movement of visible surface marked with a white ink when preparing the initial charge. Regarding the thermal expansion from the initial state, consolidated sample, to be expanded by heating to achieve isothermal condition. By applying the sufficient heating for isothermal condition and pre-consolidated sample as a charge for eliminating free spaces of preform sheets, it was possible to achieve rapid filling (35 sec) in the given open mold configuration.



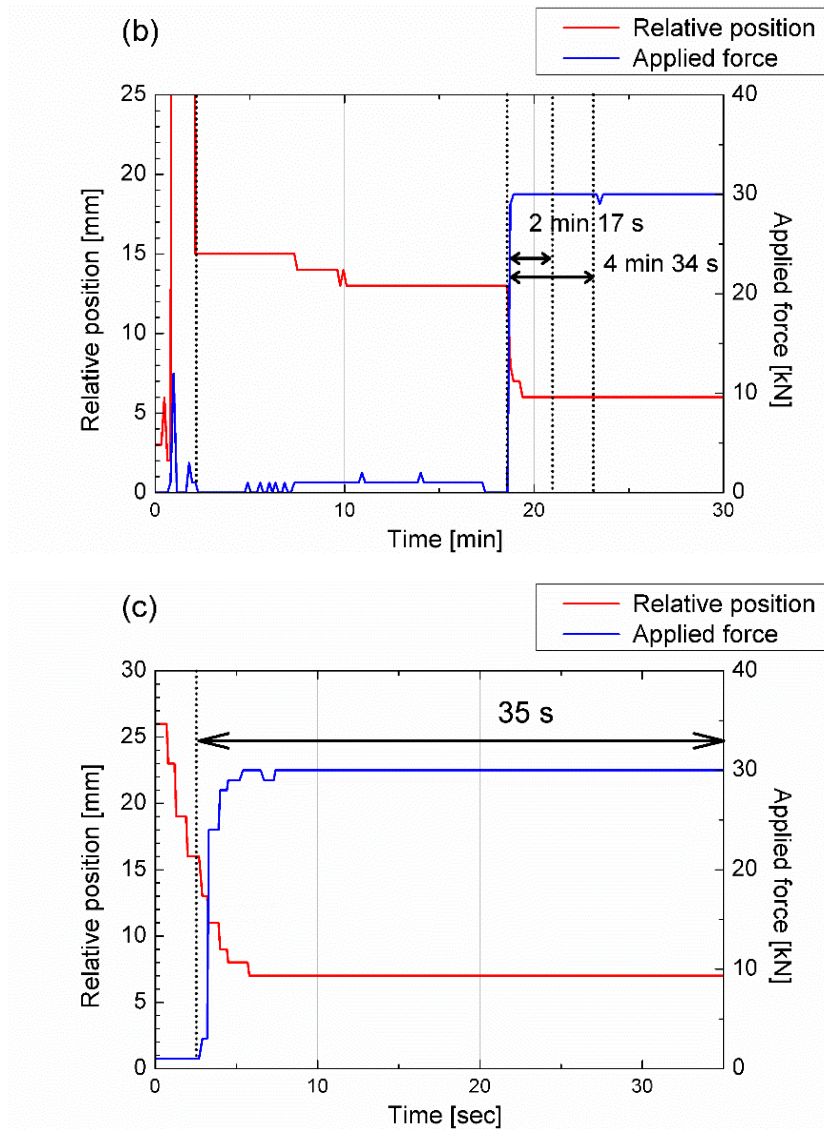


Figure 3.17. Applied force and corresponding relative position in open mold cases: (a) case A, (b) case B and (c) case C.

Fig. 3.18(a), (b) and (c) represent filled area from the charge placement in open mold cases of charges in the given mold cavity. The red line shows the initial charge dimension (90 mm \times 170 mm in case A and B, 99 mm \times 170 mm in case C) and the blue line illustrates mold dimension (upper and lower) with a rectangular shape of 125 mm wide 250 mm long from the top view except for two open areas. Two yellow areas represent open areas for observing the flow front and symmetric behaviors when squeeze flow occurred. There might be heat loss from the open areas with 40 mm long, but it was treated as negligible effects on the global behaviors of squeeze flows. All tests were carefully taken the case of flowing out of materials during molding cycles by adjusting the initial charge placement and the volume of charge. Fig. 3.18(a) shows largest unfilled areas in the given

squeeze flow condition and is hard to be considered as full filling. Meanwhile, Fig. 3.18(b) and (c) (30 kN of applied force) allowed to fill the mold cavity despite the open areas.

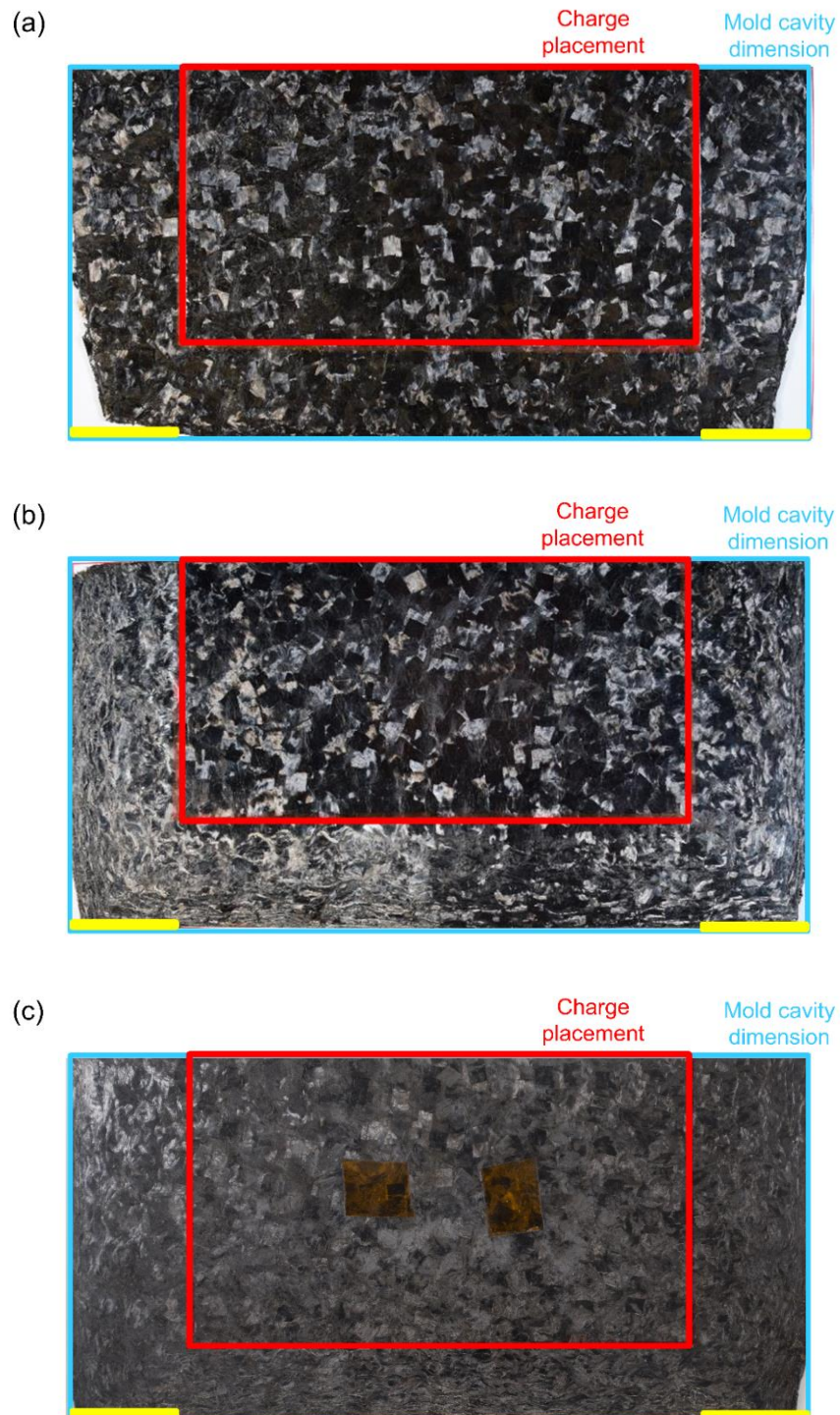


Figure 3. 18. Mold filling by squeeze flow tests using CTT: (a) case A, (b) case B and (c) case C.

Complete filling of the mold cavity was obtained using case D conditions. It is impossible to evaluate the mold filling time for case D due to the closed mold system and the absence of observable areas using a video recorder, which existed in open mold cases. Hence, it was unclear that when the initial flow occurred during phase 1 and phase 2 in the case D. However, this point can be discussed considering the data shown in Table 3. Assuming the number of preform plies and melted polymer lubrication are less influential than the effective pressure in exceeding the yield stress for flow, sufficient pressure for flow was applied to the preforms during phase 1 of case D. The entire duration of phase 1 and 2 of case D was 38 min at constant temperature: 15 min at 1.5 MPa in phase 1, 10 min at 5 MPa in phase 2, increasing force interval between phase 1 and 2 for 13 min. After the initiation of flow of phase 1, there was a post-consolidation in the rest of time for filling the mold cavity. It is not proper to describe the phase 1 as filling phase because the phase 1 may imply mold filling and immediate consolidation after the filling. The consolidation process was required to eliminate free spaces existed in the preforms, consolidate the fiber network, and facilitate resin percolation to achieve final molded samples with better homogeneity.³⁵ In contrast, for cases A and B, shorter consolidation time and lower effective pressures were used compared to those for case D, as shown in Table 3.3, the Effective pressure of 65.4 kPa did not induce the flow for cases A and B.

Table 3 - 3. Summary of applied effective pressure in squeeze flow tests.

Case	Preform plies	Applied force (kN)	Initial contact area (cm ²)	Effective pressure (kPa)	Final contact area (cm ²)	Effective pressure (kPa)	Flow
	54	1	153	65.4			Infeasible
A	54	15	153	980	313	480	Feasible
B	54	30	153	1961	313	960	Feasible
D	18	31	213	1460	313	992	
		156			313	4990	

Preforms sheets basically contain free spaces if there is no consolidation process. Also, the void content in the early stage, initial compression in phase 2, is considered as high because of lofting of the preforms,³⁶ related to the relaxation of the compressive stress occurred in the fiber network during impregnation and preform preparation. In addition, the applied load in phase 1 was low to completely eliminate internal free spaces of in the preforms and between adjacent plies. Although 0.98 MPa of effective pressure in case A and 1.96 MPa in case B initiated compressive flow, the porosity could not be sufficiently removed during the flow phase. The absence of pressure during cooling phase can originate the void formation, in particular at the surface of the molded part.²⁷ The conditions used in

case D are thought as appropriate for minimizing void formation. Internal geometry is consisting the composite system is also influenced by a flow field and resulting out-of-plane and in-plane shear during the bulk flow. Although the change might cause a variation in the internal fiber network and alignment by the formation of flow field compared to cases A and B, a fraction of each composition does not show a large variation in terms of the standard deviation. It can be concluded that the homogeneity of the formed samples is reproducible.

Table 3 - 4. Summary of fiber, resin, void content and the final strain.

Case	Mold type	Assumption	Fiber volume fraction* (%)	Resin volume fraction* (%)	Void content* (%)	Final strain ϵ_f
A	Open	Voids	49.52 (0.17)	42.81 (0.42)	7.68 (0.36)	≈ 0.51
B	Open	Voids	49.66 (0.10)	42.55 (0.15)	7.78 (0.14)	≈ 0.51
D	Closed	Voids	50.78 (0.79)	48.85 (0.88)	0.37 (0.38)	≈ 0.32
		No voids	53.18 (1.56)	46.82 (1.56)	-	

*Mean values (one standard deviation).

By employing a model of the consolidation of fiber systems,³⁵ the final strain can be defined to quantify the compaction degree by comparing between the initial and final charge dimensions according to the following relationship:

$$\epsilon_f = 1 - h_f/h_i \quad \text{Eq. 3-3}$$

Here, ϵ_f is the final strain, and h_f and h_i are the final and initial heights of sample, respectively. The void contents of case A and B shown in Table 3-4 are much higher than that of case D. The final strain of case D was lower than the other samples, indicating that the degree of compaction was lower in the closed than open mold cases. Nevertheless, the final void fraction for case D was 0.37% even in the flow end sections. These results indicate that phase separation was not significant. Fig. 3.19 shows representative micrographs of internal void formation for the three cases along the flow direction. The observation was carried out at the boundary of the initial charge and filled areas for all samples. The microscale porosity are observable for cases A and B, whereas there are no visible voids in case D at this resolution. These observation supports the void formation analysis by the burning off technique.

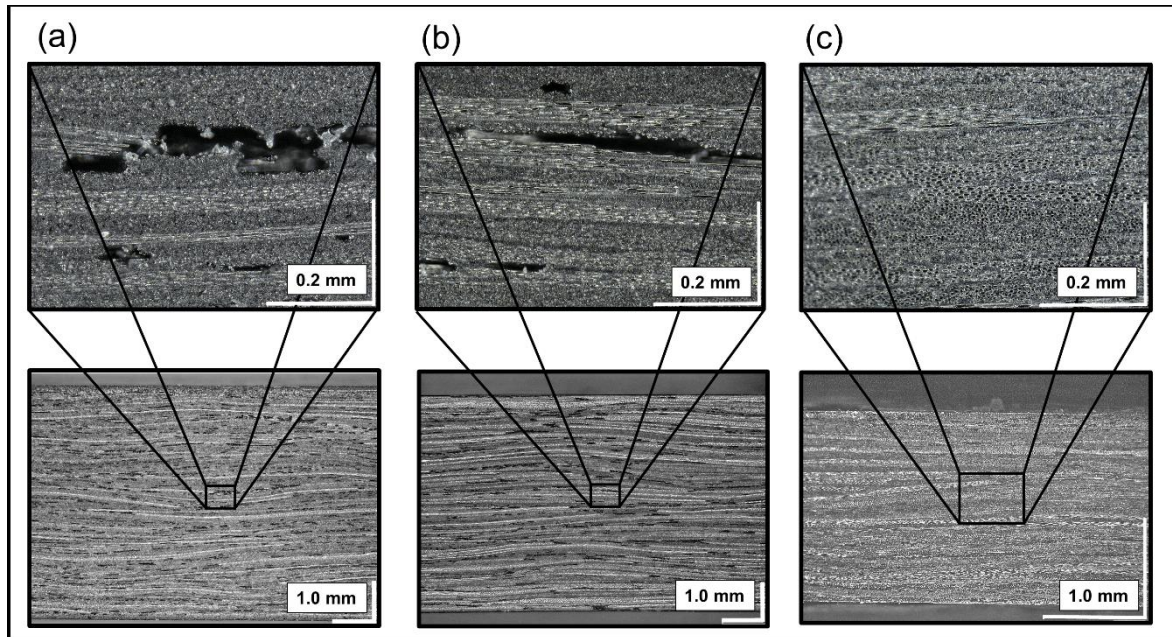


Figure 3. 19. Representative cross-sectional micrographs of CTT samples (the plane of symmetry along the flow front) formed under different conditions showing void formation: (a) case A, (b) case B and (c) case D.

Table 3-5 represents the mechanical performance in the tensile mode of specimens with a high volume fraction ($>50\%$) that experienced flow and flat panel specimens manufactured without flow. The two ends (corresponding to the middle and filling end) of specimens were gripped to conduct tensile tests. Case D exhibits high tensile strength, which is comparable to flat panel specimens with international standard. Meanwhile, shows a lower tensile modulus, to those of the panel specimens. The void content was below 1% for each sample prepared under case D conditions; consistent with former results, the longitudinal tensile properties of CFRP are not significantly affected by void content.³⁷ Thus, a possible reason for the lower modulus of the case C samples can be thought as a change in the internal microstructure. There was a large compaction with a final strain of 0.32 (compared to 0 for samples without flow) for case D. This compaction caused the instant flow field and resulting out-of-plane and in-plane shear to change the initial in-plane orientation of the preform sheets. Therefore, in the filling phase, if the initial state of fiber alignment had been designed to have in-plane orientation, the global flow would have increased fiber misalignment in any direction. In addition, the fibers were not easily aligned in the flow direction due to the high fiber content and level of networking of the fibers. Such a microstructure might affect the deterioration of the tensile modulus. The major fracture mechanism for the shorter strand size (6 mm long and 5 mm wide) was the pulling out of strands in the previous literature.¹⁸ After undergoing out-of-plane and in-plane shear, it was difficult to interpret the result from mechanical tests in a way used in the literature

because the initial geometry of the strand was deformed due to the global flow. The localized inhomogeneous, for example, regions that are resin rich or contain voids, can initiate failure during the tests. Such localized inhomogeneity can be minimized by consolidation process, and thus it was possible to achieve 96% of the tensile strength of flat panel samples in case D. Although fully characterizing the mechanism of fracture and fiber orientation would be valuable, it has not been accomplished in this study. Nevertheless, for cases using compression molding to form larger dimension samples than the initial charges used here, the effect on the mechanical performance needs to be considered when aiming good quality of final molded parts.

Table 3 - 5. Mechanical properties of squeeze flow and typical flat panel samples.

	Forming type	Specimen			Tensile modulus*	Tensile strength*
		Length	Width	Thickness		
		(mm)	(mm)	(mm)	(GPa)	(MPa)
Case D	Squeeze flow	124	25	1.97	30.6 (2.1)	375 (19)
	Closed mold					
Reference	No flow	180	30	2.05	39.3 (0.6)	391 (22)
[18]	Closed mold					

*Mean values (one standard deviation).

3.6 Concluding remarks

In this chapter, the forming characteristics of CTT materials were experimentally studied. First of all, the relationship between processing conditions and flow behaviors was studied by several case studies adopting squeeze flow tests, and influential factors were discussed. In order to achieve the purpose, we used a video camera to observe the progression of the flow front using a unique mold configuration. The observation was achievable by considering proper charge dimensions, confirmation of thermal stabilization and void reduction. Possible defects, in particular, internal void, need to be considered when designing an automated and continuous process, which is the final goal when applying such materials in mass production. A possible solution for avoiding the defects is the use of hot roller compaction to achieve a fully consolidated part prior to the forming process. Thermoplastic consolidation models have been introduced in the previous study for a compressible fluid.³⁵ In addition, the cooling phase conditions, as well as preheating condition, should be designed concerning the void formation mechanism.

A realistic and cost effective process is obtainable using an optimal combination of heating, consolidation, and forming stages. Also, if the mold filling observation was linked to apply numerical simulations in process modeling based on rheological data, the pre-consolidation process should be applied to satisfy fundamental assumptions of the approach; negligible void content and thus two phases of fibers and melted polymers. Considering the void formation and overestimation of the final height of the sample in experiments, an alternative method (pre-consolidated samples) was applied to establish a valid setting for the squeeze flow test. Lastly, several considerations related to forming applications were investigated: void formation, mechanical performance of molded parts. The sample formed by unidirectional squeeze flow had a comparable mechanical performance, exhibiting a slightly lower (95.9%) tensile strength of samples prepared without flow. It is expected that this study will contribute to the development of process modeling for CTT manufacturing and allow more efficient use of materials, as well as suggest optimal processing conditions for commercial applications. In addition, the importance of rheological characterization and thermo-mechanical properties is emphasized to construct the constitutive relationship to predict and understand the compression molding process.

Chapter 4

Characterization of Rheological Properties

4.1 Introduction

Compression molding is a widely used process for manufacturing components of large panels and other parts with complex geometries in various industrial applications. In cases when the dimension of mold charge does not exactly fit the mold cavity, the properties and mechanical performance of the final molded parts are dominantly determined by the fiber orientation and flow behavior, which depend on the mold filling.¹⁰ Therefore, studies in CFRP manufacturing have concerned on characterizing and predicting the mold filling behaviors, However, clarifying the flow mechanism and modeling the mold filling process is difficult because establishing an appropriate constitutive equation is inhibited by the presence of carbon fiber fillers in the system. Several decades ago, Barone and Caulk (1985, 1986) studied the flow behavior of SMC.^{18,38} Among diverse studies on the rheological properties of fibrous reinforced thermoplastics, most of the studies of flow behaviors have primarily focused on PEEK, PP as the polymer matrix. The macroscopic squeeze flow behavior of aligned fibers was investigated by researchers applying possible fluid models,³⁹ and in recent years, the prediction model of squeeze flow behavior using a 2D finite element method attained considerable attention.²² Törnqvist *et al.* studied the rheological properties of fiber reinforced thermoplastic composites by adopting the Carreau model based approach in order to illustrate the flow property of molten PP behaviors.⁴⁰ In addition, Thomasset *et al.* used experimental methods and theoretical models of fiber-filled polymers to validate the rheological properties of PP filled with long glass fibers.⁴¹

In consideration of these previous studies, the objective of the study presented here is to reveal the flow mechanism of a thermoplastic polymer matrix consisting of PA6 and carbon fiber. Because of CTT's high fraction of carbon fibers ($\approx 55\%$) and structural consistency, identifying the relevant flow mechanism is limited when using conventional measurement approaches in rheological characterization. Also, because of the volume fraction and packing geometry of carbon fibers in the

composite system, it may exhibit high yield stress compared to the melted polymers. Therefore, the Cox-Merz rule cannot be applied to describe the rheological behavior when using a rotational rheometer to measure the behavior.⁴² However, Servais *et al.* proposed a model for planar random fiber filled suspensions, which represent elastic deformation below yield stress and viscous behavior after yield point, to describe the unique behavior of such materials in both fiber and fiber bundle suspensions.⁴³⁻⁴⁵ Based on these studies, the goal of this section is to systematically study the relationship between CTT's internal structure and its rheological characteristics. Moreover, in order to validate the proposed micro-mechanical model, based on the rheological measurements of the molten polymer matrix and essential assumptions in terms of the system's internal packing geometry, is evaluated. The work presented here conveys valuable insight that can improve processing efficiency and expand the range of forming applications in which CTT can be applied.

4.2 Theory

This section represents the proposed methodology, which applies the theory of sheet forming by compression molding because the CTT manufacturing generally involves the stacking of pre-formed sheets, and is therefore highly affected by the characteristics of sheet forming. At least four anisotropic viscosities are required to construct the constitutive interrelation between stress and deformation rate, even if highly concentrated suspensions is assumed to be a transverse isotropic and incompressible properties.¹⁶ Among these constants, assessing the out-of-plane shear viscosity of suspensions is an essential one to analyzing the sheet-forming process because the material constants are connected to the deformation mode. In particular, the axial extension in the fiber direction, in CTT's multi-axial in-plane, is restricted by dense networking structure of fibers. Also, assuming a narrow gap and no slip, the dominant deformation mode can be simplified as shear deformation mode using approximated solutions of the governing equations: the equations of motion and mass conservation.^{12,16} In addition to theoretical approximation, shear flow is easily measured in a laboratory environment, and thus it is the most frequently used mode for characterizing flow behavior during compression molding. Consequently, the deformation mode that is measured here is out-of-plane shear for suspensions.

4.2.1 Polymer melt rheology

Rheological studies of polymer melts have been introduced in a lot of various investigations in the polymer processing field. The generalized Newtonian fluid (GNF) models were frequently used to account for the non-Newtonian behaviors of the molten polymer, for example, shear thinning behavior. In particular, the models are valid to describe precisely the shear rate dependency of the

molten polymer. The linear viscoelastic (LVE) models represent the dynamic rheological response of molten polymers below the particular strain of the linear viscoelastic response. Achievable results strongly depend on macro-molecular structure of polymers. The nonlinear viscoelastic (VE) models enable to describe most of the flows, such as steady, dynamic shear and extensional flows. The models facilitate to construct constitutive equations accurately and thus predict most of the rheological phenomena.⁶ However, numerical complexity of LVE and VE models let many researchers utilize GNF models as the primary approach.

In order to build the viscosity model for fiber suspensions based on micro-mechanics at interaction points, first of all, it is required to describe the viscosity of polymer constituents. Especially, the viscosity dependence on the shear rate is the primary focus in general. Three possible GNF models have been selected to represent the rheological behaviors (shear viscosity models) of polymer melts in the present study: the Carreau three-parameter model, Eq. 4-1; the Cross three-parameter model,⁶ Eq. 4-2; and the Carreau-Yasuda five-parameter model, Eq. 4-3.⁴⁶

$$\eta(\dot{\gamma}) = \eta_0 [1 + (\lambda \dot{\gamma})^2]^{(n-1)/2} \quad \text{Eq. 4-1}$$

$$\eta(\dot{\gamma}) = \eta_0 / \left[1 + \left(\frac{\eta_0}{\tau^*} \dot{\gamma} \right)^{n-1} \right] \quad \text{Eq. 4-2}$$

$$\eta(\dot{\gamma}) = \eta_\infty + (\eta_0 - \eta_\infty) [1 + (\lambda \dot{\gamma})^a]^{(n-1)/a} \quad \text{Eq. 4-3}$$

A typical viscosity plot for the shear thinning polymer melt has three distinctive regions: zero shear viscosity region (1st Newtonian plateau region), shear thinning region and transition region lying between the Newtonian plateau and shear thinning regions. The zero shear viscosity η_0 denotes viscosity in the plateau region at low shear rates. If the material exhibits 2nd Newtonian plateau, η_∞ is the infinite shear rate viscosity at high shear rates. λ is a parameter with units of relaxation time, which is related to horizontal position of the transition region. n is a dimensionless Power Law index that defines the slope in the shear thinning region. τ^* is the critical stress point at which the viscosity of the polymer melt η transitions from the Newtonian plateau region in the Cross model. a is the adjustable Yasuda constant in Carreau-Yasuda five-parameter model, which determines the shape in the range of transition region. $\dot{\gamma}$ is the shear rate representing the x axis when drawing shear viscosity of materials.

The parameters involved in the GNF models are achievable by applying Cox-Merx rule when using oscillatory rheometer in LVE region regarding the strain range. These parameters involved in the

GNF model can be experimentally determined by using a fundamental oscillatory rheometer and applying the Cox-Merz rule.³⁴ Many studies on the suspension rheology of a wide range of materials, the Carreau model is widely accepted GNF model that accounts for the low shear rate Newtonian region, nearly horizontal tendency in the region, as well as the shear thinning behavior. The Cross model is considered as a suitable model for describing semi-crystalline polymers. The Carreau-Yasuda model is one of the flexible models due to the existence of five parameters, which can be adjustable. However, the Carreau-Yasuda model is only used to describe the rheological properties of neat polymer melts because the model implies mathematical complexities. Lastly, the temperature dependent rheological properties have not been considered for simplicity and conveying one clear message of this study. Therefore, all the experiments were carried out in isothermal condition after the sufficient thermal equilibrium at a constant temperature.

4.2.2 Suspension rheology: micro-mechanical model for highly filled fiber suspensions

As referred in the previous section, one research proposed a theoretical model for planar, randomly oriented concentrated carbon fiber suspensions using the Rutgers-Delaware relationship. This relationship is the essential link to develop suspension rheology of such materials, which can have particular yield stress. The relationship implies the superimposition of a steady-state viscosity η as a function of shear rate $\dot{\gamma}$, and a complex viscosity $|\eta^*|$ as a function of an effective shear rate (defined as the product of strain amplitude γ_m and angular frequency ω):³⁴

$$|\eta^*(\gamma_m \omega)| = \eta(\dot{\gamma}) \quad \text{Eq. 4-4}$$

It is possible to apply this interrelation to materials that represent linear viscoelastic (LVE) behavior below the yield stress, and viscous behavior above the yield stress.³⁵ [35] Concerning studies on the micromechanical models of fiber suspension rheology,³⁰⁻³² the models were established for the complex viscosity of suspensions including parameters based on the packing geometry of mat structure fibers and the rheological behavior of polymer melt constituents (PP) of suspensions under both steady-state and oscillatory shear deformation. Hence, the proposed methodology can be established based on the following fundamental assumptions:

1. Fibers are in-plane randomly oriented and transversely packed.
2. All interactions are associated with the points of contact between fibers.
3. The surface forces, which are generated at the contact points, contribute significantly to the bulk stress.
4. Hydrodynamic lubrication and Coulombic friction are the dominant mechanisms of fiber-fiber interaction.
5. Fibers are regarded as straight cylinders with slender geometry, having uniform length l

over the diameter $d \gg 1$.

6. There is no rotation of fibers around the in-plane axis, the axis perpendicular to the plane of orientation, or even their own axes.
7. Fibers are considered to be well dispersed, and thus suspensions are statistically homogeneous with a planar orientation distribution.

The bulk stress σ can be considered as the sum of two stress components in consideration of rheology of particle filled suspensions: $\sigma = \sigma^{(p)} + \sigma^{(l)}$, where the stress arising from presence of particles is $\sigma^{(p)}$, the stress related to liquid constituent is $\sigma^{(l)}$. The liquid stress is not regarded in this study because the liquid stress contribution to the bulk stress is negligible in the case of high concentration of fiber fraction.³⁰ This approximation of stress components is considered acceptable. Therefore, the arising from the presence of particle is dominant stress in the case of high concentration of fiber fraction. In addition, the scope of mechanics is constrained to contact points of fibers and the, suspension stress can be regarded as the sums of representative set of fibers occupying volume V with normal force f_n , tangential friction force f_f and hydrodynamic lubrication force f_h arising at the contact points. X denotes the location of a contact point.

$$\sigma \approx \sigma^{(p)} = \frac{1}{V} \sum_{\text{fibers}} \sum_{\text{contact points}} (f_n + f_f + f_h) X \quad \text{Eq. 4-5}$$

Fig. 4.1(a) and (b) show the morphology observation of CTT by X-ray computed tomography. CTT is sufficiently characterized by a high volume fraction of prepregs and well-defined manufacturing process. Orientation distribution is highly planar (in the plane of preform sheet), and out-of-plane orientation is quite limited compared to the in-plane orientation.

As studied in Chapter 3 regarding the fiber volume fraction and observation of the internal geometry of CTT systems, there existed many contact points between fibers. The particle stress, cylindrical fibers in the case of CTT, derives from forces acting on the fiber surfaces. Two relevant surface forces at the fibers' contact point lead the primary contribution to the bulk stress, as shown in Fig. 4.2. Because of the structural stability of CTT, regarding the consistent quality of molded parts and the less amount of out-of-plane misalignment, it is possible to embrace the written assumptions. The fifth assumption is acceptable as well because the fibers are precisely prepared by preform preparation and the molding process. The significant point of the fifth assumption is that CTT sample manufacturing does not involve the processes such as extruders, injection molding and compression molding with excessive normal force on the orientation plane; therefore, there would be negligible fiber breakage during the manufacturing. The schematic illustration of the contact between two fibers and their interaction mechanism is shown in Fig. 4.2, and specific explanation of the material fabrication procedures is described in the materials section.

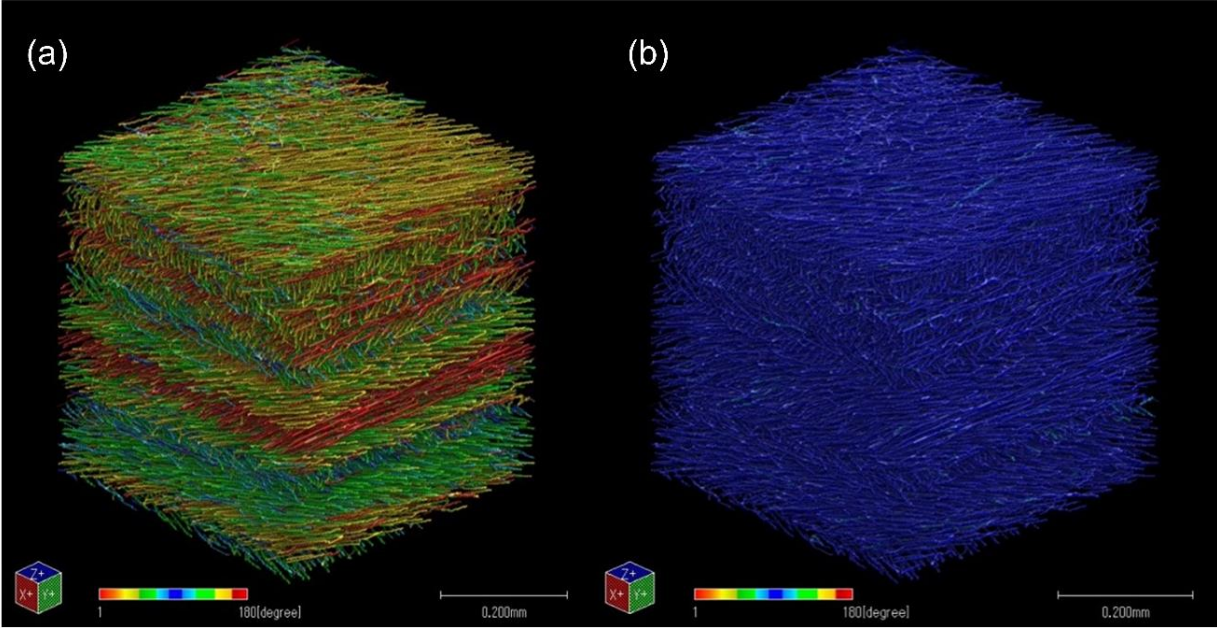


Figure 4. 1. Fiber distribution in CTT observed by X-ray computed tomography: (a) in-plane orientation and (b) out-of-plane orientation (adapted from [49]).

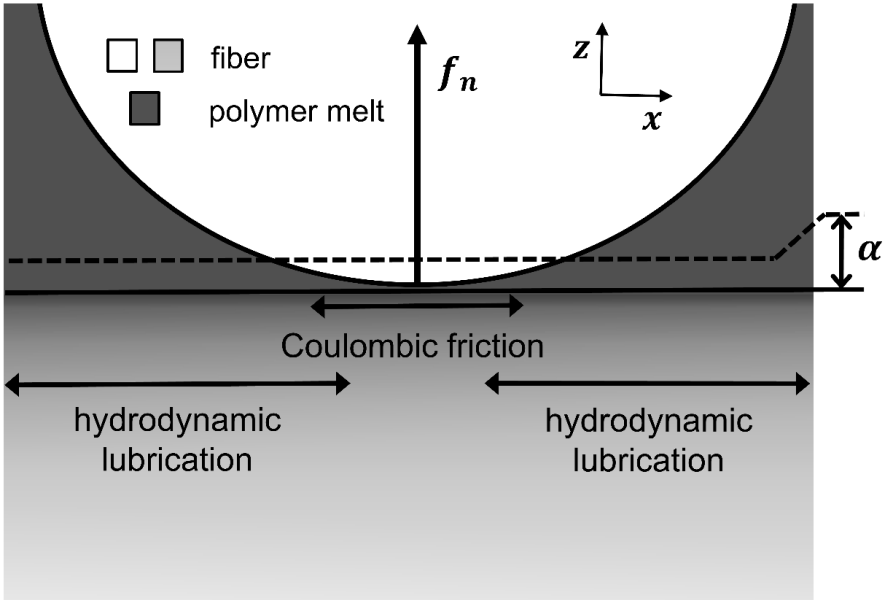


Figure 4. 2. Schematic representation of relevant surfaces forces at contact points (Adapted from [43]).

4.2.3 Model development

The scope of this study focuses on oscillatory shear measurements and the relevant analysis by applying the Rutgers-Delaware relation. The steady-state shear measurement of highly filled suspensions exhibits a higher possibility of fracture than the oscillatory shear measurement. The crack propagation associated with this possibility influences the overall measurements and possibly leads non-homogeneous flow. Furthermore, steady-state shear testing can induce variation in the initial fiber orientation (prepared for planar random), resulting in distorted experimental results. On the other hand, oscillatory shear testing can partially minimize the possibility of fracture at low strain amplitudes. Consequently, steady state viscosity model for fiber suspension form is rearranged in the form of complex viscosity by applying the Rutgers-Delaware relationship from Eq. 4-6 to Eq. 4-7.⁴⁵

The packing stress P and the friction coefficient k_f within the friction force term in the model equation (Eq. 4-6) can be combined into yield stress because the yield stress can be presumed to be caused by the friction within the fiber network and consistency.⁴³ Within this framework, the micromechanical model of complex viscosity in carbon fiber suspensions under out-of-plane shear can be rewritten in the form of the Herschel-Bulkley fluid model by deriving the Carreau three-parameter model and the Cross three-parameter model as shown in Eq. 4-7 and 4-8, respectively:

$$\eta_{sp} = k_f P (\dot{\gamma})^{-1} + k_h \frac{16}{\pi^2 d \alpha} f \Phi^2 \eta_0 \left[1 + \left(\lambda \frac{d}{\alpha} \dot{\gamma} \right)^2 \right]^{n-1/2} \quad \text{Eq. 4-6}$$

$$|\eta_{sp}^*| = \tau_y (\gamma_m \omega)^{-1} + k_h \frac{16}{\pi^2 d \alpha} f \Phi^2 \eta_0 \left[1 + \left(\lambda \frac{d}{\alpha} \gamma_m \omega \right)^2 \right]^{n-1/2} \quad \text{Eq. 4-7}$$

$$|\eta_{sp}^*| = \tau_y (\gamma_m \omega)^{-1} + k_h \frac{16}{\pi^2 d \alpha} f \Phi^2 \eta_0 / \left[1 + \left(\frac{\eta_0 d}{\tau^* \alpha} \gamma_m \omega \right)^{n-1} \right] \quad \text{Eq. 4-8}$$

where τ_y represents the combined yield stress; k_h denotes the hydrodynamic lubrication coefficient, which corresponds to the average area around the contact points between two intersecting fibers; α is the shear gap, which corresponds to the average thickness of the thin polymer film around the contact points, which is characterized in the material section (Fig 4.3); f is the distribution function of the in-plane fiber orientation.⁵⁰ The value of f is $2/\pi$ for in-plane random orientation ideally, whereas 0 for perfect alignment; Φ is the fiber volume fraction of the suspension, which is measurable using the ‘burning off’ test as described in Chapter 3; and η_0 , λ , τ^* , and n are the rheological parameters of neat polymer matrix consisting the composite system. Three parameters are assessable using widely used rheometers, such as a capillary rheometer, a rotational rheometer and a viscometer. The rheological behavior of the matrix contributes to the entire suspension viscosity by defining the shear gap thickness α around fiber interactions points. The left

term and right term in both Eq. 4-7 and Eq. 4-8 separately express two competing elements: Coulombic friction and hydrodynamic lubrication, which together determine the entire complex viscosity. The comparable relationship between viscosity and shear rates has been found in the previous studies on rheological characterization of thermoplastic composites as well.⁴⁰

4.3 Experimental procedures

4.3.1 Materials

Fig. 4.3 describes the overall procedures for CTT flat panel (cuboid) samples manufacturing. Two types of unidirectional semi-impregnated sheets with an average thickness of 44 μm were provided by Industrial Technology Center of Fukui Prefecture for this research. The thin prepreg sheets are fabricated following the process is shown in Fig. 4.3. Commercial PA6 film products (Diamiron™ C, Mitsubishi Plastics, Inc.) and carbon fiber tows (TR 50S, Mitsubishi Rayon Co., Ltd., T700SC, Toray Industry, Inc.) are used in this process. Spreading tows and impregnation of film products are common techniques to fabricate the prepreg sheets. One type of materials with relatively high volume fraction (abbreviated CTT55, means volume fraction Φ of 55%) is fabricated by TR50S and 20 μm thick Diamiron™ C film. In comparison, another type of materials with relatively low volume fraction (abbreviated CTT44, means volume fraction Φ of 44%) is fabricated by T700SC and 25 μm Diamiron™ C film.

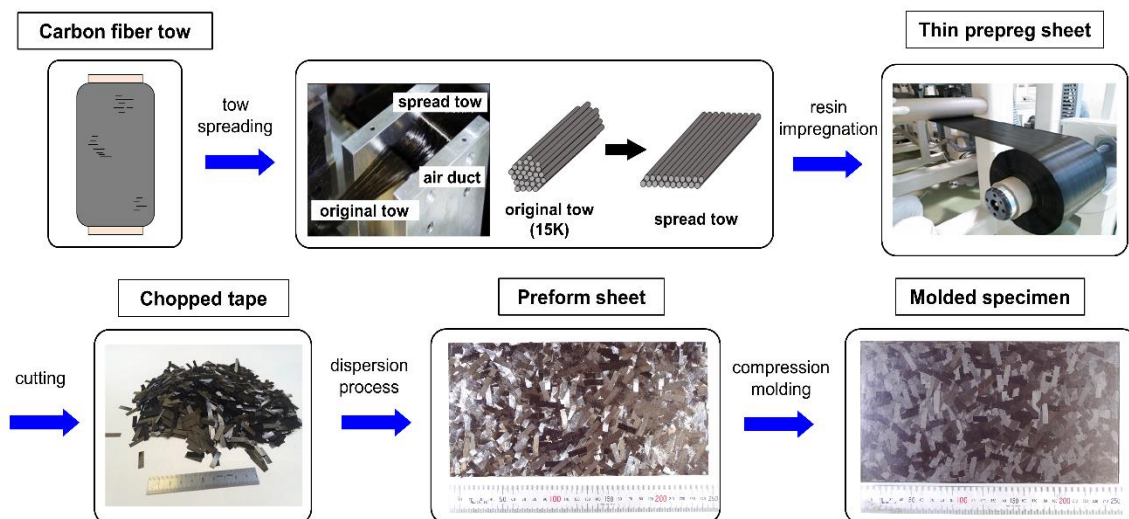


Figure 4. 3. Overview of production of flat panel samples using CTT.

Those two types of prepregs were designed to investigate influences of Φ on rheological behaviors presented in this study. The fiber volume fraction Φ of molded CTT55 sample was $\approx 55\%$, as stipulated in the previous research.¹⁷ Φ of molded CTT44 samples was measured by ‘burning off’ similar way described in Chapter 3. The density and weight of each sample were assessed employing a density meter (MDS-300, Alfa Mirage Co., Ltd.) and a digital scale with a precision of four decimal places. The weight and density of composite samples were measured by two devices. Subsequently, the weight of fibers W_f was determined by weighing the weight difference between a container and the sum of the container and fibers left in the container after finishing the decomposition process (burning off) in a nitrogen atmosphere for 2 h at a constant temperature of 500°C. In order to make sure the weight decrease was completed (complete decomposition of polymer matrix), the weight after 1 h and 2 h was compared and there was no additional change at two check points. Consequently, Φ of each sample could be calculated using Eq. 4-9, where W is weight, V represents volume, ρ is density, and the subscripts f , c , and indicate the fiber and composite respectively. W_c , ρ_c and W_f are measured values and $\rho_f = 1.14 \text{ g/cm}^3$ is known value provided by material supplier. The averaged value is 43.57% and one standard deviation is 0.29% when using five samples with 20.0 mm long, 20.0 mm wide and 1.96 mm thick (averaged five samples). Therefore, the material could be abbreviated CTT44 in this section.

$$V_f = \frac{(W_f/\rho_f)}{(W_c/\rho_c)} \text{ Eq. 4-9}$$

The preparation of preform sheets has been introduced in CTT fabrication. The aim of preparation is to improve the controllability of the molding process and to facilitate the planar random orientation of fibers. Such structural considerations aim at minimizing the out-of-plane misalignment of the carbon fibers because the out-of-plane misalignment may degrade the mechanical performance of molded specimens. In order to fabricate the preforms, prepregs are precisely cut (width 5 mm \times length 6 mm) using a digital cutting machine (Zund) with a maximum deviation of ± 0.02 mm and a customized cutter in each direction.

Preform fabrication involves the equivalent steps described in the material section in Chapter 2. To sum up the steps briefly: Planar random orientation of chopped tapes is achieved by stirring a certain amount (20-23g) of chopped strands (5 widths and 6 mm length) in a container filled with water. Water flows out through an exit at the bottom of the container, while a fine mesh filters the chopped tapes right above the exit. The frame of fine mesh width is a rectangular shape (25 \times 25 mm), and the absorbed water in the sheet is evaporated from the sheet at the boiling point of water for 3 min. The sheet is heated above the melting point (220°C) of the polymer matrix with compression for 1

min to create the forms of preform 'sheet'. Although the preform sheets are partially sheets with internal free spaces, full impregnation is achievable after the particular molding process. Preform sheets (120 mm wide and 245 mm long) were prepared to conform the dimension of mold cavity (125 mm wide and 250 mm) without wrinkles and voids.

In order to produce 2 mm thickness samples in both cases (CTT44 and CTT55), preform sheets were prepared in one compression molding cycle termed as the compression molding in Fig. 4.3. Basically, transverse squeeze flow, resin percolation, interply shear and intraply shear are known as significant experimental aspects.¹⁰ If one assume one preform ply has different interply shear and intraply shear viscosities (resistance to flow), unifying the number of preform sheets would make it possible to facilitate valid comparison. Therefore, 12 plies ($90.5 \text{ g} \pm 0.5 \text{ g}$) of the CTT44 preform and 12 plies ($95.5 \text{ g} \pm 0.5 \text{ g}$) of CTT55 were used to quantify each molding cycle and achieve the dimensional conformance of 2 mm thickness before the drying process in a vacuum oven. The preforms were dried using a vacuum dryer to avoid degradation of the polymer constituent for over 12 hours at 90°C .

For equivalent molding process, a Laboratory Press 30T (Pinette Emidecau Industries, the maximum force of 30 ton) was employed in the compression molding process. It is possible to precisely control and monitors the processing conditions (platen temperature, applied force, and relative platen positions). Each platen (upper and lower) consists nine heating areas with their proportional-integral (PI) controllers and cooling occur in each platen, and controlled by water and air solenoid valves. The temperature and force setpoints at upper and lower platens (different from customized mold, which is fitted with two platens) are recorded by a data acquisition system. In addition to the system, monitoring the internal mold temperature in real time was possible due to thermocouple probes embedded in the upper and lower molds. Such precise measuring systems facilitates an effective analysis of the processing conditions.

All molding cycles were accurately assigned by the user-defined recipe for processing steps. In the cycles, setpoints of upper and lower platen temperature are 265°C , which corresponds to $260^\circ\text{C} \pm 2^\circ\text{C}$ of upper and lower molds, directly detected from embedded thermocouple probes in the molds. The temperature setting constantly maintains except the cooling stage. After the insertion of prepared preform sheets at 265°C of platens, the molding cycle starts. A force begins with 31 kN, which corresponds to 1 MPa on the dimension of molded samples for 15 min and then the force is applied with a gradual increase up to 156 kN for 10 min, which corresponds to 5 MPa on the dimension. Then, the cooling step is also considered to have a same cooling rate ($20^\circ\text{C}/\text{min}$), and the cooled samples are ejected at 70°C ($T_g = 70^\circ\text{C}$ of the PA6 matrix). Identical cycle steps for both materials (CTT44, CTT55) were employed because it is clear that the process conditions influence the internal geometry of composite constituents as resulting properties of molded samples. The molded samples

(125 mm wide 250 mm long) are cut into 2 mm diameter for dimensional conformance with circular dimension accessory of rheometer used. Table 4-1 summarizes fundamental parameters, such as chopped tape dimension and the molding condition related to the fabrication of CTT samples.

Table 4 - 1. Fundamental parameters of two types of CTT samples.

Properties (Unit)	CTT 44	CTT 55
Prepreg sheet thickness (μm)	≈ 44	
Type of fiber	T700SC	TR 50S
Chopped tape length (mm)	6	
Chopped tape width (mm)	5	
Molding temperature ($^{\circ}\text{C}$)	$260 \pm 2^{\circ}\text{C}$	
Molding pressure (MPa)	5	
Molded specimen thickness (mm)	1.98 ± 0.3	1.96 ± 0.03

During measurements using rotational rheometer and the construction of shear viscosity model for CTT, the material is considered to be a highly concentrated fiber suspension. In regards to the shear viscosity model, it is necessary to determine the shear gap α . By considering a geometry of carbon fibers and polymer melt in micro-scale unit, it is assumed here that a quarter of the cylindrical fiber is embedded in a cubic unit volume without voids, as illustrated in Fig. 4.4. As a result, α is determined with respect to the \emptyset of the molded CTT samples. Therefore, the shear gap of lower volume fraction case (CTT44) is thicker than that of higher volume fraction case (CTT55).

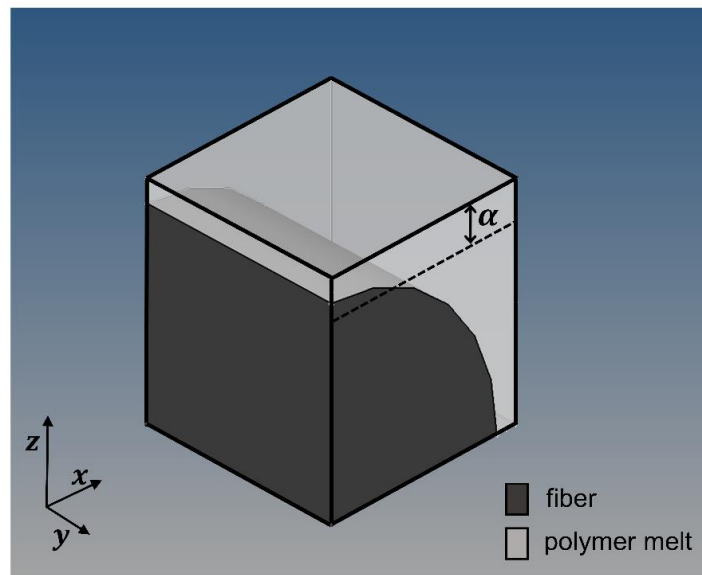


Figure 4. 4. Schematic representation of shearing gap in a cubic unit volume.

The geometric parameters for the construction of shear viscosity models are given in Table 4-2. Fiber length l corresponds to the length of chopped tape dimension because the uni-directional prepregs are chopped into the strands. The fundamental parameters relevant to all of these procedures are summarized in Table 4-2. It is expected that the fibers are uniformly dispersed, and thus the constituents have sufficient homogeneity throughout the molded samples.

Table 4 - 2. Summary of geometric parameters for modeling two types of CTT.

Properties (Unit)	CTT 44	CTT 55
Fiber volume fraction ϕ (-)	≈ 0.44	≈ 0.55
Fiber diameter d (μm)		7
Fiber length l (mm)		6
Shear gap α (μm)	2.62	1.88
Distribution function of in-plane orientation f (-)		$2/\pi$

Samples of PA6 were fabricated using identical materials with resin constituent (Diamiron™ C) of prepregs. A laboratory scale extruder (Hand Truder PM-1, TOYO SEIKI Co., Ltd.) and a customized mold cavity (15mm wide, 100 mm long and 2 mm thick) were employed to fabricate the samples. Before the fabrication, film products (50 μm thick, known as equivalent properties to thin films) were snipped into small pieces (25 \times 25 mm) because the material form is film type and had difficulties in inserting large films into the entrance of cylindrical container (diameter 12 mm). Then, there are two sequential steps: 230°C for 3 min for melting (melting temperature $T_m=220^\circ\text{C}$, PA6),⁶ the identical temperature for 5 min for eliminating voids. The fabricated samples were cut into the identical square dimension (15 \times 15 mm) for polymer rheology tests with a thickness of 2 mm. One of the significant concerns is to eliminate voids by employing adequate thermal condition. Another concern is to unify the heating condition as well as cooling condition, and thus all samples undergo an equivalent thermal history and crystallization degree. Thus, the injected polymer melt into the mold cavity is cooled down to 70°C using cooling circuits embedded in the mold.

4.3.2 Melt rheology measurement

A stress-controlled MCR 302 rotational rheometer (Anton Paar) with a parallel plate accessory was employed for oscillatory shear and stress ramp tests. The accessory is composed of two circular aluminum plates with diameters of 20 mm. Heated nitrogen (N_2) gas flowed into a convection chamber in order to induce a nitrogen blanket for the measurement. The temperature condition was

set at 250°C with a maximum deviation of 1°C for all of the measurements through convection. All tests including melt rheology, yield stress, and suspensions rheology were performed at 250°C, because the temperature is known as sufficient for forming applications in Chapter 2 and 3. If the temperature is different, analysis of results should be considered as a different case because of the strong temperature dependency of polymer melt on viscosity tendency. Despite the longer preheating time in cases of composite samples, 250°C of temperature was applied to all tests to have consistency and avoid conflicting experimental conditions when establishing suspension rheology models.

The melt rheology of the polymer matrix was measured using cut cuboid samples (15 × 15 mm, 2 mm thickness) that were cut from injection-molded parts for polymer rheology tests. For facilitating isothermal condition and melt rheology during measurements, initially, each specimen was placed on the lower plate. And then the gap between two plates was reduced until the upper plate nominally contacted the specimen. After heating for melting the sample and thermal equilibrium the specimen at 250°C for 5 min, above the melting temperature of PA6 (220°C), the gap was instantly reduced to 1 mm. In order to minimize measuring errors originated from dimensional deviation from the ideal assumption on specimen geometry (perfectly cylindrical geometry), the squeezed out part from the circular dimension was eliminated by a trimming tool. Because the total volume of initial cuboid sample (450 mm³) is much larger than the reduced cylindrical volume during measurement between two circular accessories (314 mm³), it is possible to measure rheological properties with negligible dimensional errors.

The entire tests were performed at a constant measuring gap of 1 mm, and rheological responses were recorded by the equipped data acquisition system. The angular frequency was set to range from 10⁻¹ to 100 rad/s in the oscillatory shear mode. The tests are also known as frequency sweep test because the tests cover a wide range of angular frequency. The angular frequency was set to range from 10⁻¹ to 100 rad/s in the oscillatory shear mode. Regarding the setpoint of strain amplitude (1% in this study), the linear-viscoelastic region (LVR) of the polymer melts was assumed to be below 1% of strain in oscillatory shear deformation, which is acceptable in most cases of polymer melts in general.⁴²

4.3.3 Yield stress measurement

Regarding rheology of complex fluids, such as networking polymers and suspensions, the yield stress τ_y is a property associated with the fluids where the material does not flow unless the applied stress exceeds a critical stress value. There are several methods for characterizing τ_y , for examples, a numerical model fitting, a stress growth tests and an oscillation amplitude sweep test. Among the methods, a stress ramp test is one of rapid and easiest methods for assessing this value, in which stress values are assigned following a linear profile and the apparent yield stress value is evaluated using a stress-controlled rheometer.⁵¹ From the results of the test, viscosity peak is observable and,

a sudden decrease in the viscosity peak represents the yield value of yield stress fluids during measurements.

The stress-controlled rotational rheometer was also employed with a parallel plate accessory for stress ramp tests. Dimensional conformance between the circular accessory (20 mm diameter) and fabricated CTT samples was precisely measured. The first step of measurement is preheating isothermally at 250°C for 30 min, which aimed at the complete melting of the polymer matrix. Thermal diffusion throughout samples was thought as low efficiency because the experimental apparatus has convection heating system by heated N₂ gas instead of direct conduction from the heat source. Oscillatory shear tests rather than steady-state shear tests were carried out, with a constant angular frequency of 1 rad/s, in order to minimize the influence of slip and fracture on the viscosity data. The stress was assigned to increase linearly, literally means the stress ramp. The value of yield stress by the stress ramp test replaces the packing stress experiment and fiber pull-out test as expressed in Eqs. 4-7 and 4-8 because of the constraints on resin percolation and the dense packing geometry of fibers in the case of molded CTT samples.

4.3.4 Suspension rheology measurement

The rotational rheometer was used with an identical for stress suspension rheology tests. In order to measure the CTT suspension rheology, oscillatory shear tests were conducted using circular specimens, which had diameters equivalent to the parallel plate accessory (20 mm). Most of the conditions were similar to the polymer rheology measurement, except with regard to the normal force and preheating because sufficient preheating is necessary for highly filled composite systems. Identical preheating time (30 min) was applied to CTT samples prior to the measurements. The thicknesses of each specimen were determined after the normal force on the specimen reached an equilibrium ranging from 2 N to 8 N in the case of CTT44, whereas the normal force ranged from 9 N to 20 N in the case of CTT55 samples.

Controlling the normal force range is necessary because the normal force range may change in rheological results due to the change of packing stress, which affects yield stress of one sample. Therefore, low normal force is undesirable in terms of slip occurrence of the samples during measurement, and high normal force was undesirable as well in terms of overestimation of packing geometry effects. According to the previous research, an increase in fiber content in the composite samples resulted in higher deformation resistance, leading to higher loading forces.¹ Regarding the nature of composite samples, the normal forces range was empirically set, enabling gradual change of plot tendency in a set of series at various strain amplitudes.

The carbon fibers in the composite samples were considered to be oriented following the plane of the parallel plates. The fibers may have been rotationally limited, as assumed in the theory section because the thickness of the flow domain (2 mm in both CTT samples) was sufficiently smaller

compared to the fiber length (6 mm). In addition, gap size effects may be considered as negligible because the ratio of the gap size to the fiber diameter was higher than 200 in composite samples. The tests were implemented by modulating an angular frequency range from 10^{-1} to 200 rad/s at various strain amplitudes: 0.05%, 0.1%, 0.5%, 1%, 3%, 5%, 7% and 10%. The frequency range and strain amplitudes were adjusted to allow observation of the clear variation at high effective shear rates.

4.4 Results and discussion

4.4.1 Polymer matrix shear viscosity

As a first step, the shear viscosity of CTT's polymer matrix was experimentally characterized in dynamic modes of a rotational rheometer. It is obvious that the shear rate range from measurements has to match with the range of the actual processing. An upper limit on the measurements may be adequate because the compression molding procedure has a relatively low upper limit for the shear rate—up to 100 1/s—compared to that of techniques, which involves to large deformation in short time. For example, analysis of extrusion or injection molding or mixer is required to measure rheology at high shear rate. However, employing typical experimental devices for obtaining at high shear rate range, e.g. capillary rheometer, is not achievable in the case of high content and because it is difficult to flow materials in the exceptionally narrow path of capillary shaped geometry even at above the melting temperature. Also, packing geometry of composite system cannot be considered in the geometry. The rotational rheometer is one of possible option regarding the constraints of experimental usage.

Fig. 4.5 shows three GNF models that provide precise illustrations of the shear viscosity plots of the polymer melts in the valid shear rate range. In the figure, the filled dots indicates experimental results. Assigned angular frequency ω can be converted to shear rate by applying Cox-Merz rule in assumed linear viscoelastic region.⁴² Measuring points of angular frequency were identical in three representative samples, and thus it is possible to average complex viscosity values of three samples. The maximum coefficient of variation (CV) is 4.7% at first measuring point at 0.1 rad/s, and the minimum CV is 2.3% at 0.25 1 rad/s. The range of CV represents the reproducibility of this test.

The dotted red line represents the Carreau three parameter model, Eq. 4-1; the dashed blue line represents the Cross three parameter model, Eq. 4-2; and the solid black line represents the Carreau-Yasuda model 5 parameter model, Eq. 4-3. The parameters in the GNF models can be obtained by the functional fitting of experimental results, and those are in Table 3-3. Non-linearity and deviation from the numerical expression of each equation with multiple variables make it difficult to the functional fitting of each GNF model. Therefore, coefficient of determination r^2 originated from statistical concept, quantifies the deviation of model equations from measured values can be simply calculated ($r^2 = 1 - \text{error sum of square}/\text{total sum of square}$). When comparing r^2 in three

cases models, the Carreau model is 0.93; the Cross model is 0.99; the Carreau-Yasuda model is 0.93. This result implies the Cross model is well fitted to experimental data. It is understandable the measured PA6 melt has unclear Newtonian plateau region at low shear rate and the Carreau and Carreau-Yasuda models inherently implies clear Newtonian plateau region at low shear rates. The Cross model shows better agreement at low shear rates compared to the results from the other models

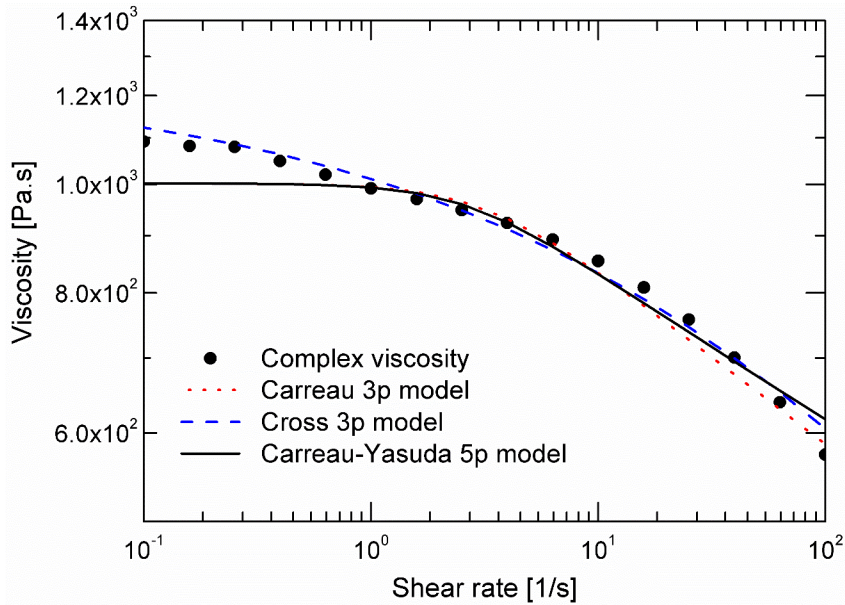


Figure 4. 5. Complex shear viscosity of PA6 and functional fitting to three Newtonian fluids (GNF) models.

Table 4 - 3. Rheological parameters for three generalized Newtonian fluids (GNF) models.

Model type	Parameters (Unit)	Value
Carreau model	Zero shear rate viscosity η_0 (Pa·s)	1002
	Relaxation time λ (s)	0.31
	Power Law index n (-)	0.84
Cross model	Zero shear rate viscosity η_0 (Pa·s)	1245
	Critical stress τ^* (Pa)	1.05×10^5
	Power Law index n (-)	1.33
Carreau-Yasuda model	Zero shear rate viscosity η_0 (Pa·s)	1002
	Infinite shear rate viscosity η_∞ (Pa·s)	113
	Relaxation time λ (s)	0.38
	Power Law index n (-)	0.84
	Yasuda constant a (-)	2.08

GNF model plots exhibit acceptable overall tendencies, although there is a deviation from the experimental results in the low shear rate region. Establishing a micromechanical model for shear viscosity is possible because the slight deviation at low shear rates is negligible compared to the predominance of yield stress in Eq. 4-7 and 4-8.

4.4.2 Suspension yield stress

Fig. 3.6 illustrates the yield stress as assigned by setting experimental conditions. The experiments were conducted by ramping the shear stress linearly with even intervals between two measuring points. Following this procedure, monitoring the strain amplitude with high precision is possible. In the figure, the assigned shear stress values are indicated by solid dots, and open dots illustrate the resulting shear strain. Based on the shear strain amplitude's slope variation, two curve segments show

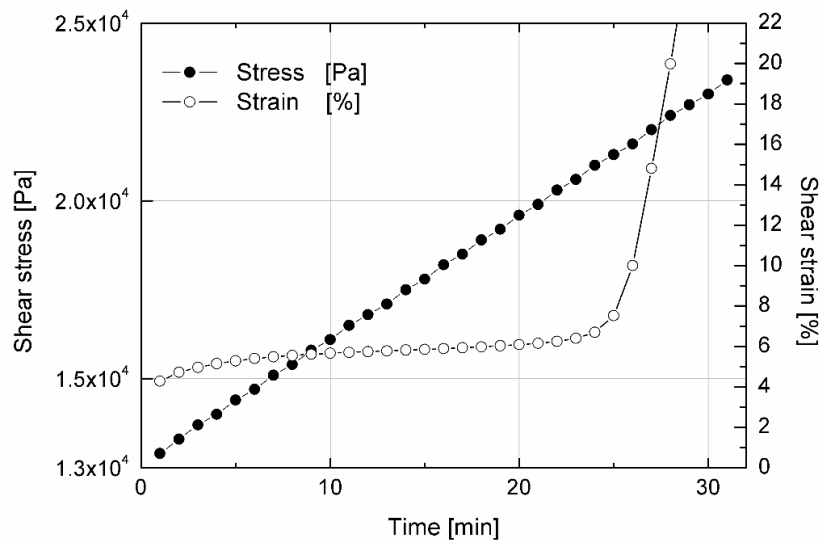


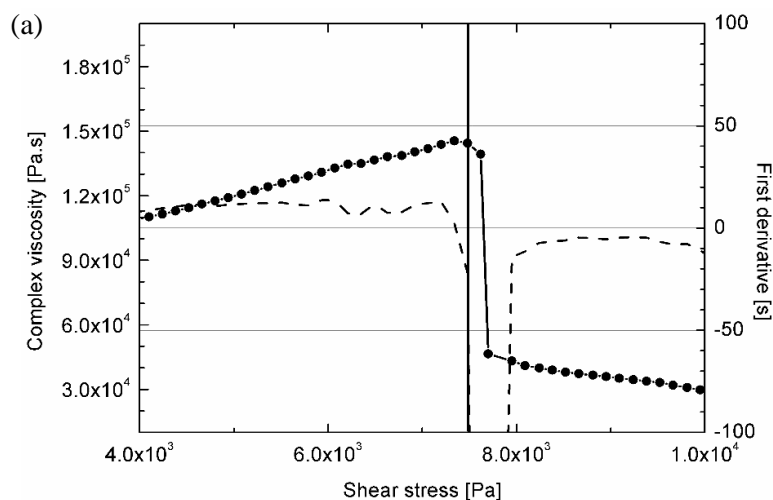
Figure 4. 6. Representative plots showing shear stress and strain over time in stress ramp test: CTT55 sample.

in a change of viscoelasticity during measurements. The first segment represents a linear tendency below the apparent yield stress. In this segment, the specimen is undergoing pseudosolid deformation, representing a linear viscoelastic (LVE) response that is dominantly induced by the packing geometry of the carbon fibers and Coulombic friction at contact points of those. Hence, strain rate is almost constant with a limited variation even though the stress is increasing linearly. After 22 min, the slope change reveals the beginning of shear flow due to the transition of linear viscoelasticity of samples during the measurement.

To evaluate the apparent yield stress of two types of CTT suspensions, the relation between complex viscosity and shear stress for two types of CTT suspensions is drawn in Fig. 4.7(a), (b), (c), (d) and

4.8 (a), (b), (c), (d) using four samples in each case. The shear stress ranged from 1 kPa to 10 kPa for CTT44 suspensions, while the range was from 13 kPa to 30 kPa for CTT55 suspensions. The ranges were achievable a lot of trials and errors to select the adequate range showing clear viscosity decrease at a certain point. A peak in complex viscosity indicates the point at which the specimen yields and its complex viscosity consequently decreases as shear stress increases. The decrease of complex viscosity reveals the beginning of shear flow due to the transition of linear viscoelasticity. This point allows the evaluation of each sample as the apparent yield stress of the suspension viscosity. The onset point of viscosity decrease is determined as a first derivative function of complex viscosity below zero for CTT44 suspensions, whereas the point is determined as first derivative below -20 for CTT44 suspensions. Overall responses from linear shear deformation in each suspension case are different, and a consequent derivative function is entirely different.

In order to demonstrate the validity of tests in evaluating the yield stress of CTT suspensions, repetitive experiments were carried out under the same conditions. Four samples of CTT44 exhibit 6.6 kPa of yield stress with CV of 25.8%. In comparison, the same number of CTT55 samples represents 17.8 kPa of yield stress with CV of 12.7%. The difference of CV can be considered as sample homogeneity and consistency of packing geometry of fibers. Recalling the theory section, the essential assumption includes statistically homogeneous of suspensions with a planar orientation distribution. Therefore, CTT55 can be thought as better agreement with the assumption. The complex viscosity below the yield stress indicates the integrated response of packing geometry and a consequence friction at interaction point. Considering the volume fraction ϕ of each material, contact points per unit volume is higher in the case of CTT55 than CTT44. Therefore, the yield stress is high due to ϕ is understandable. The friction coefficient k_f , which contributes to the yield stress, is known as being dependent on normal force at micro-scale in terms of tribological aspect.



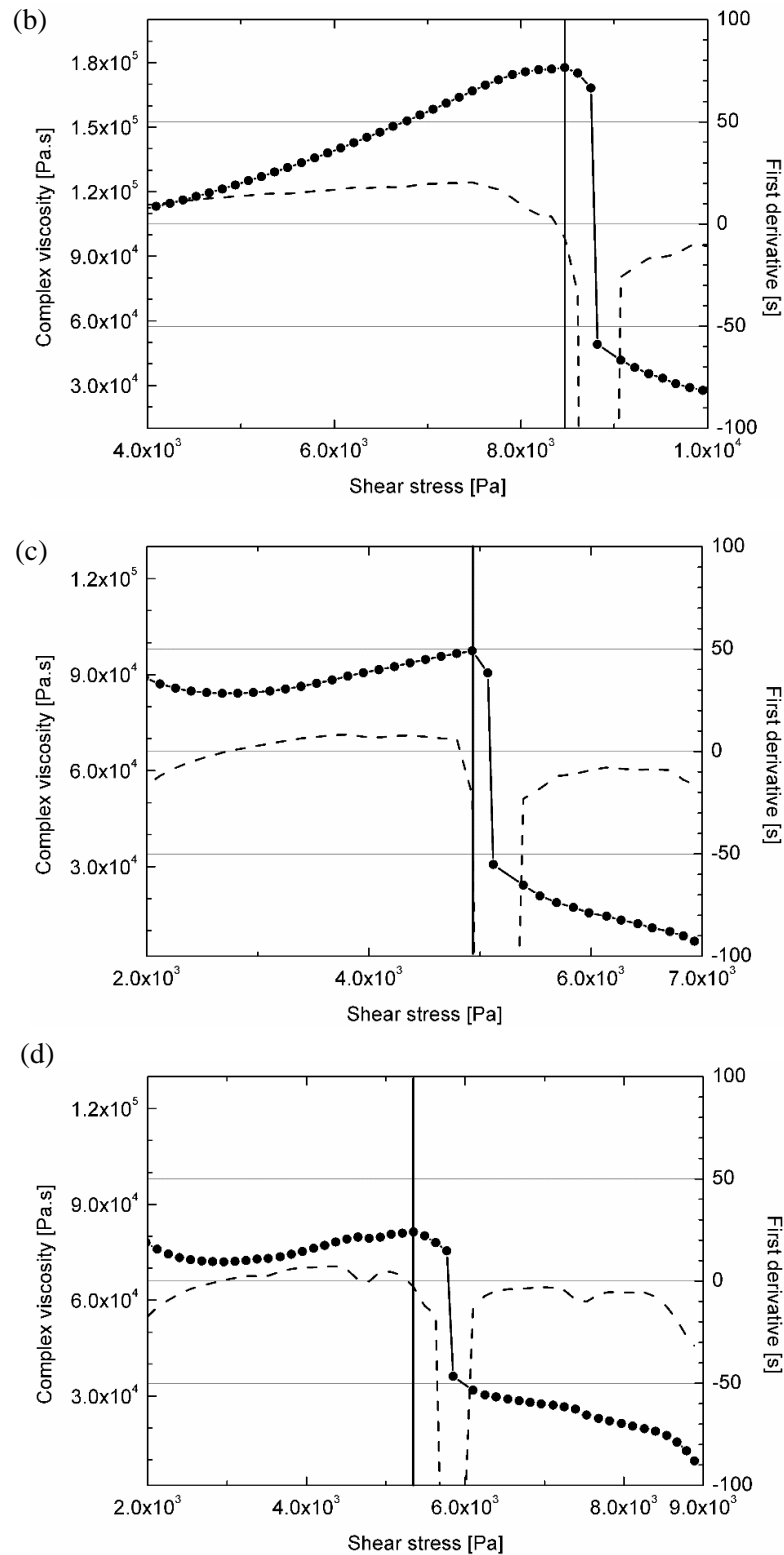
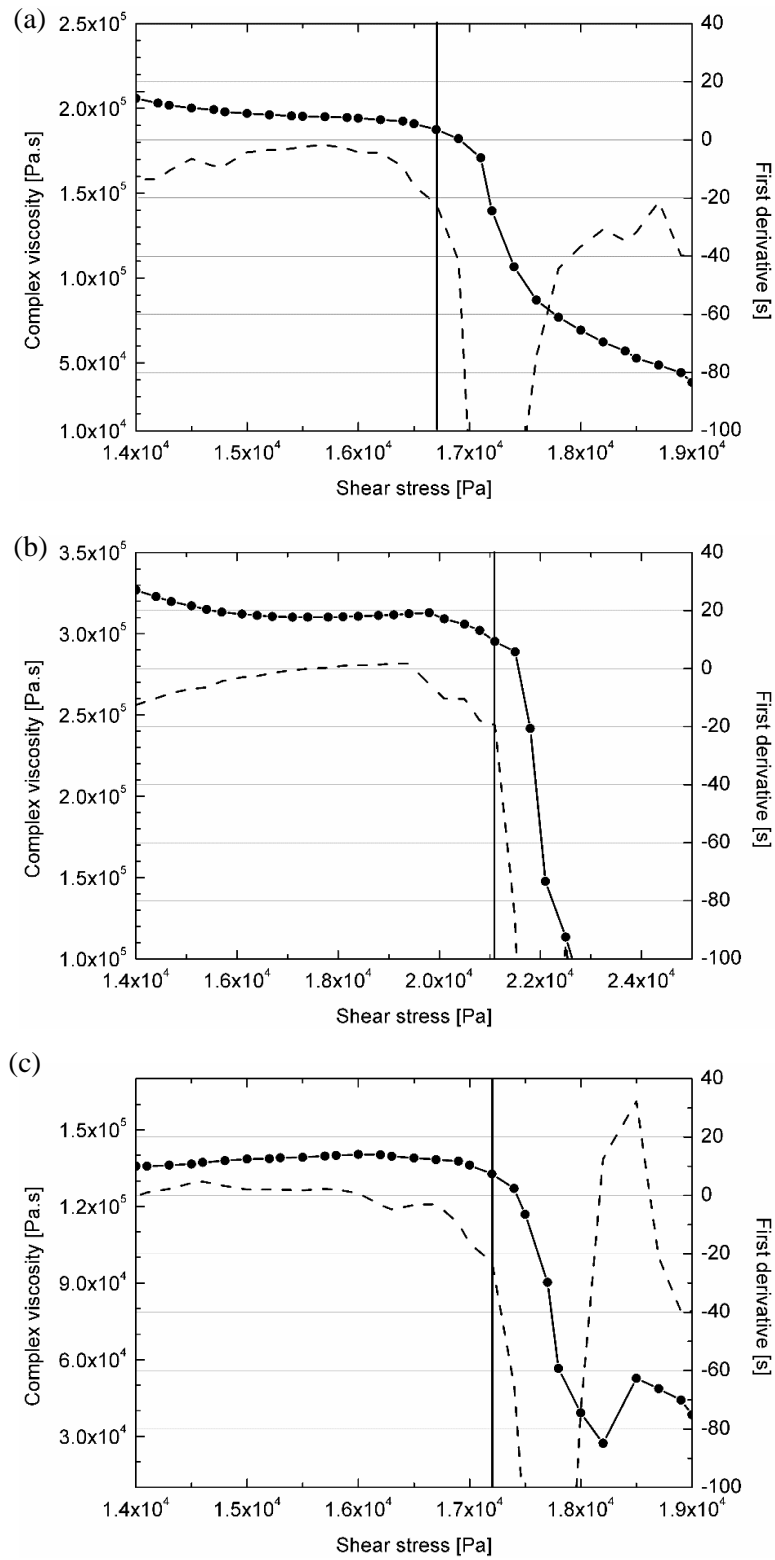


Figure 4. 7. Yield stress evaluation for CTT44 suspensions by complex viscosity peak: (a) sample 1, (b) sample 2, (c) sample 3 and (d) sample 4.



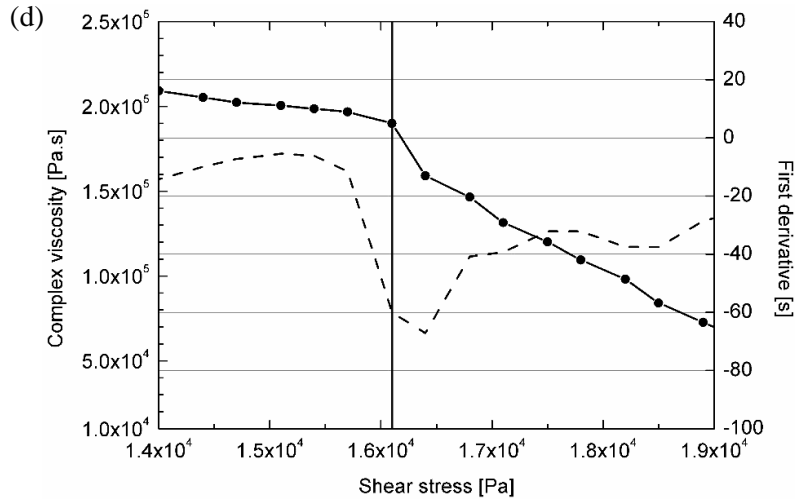


Figure 4. 8. Yield stress evaluation for CTT55 suspensions by complex viscosity peak: (a) sample 1, (b) sample 2, (c) sample 3 and (d) sample 4.

In several CTT44 samples, instant fracture initiates at low shear stress than the assigned maximum stress point (10 kPa) as presented in Fig. 4.7(c) at ≈ 7 kPa and (d) at ≈ 9 kPa, respectively. Although oscillatory shear testing can minimize the possibility of fracture, relatively weak packing geometry of CTT44 may induce a crack initiation at an arbitrary position in low shear stress range. Because of the low ϕ , the polymer matrix is widely located in CTT44 sample, leading a small number of the contact points. In CTT55 samples, such fracture does not occur at least 19 kPa of shear stress even though shear stress ranges in a higher stress level. The yield stress value is imported into the friction force terms in Eqs. 4-7 and 4-8 to establish suspension rheology model for two types of suspensions. A relatively high yield stress is found in previous studies in highly filled suspensions.^{22, 40}

4.4.3 Suspension shear viscosity

As shown in Fig. 4. 9(a) and (b), complex viscosity could be related to the effective shear rate function, which was defined as the product of the strain amplitude γ_m and the angular frequency w at various strain amplitudes. The plots were established by multiplying the results of angular frequencies at the assigned strain amplitude. Despite the absence of steady-shear test results, the superposition indicated by Eq. 4-4 was observed above the strain amplitude of 3% in both cases of CTT suspensions. In the figure, the solid dots represent complex viscosity above the strain amplitude, whereas the open dots illustrate complex viscosity below the strain amplitude, representing the linear viscoelastic solid region. Eqs. 4-7 and 4-8 are also illustrated in Fig. 4.9(a) and (b) by the dotted red line and the dashed blue line, respectively. In the models, k_h was defined as the hydrodynamic lubrication coefficient, which corresponds to the average area at the contact points. The coefficient was determined by functional fitting to the complex viscosity results of $196 \mu\text{m}^2$ for CTT44 case and

121 μm^2 for CTT55 case. Because the fiber content of CTT44 is less than that of CTT55, it can be deduced that the lubrication effects are larger in the former case than the latter case.

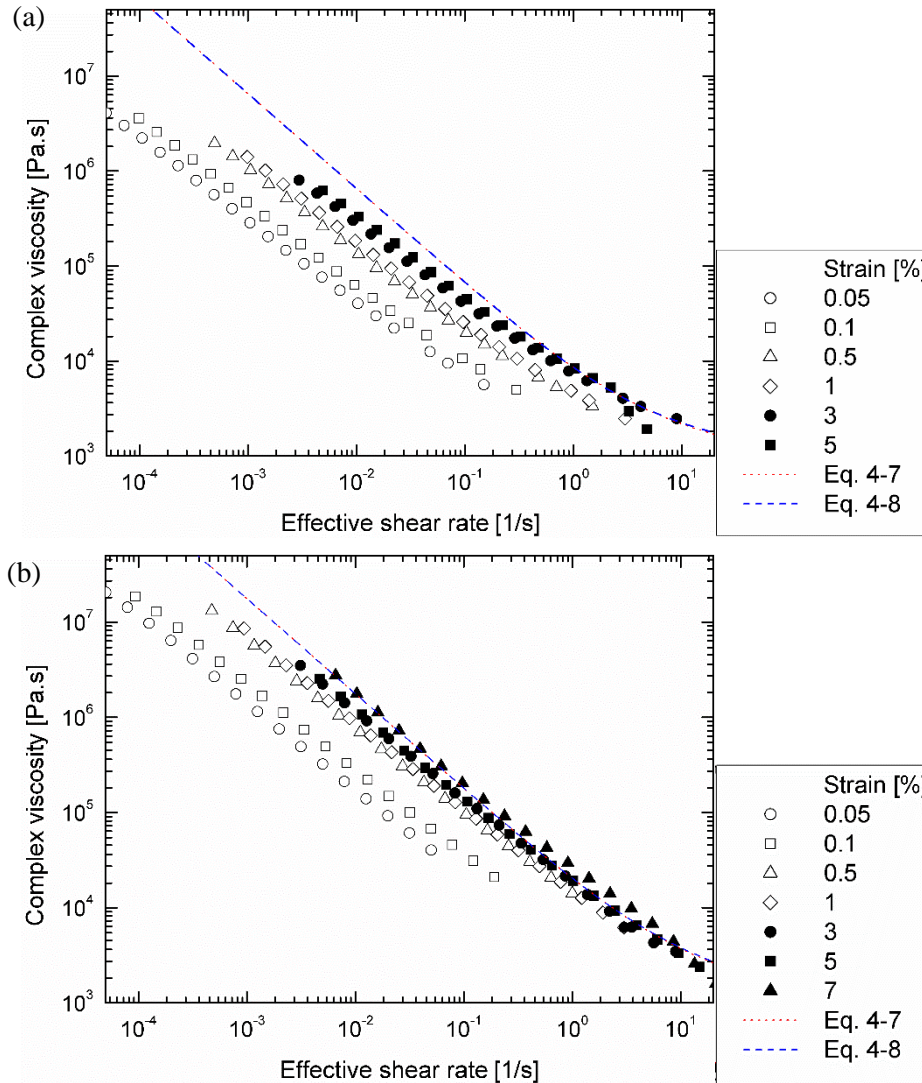


Figure 4. 9. Complex viscosity as a function of the effective shear rate at various strain amplitudes: (a) CTT44 and (b) CTT55.

The complex viscosity results above the strain amplitude of 5% can be categorized into distinctive regions depending on the range of effective shear rates. The first region shows the predominance of a pseudo-solid behavior with the log-log slope of -1 below the effective shear rate of 1/s. In this region, a relatively high yield stress covers the Newtonian Plateau, which is related to the rheological behavior of the polymer matrix. Therefore, two viscosity models exhibit identical viscosity plots in this region. The second region indicates viscoelastic behavior, which is caused by combined effects of Coulombic friction and hydrodynamic lubrication at contact points between the fibers above the

effective shear rate of 1/s. It is possible to observe partial frictional and viscous responses in this region based on the change in the slope. In the case of highly concentrated fiber suspensions, it is not possible to completely eliminate Coulombic friction contribution even at high effective shear rates. Therefore, pseudo-liquid behavior cannot dominate the viscosity results, showing only a slight slope variation. Despite the different descriptions of the two CTT suspension models in Eq. 4-7 and 4-8, no clear difference is apparent on the log-log scale. Both models are expected to be valid for flow analysis because the models have the form of the Herschel-Bulkley fluid model. The micro-mechanical model derived from the Cross fluid model more precisely illustrates the viscoelastic behavior of both CTT suspensions, compared to that of the Carreau model, when the influence of the polymer matrix lubrication on the models is considered.

The general tendency is different depending on the fiber content. Fig. 4.9(a) displays the overestimation of the shear viscosity determined by Eq. 4-7 and 4-8 at low shear rates. This overestimation is attributed to the ideal assumption that there is no rotation of fibers around the in-plane axis, transverse axis, or the fiber's own axis; however, there might be variation in the initial fiber geometry during measurements. In addition, other discrepancies may exist, such as the bending of carbon fibers and/or imperfect in-plane random orientation.

The value of $\tan \delta$ represents the ratio of the dissipated mechanical energy to the stored energy per cycle during dynamic tests.⁶ In other words, $\tan \delta$ Reveals the relative proportion of viscous components to elastic components in the oscillatory deformation mode. Therefore, this value is typically utilized to analyze the flow characteristics of viscoelastic materials. Fig. 4.10 shows $\tan \delta$ plots of CTT55 suspensions with varying angular frequencies and strain amplitudes. From strain amplitudes of 0.05 to 5%, $\tan \delta$ grows with the increase in the strain amplitude because the relative elasticity of the suspension decreases with the growth of the strain amplitude. Above the strain amplitude of 5%, the $\tan \delta$ values converge to 0.5 at low angular frequencies, below approximately 10 rad/s. This suggests that the experiments already exceed the particular level of strain amplitude, and represent the saturated viscoelastic behavior above 5% amplitude. After termination of the entire measurement procedure, the fracture of the specimens is easily identified in the cases of 7% and 10% amplitude, whereas there is no such phenomenon at the 5% amplitude. Therefore, it can be deduced that the former cases suffered crack propagation and fracture during the measurements. A drastic increase in $\tan \delta$ is identified at 50 rad/s in the 7% amplitude test and at 20 rad/s in the 10% amplitude test. Such phenomena represent the complete separation of specimens induced by the fracture, which thus influences the viscosity results in these two cases.

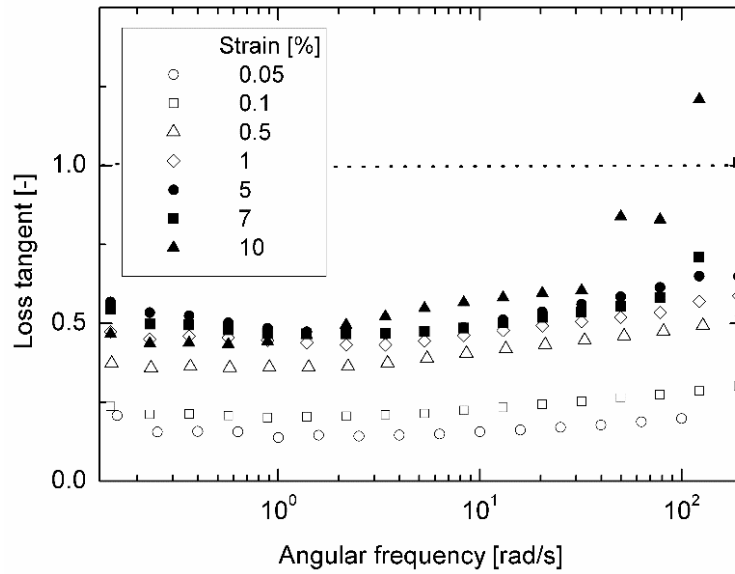


Figure 4. 10. Loss tangent with varying angular frequencies and strain amplitudes for CTT55 suspensions.

Fig. 4.11 shows filler effects on complex viscosity for two types of CTT suspensions. Both suspensions show pseudo-solid behaviors at low shear rate region and viscoelastic behavior at high shear rate region presented as solid dots: circle dots for CTT44 suspensions and square dots for CTT55 suspensions. The open dot represents Cross based shear rate viscosity of PA6 matrix. The absolute value is lower in the case of CTT 44 because of the difference of yield stress and shear gap effects, and eventually being closer to the flow behavior of the polymer

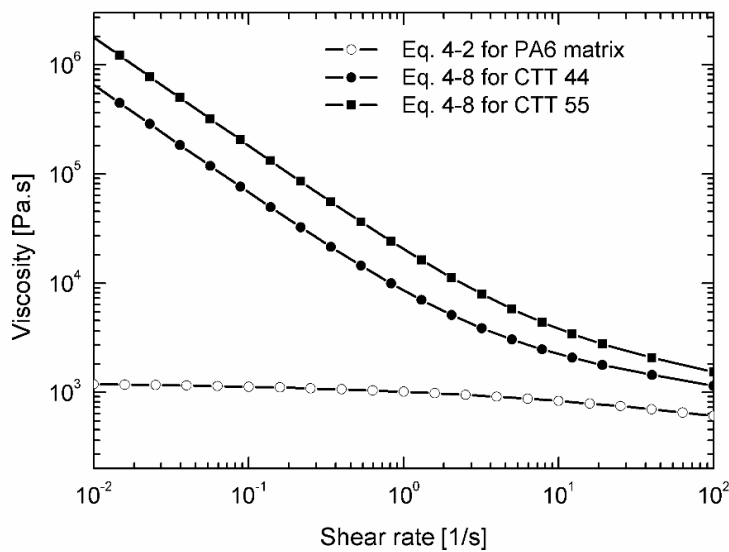


Figure 4. 11. Filler effects of CTT suspensions on viscosity plots.

matrix. The multiple plots clearly show the filler effect on polymeric behaviors with increasing the filler content. Increasing filler concentration causes interaction of fiber friction, whereas melt polymer behavior, located in polymer film at interactions points of fibers, is less influential as filler content increases.

4.5 Concluding remarks

The rheology of highly concentrated CTT suspensions has been characterized by applying experimental methodologies and theoretical models. The rheological properties have been determined by adopting the Rutgers-Delaware relationship and constructing micromechanical models. CTT specimens fabricated from two types of thin prepreg sheets present homogeneous constituents and dispersion of fibers in the flow domain, enabling the rheological analysis in an oscillatory shear mode. A shearing flow mechanism for CTT suspensions has been established by micromechanical models, and oscillatory shear experiments have shown the validity of this approach. The yield stress of CTT suspensions is assessed from the viscoelastic response determined by an oscillatory stress ramp test. The complex flow behavior of CTT suspensions can be expressed in the form of the Herschel-Bulkley fluid model with high yield stress. Three distinctive regions are identified in the viscosity results and models: a linear viscoelastic region below a strain amplitude of 1%, a predominantly pseudo-solid behavior region at low effective shear rates, and a transition region combining frictional and viscous components at high effective shear rates. Because of the consistent contribution of strong friction interaction to the bulk stress, it is not possible to observe the region where pseudo-liquid behavior dominated in the viscosity results, even at high effective shear rates.

The results give an explanation on the mechanism of flow behaviors studied in Chapter 2. In Chapter 2, despite the high concentration of carbon fiber suspensions exhibited rapid mold filling in the range of few min without a phase separation in cases properly set test conditions. Although there should be additional discussion of the mechanism by following studies, findings in this study reveal one part of flow mechanism: friction contribution and lubrication contribution to the bulk stress applied by shear deformation mode. Friction contribution increases with a high fraction of fibers due to lots of interaction points for CTT55 suspension (fiber geometry can be regarded as similar in both cases of CTT44 and CTT55, interactions points between fibers are many in the unit volume of flow domain because the volume fraction is high). It causes the increase of resulting friction effects: high yield stress in out of plane shear mode. The lower value of lubrication coefficient, $121 \mu\text{m}^2$ for CTT55 suspensions, than that for CTT44 suspensions also supports this interpretation based on the internal geometry of specimens. Although such high content of fibers (44–55%) causes less influential of polymer melt behaviors, lubrication contribution is small for CTT55 due to the filler content, which corresponds to the average area at the contact points.

It is expected that this study will contribute to establishing models for manufacturing process by giving constitutive equations of out of plane shear viscosity. From this baseline, developing constitutive equation would be valuable to extend theoretical validity using several case studies on fiber filled thermoplastic composites with different internal geometry. If this kind of study is accumulated and finally linked with numerical applications to predict flow behaviors, it would contribute to design economical CTT manufacturing by predicting the flow behavior of CTT. Such predictions would minimize material waste, and could also be used to optimize cost-effective mold designs for commercial applications.

Chapter 5

Characterization of Thermal Expansion Behaviors

5.1 Introduction

The ultimate goal of this thesis is to establish a baseline for simulating compression molding process in CTT manufacturing. When compressing the material during the process, the pressure applied by normal force on the material is the only driving force inducing squeeze flow. Therefore, calculating the accurate pressure distribution throughout the material is the most important information in numerical simulation. The generation of pressure distribution is partially influenced by the thermal expansion of the material. In order to figure it out the magnitude of thermal expansion, this analysis is planned.

As previously studied CTT system, the material possesses high specific strength, high specific modulus. Although thermo-mechanical behavior plays a significant role when manufacturing the composite material, thermal expansion properties are considered as negligible effects. This is because adjusting processing condition can compensate the influences of thermal expansion on the dimensional change in practical manufacturing scales. Fundamentally, the properties are inherent properties of combined effects of composite constituents: a polymer matrix and carbon fibers. Adopting classical method allowed one to characterize the properties by using flat panel samples were used, which can be treated as in-plane isotropic.⁵²

There are three types of linear coefficient of thermal expansion (CTE) in the cases of orthotropic materials. In the case of CTT, expansion through thickness direction may have the largest compared to those of longitudinal direction and transverse direction according to the revealed internal structure of carbon fibers and their networking structure in CTT system, in-plane quasi-isotropic. This is related to friction between fibers and negative CTE of carbon fiber in the axial direction, or longitudinal, of fibers (α_{fl}), whereas positive CTE of the fiber in radial direction (α_{fr}).⁵³

Two types of coefficient of linear expansion are considered in this study: $\alpha(T)$ (differential coefficient of linear thermal expansion), $\bar{\alpha}(\Delta T) = (\Delta l/l_0)/\Delta T$ (mean coefficient of linear thermal expansion); l_0 is the initial length; ΔT is the difference between two temperatures; Δl is the change in length over the temperature range. Hence, $\alpha(T)$ is the respective slope of the tangent at a certain temperature, whereas $\bar{\alpha}(\Delta T)$ is the slope of a secant in a designated temperature range. Fig 5.1 clearly illustrates the difference between two characteristics. The properties are separately used to represent the tendency below glass transition and above the transition, are specifically described in the ‘results and discussion’ section.

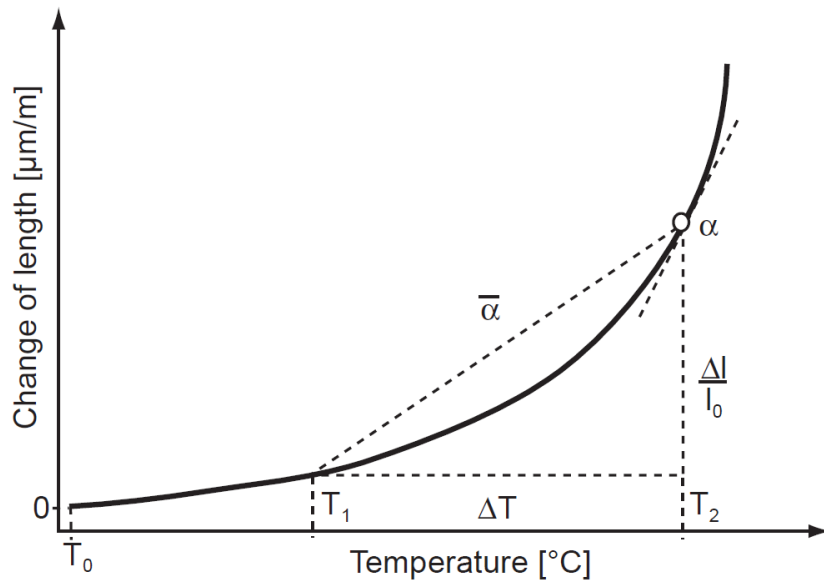


Figure 5. 1. Evaluation of the mean (ΔT) and differential $\alpha(T)$ coefficients of linear thermal expansion [13].

5.1 Experimental procedures

5.1.1 Specimen preparation

In order to manufacture 4 mm thickness samples using high volume fraction 44 μm prepregs, abbreviated to CTT55 in Chapter 4. Preform sheets preparation shares the methodology in Chapter 4, unifying the weight of one cycle of preparation (20-23g) and the dimension of chopped strands (5 mm \times 6 mm). Subsequently, by specifying the number of preform plies (24 plies), one molding cycle used 190.5 g \pm 1.0 g of preform sheets to achieve the dimensional conformance of 4 mm

thickness. The preforms were dried using a vacuum dryer to avoid degradation of the polymer constituent for over 12 hours at 90°C prior to the molding process.

For equivalent molding process, a Laboratory Press 30T (Pinette Emidecau Industries, the maximum force of 30 ton) was employed in the compression molding cycle. In molding cycles, setpoints of upper and lower platen temperature are 265°C, which corresponds to 260°C ± 2°C of upper and lower molds, directly measured from embedded thermocouple probes in the molds. The temperature setting constantly maintains except the cooling stage. After the insertion of prepared preform sheets at 265°C of platens, the molding cycle starts. A force begins with 31 kN, which corresponds to 1 MPa on the dimension of molded samples for 15 min and then the force is applied with a gradual increase up to 156 kN for 10 min, which corresponds to 5 MPa on the dimension. Then, the cooling step is also considered to have a same cooling rate (20°C/min), and the cooled samples are ejected at 70°C ($T_g = 70^\circ\text{C}$ of the PA6 matrix).

The molded samples (125 mm width as x-axis, 250 mm length as the y-axis, the average thickness of 4 mm as z-axis) were cut into cubic geometry (4 mm in each direction) using diamond blade saw with a maximum deviation of 0.05 mm to characterize anisotropic thermal expansion in principal directions. Although composite samples have dimensional variation in practical applications, caused by shrinkage during cooling process or inhomogeneity of internal fiber structure, specimens with dimensional conformance were sorted and selected for precise measurement. The cubic dimension aimed at having plane-parallel contact surfaces in the direction of each measurement. Dimensional accuracy was considered as very important because the measuring scale is very small and one unit of chopped strand is larger than the height of measurement.

Thermal expansion of polymer matrix is assumed to have isotropic properties. Fig. 5.2 represents schematics of aligned fibers in unit volume of the uni-directional composite system. Unlike the injection molded part, the compression molding process did not contain the processing direction in cases using fitted charge with mold cavity dimension. Also, due to the geometric concerns and preforms with planar random orientation in x-y plane of chopped uni-directional strands, α_{fl} (CTE of fibers in longitudinal direction, negative in general) equivalently affects to α_{ci} (in plane CTE of composite) along the x and y axes, and those are thought as having negligible difference. However, the only CTE along x axis was measured to exclude the scope of discussion on unknown variables of sampling direction. α_{fr} (CTE in radial direction, positive in general), CTE of polymer matrix and their combined effects related to the internal geometry composition are influential factors on the results of CTE along z (α_{ct} , through thickness CTE of composite).

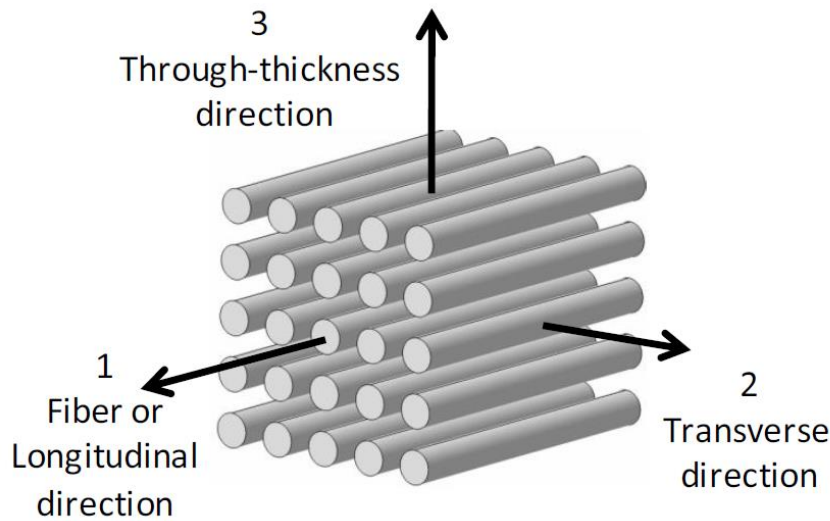


Figure 5. 2. Schematic representation of fibers aligned in uni-directional system [54].

5.1.2 Apparatus

Thermo-mechanical analyzer (TMA 7100, Hitachi High-technology) was employed to measure the change in a dimension of the test specimen with an accuracy of $0.01 \mu\text{m}$. Specimen preparation and test conditions follow general international standards for Thermo-mechanical analysis (TMA).⁵⁵ Fig. 5.3 shows a typical illustration of TMA apparatus, which is also used in this study. The dimensional change was recorded as a function of both time and temperature to generate TMA curve from which the CTE can be evaluated. All specimen is a cubic specimen 4 mm in length, width, and height. Applied pressure on the specimen, in a unit of Pascal, is determined by a measured contacting force 0.038 N with a circular contact area of a circle in 3.5 mm diameter normal to the upper surface plane of the specimen. The choice of probe type, quartz glass probe in this study, depends on the geometry of the specimen. The loaded probe kept constant four kPa on the contact plane in the entire test procedure, which is specified in the standard used ($4.0 \text{ kPa} \pm 0.1 \text{ kPa}$).

Nitrogen gas was used as a purge gas to prevent oxidation. Maintaining a constant gas flow within a flowrate of 100 ml/min. The temperature of the specimen at constant rate of $5 \text{ }^\circ\text{C}/\text{min}$ of sequential steps was assigned in order to eliminate thermal and mechanical effects in the specimen; 1st heating from 20°C to 210°C , cooling from 210°C to 20°C and finally 2nd heating from 20°C to 210°C . 1 min of interval existed between heating and cooling steps for thermal stabilization to link each step. Although the actual processing temperature in CTT manufacturing approximately ranges from 250°C to 270°C , above T_m of PA6 matrix ($\approx 220^\circ\text{C}$),⁶ the range was not detectable due to the adhesion problem when exceeding temperature above T_m . The possibility of giving damage on a quartz probe by the adhesion is not preferable, and an indirect method (extrapolation from a measuring range) can be the way of deducing the anisotropic CTE at the processing temperature.

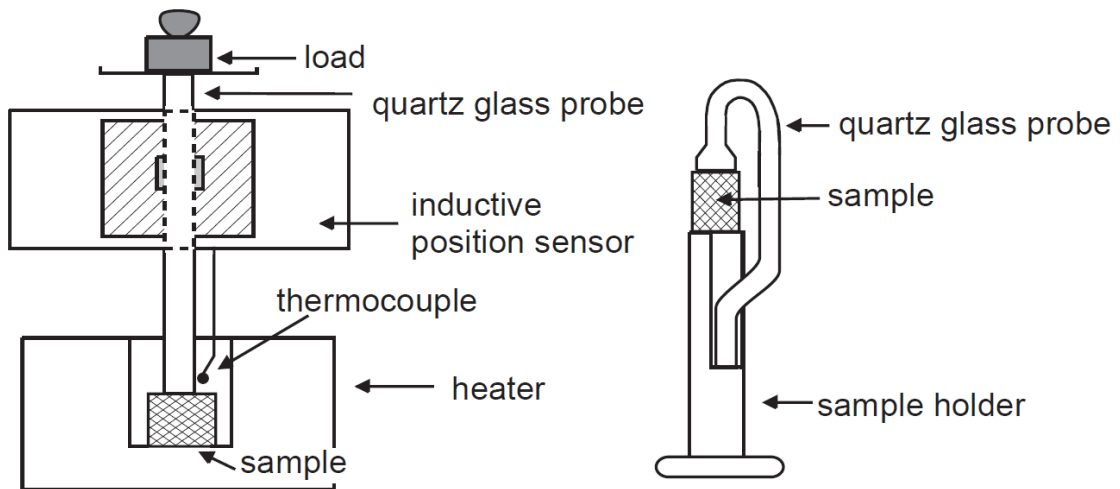


Figure 5.3. Schematic diagram of thermo-mechanical analysis (TMA) apparatus [13].

5.2 Results and discussion

5.2.1 Influences of thermal and mechanical history

Fig. 5.4 depicts an example of the influence of thermal and mechanical history for CTT specimen used. $\Delta l/l_0$, change of length, was calculated by the recorded length change and the initial length at ambient temperature. The 1st heating phase in a TMA measurement offers information about the thermal and mechanical history, processing influences, and so forth in specimen manufacturing. A 2nd heating phase, proceed by controlled cooling, exhibits information regarding purely material behavior. The objective of this study is to obtain inherent constants of materials regardless of thermal and mechanical history, which depend on the applied forming technique. There is a clear difference of two measured data. The sudden shrinkage on reaching the T_g in the 1st heating phase is hardly observable. The thermo-mechanical behavior of thermoplastic composite with high volume fraction (>50%) may have different behavior from the neat thermoplastic specimen. The 1st heating and cooling curves are excluded and then the 2nd heating curve is selected when evaluating CTE in two directions because the curve directly represents material specific behavior.

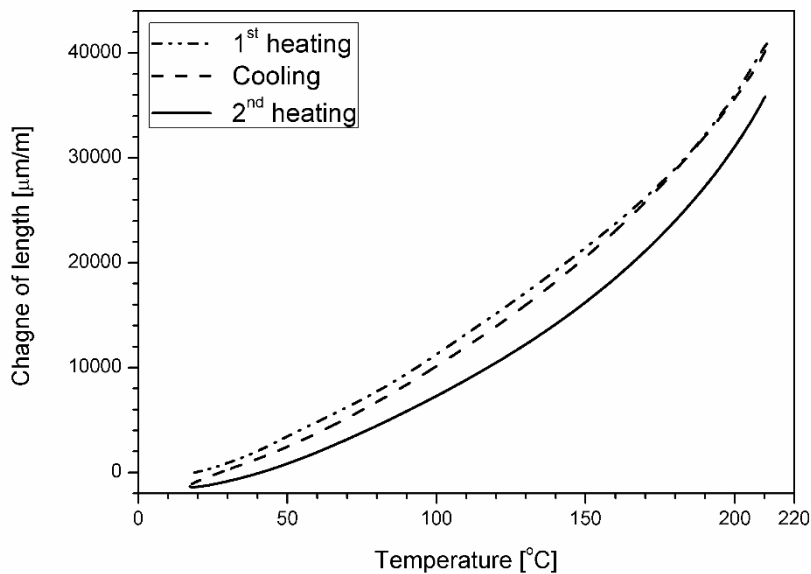


Figure 5. 4. Change of length of CTT specimen during controlled 1st and 2nd heating and cooling; normal probe, $l_o = 4.0$ mm, specimen cross-section approx. 4×4 mm, applied load 0.038N, heating or cooling rate 5 °C/min.

Fig. 5.5 shows reproducibility plots for through thickness specimens regarding change of length along the z-axis. These results are differentiated to evaluate α_{ct} , through thickness CTE of composite. As considered previously, the curve continues with a greater increase. Three curves exhibit analogous tendency in the given identical test procedure except slight deviation, which may be originated from difference of the specimen dimension and the temperature interval measured. The initial length of each specimen was measured at ambient temperature right before the test procedure as summarized in Table 5-1. The change of length at the maximum temperature represents approximately 0.035 $\mu\text{m}/\text{mm}$ in the direction of measurement. The slope at low temperature shows linear increase, which directly deliver α_{ct} of the specimens.

Table 5 - 1. Initial length measured at ambient temperature.

Initial length l_o	In-plane CTE	Through thickness CTE
	α_{ci} specimen (mm)	α_{ct} specimen (mm)
Sample 1	3.999	3.976
Sample 2	4.036	4.007
Sample 3	4.023	4.024
Average	4.019	4.002

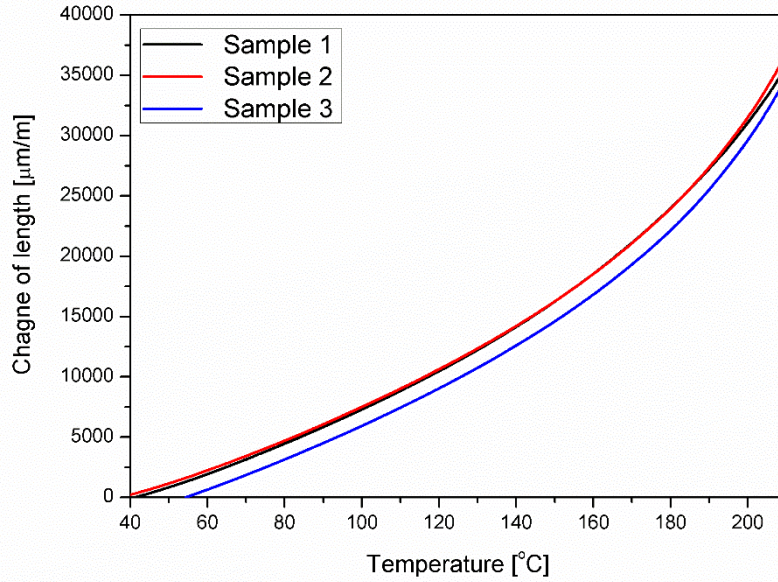


Figure 5. 5. Reproducibility plots of change of length for through thickness expansion specimens; normal probe, $l_o = 4.0$ mm, specimen cross-section approx. 4×4 mm, applied load 0.038N, heating rate 5 °C/min.

5.2.2 Anisotropic thermal expansion coefficients

At the glass transition, semi-crystalline thermoplastics undergo stepwise changes of thermal expansions. Semi-crystalline thermoplastics including PA6 exhibits a small change of length below the glass transition T_g up to roughly 70°C in cases of PA6. Therefore, CTE curves of PA6 are found to have a nearly constant CTE ($80 \mu\text{m}/\text{m}^\circ\text{C}$) below T_g .¹³ Therefore, $\bar{\alpha}(\Delta T)$ (Mean coefficient of linear thermal expansion) was evaluated by the slope of change of length plots using three through-thickness and in-plane specimens, calculated from a temperature difference of 20 and 70°C . As the temperature exceed T_g , CTE encounters significant non-linear change to the maximum measuring temperature at 210°C . Hence, in order to evaluate α_{ct} and α_{ci} , Fig. 5.6 is plotted as a function of temperature. Employing data analysis program (Origin, © OriginLab Corporation), the first derivative of a function is defined as:

$$f'(x) = \lim_{h \rightarrow 0} \frac{f(x+h) - f(x)}{h} \approx \lim_{h \rightarrow 0} \frac{f(x+h) - f(x-h)}{2h} \quad \text{Eq. 5-1}$$

where the h is sufficiently small, we can use a centered difference formula to approximate the derivative. Even though the derivative function depends on the measured interval in x-axis of plots, the software treats discrete data by the transform of the centered difference formula and calculates

the derivative at point of $P_i(x_i, y_i)$ by taking the average of the slopes between the point and its two closest neighbors in practice. Eventually, the derivative function applied to discrete data points can therefore be written:

$$f'(x_i) = \frac{1}{2} \left(\frac{y_{i+1} - y_i}{x_{i+1} - x_i} + \frac{y_i - y_{i-1}}{x_i - x_{i-1}} \right) \text{ Eq. 5-2}$$

From that numerical approximation, Fig. 5.6 illustrates through thickness CTE α_{ct} of a CTT specimen during 2nd heating using 3 samples. Even below the T_g , thermo-mechanical behavior is not only originated from the polymer matrix behavior but also originated from carbon fiber expansion in radial direction (positive). Therefore, slight increase occurs in the region. Also, when reaching melting temperature T_m of PA6 (220°C) causes a drastic increase of α_{ct} . The rearrangement of polymer chain in molecular scale causes an increase in the order of magnitude near to the temperature. In the case of neat polymer, the expansion approximately reach to 400 $\mu\text{m}/\text{m}^\circ\text{C}$ in the reference literature.¹³ Discretized data analysis is relevant to measuring points, which are very fine in the present study. The noise like behavior is about the temperature instability between two measuring points and, the sensitive measurement was performed in different measuring points. Although smoothing the plots by sorting and reducing data points is possible, the plots are drawn by using the raw data to avoid data distortion. The tendency of plot reveals the influences of polymer matrix, fiber expansion and their structural characteristics on the TMA of composite specimens.

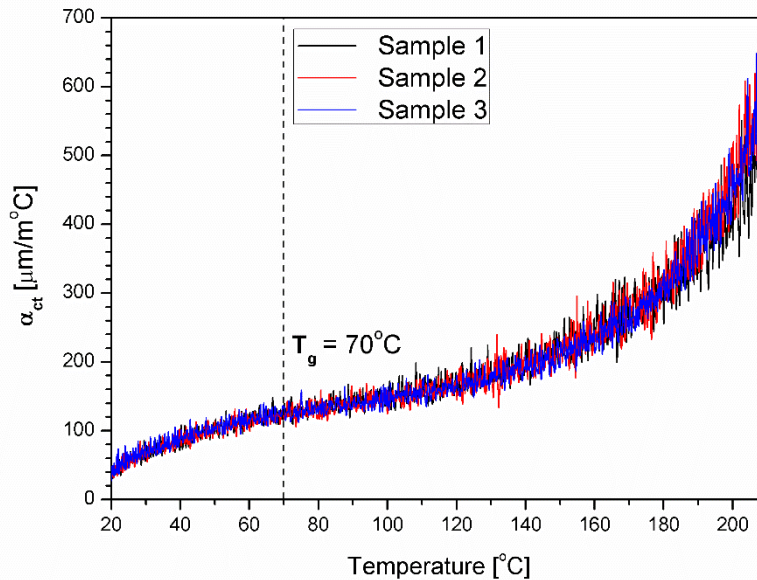


Figure 5. 6. Through thickness CTE of three CTT specimens during 2nd heating; normal probe, $l_o = 4.0$ mm, specimen cross-section approx. 4×4 mm, applied load 0.038N, heating or cooling rate 5 $^\circ\text{C}/\text{min}$.

This Fig. 5.7 clearly shows that in-plane CTE is small, whereas through thickness CTE shows a large value in the order of magnitude. To quantify and summarize the difference, $\bar{\alpha}(\Delta T)$ was evaluated by assuming linear slope, calculated from a temperature range from 20 to 70°C. From 70°C to 210°C, the maximum values of α_{ct} and α_{ci} were assessed respectively. Table 5-2 summarizes the evaluation. When considering maximum values in the temperature range above T_g , α_{ct} is 42 times larger than α_{ci} . In the case of $\bar{\alpha}(\Delta T)$ through thickness $\bar{\alpha}(\Delta T)$ is 29 times larger than in plane $\bar{\alpha}(\Delta T)$. Recalling the objective of this study, thermal expansion during forming process is the scope of discussion. This difference in order of magnitude allows to assume in-plane CTE is negligible compared to the through thickness CTE and simplify the volumetric change during forming application by employing thickness direction change.

Table 5 - 2. Comparison of in-plane CTE and through thickness CTE of CTT specimens.

	$\bar{\alpha}(\Delta T)^*$ $\Delta T = 20^\circ\text{C} - 70^\circ\text{C}$	Maximum $\alpha(T)^*$ $T \text{ range} = 70^\circ\text{C} - 210^\circ\text{C}$
α_{ci} ($\mu\text{m}/\text{m}^\circ\text{C}$)	3.07 (1.97)	16.32 (1.26)
α_{ct} ($\mu\text{m}/\text{m}^\circ\text{C}$)	91.18 (1.56)	686.93 (17.69)

*Mean values (one standard deviation).

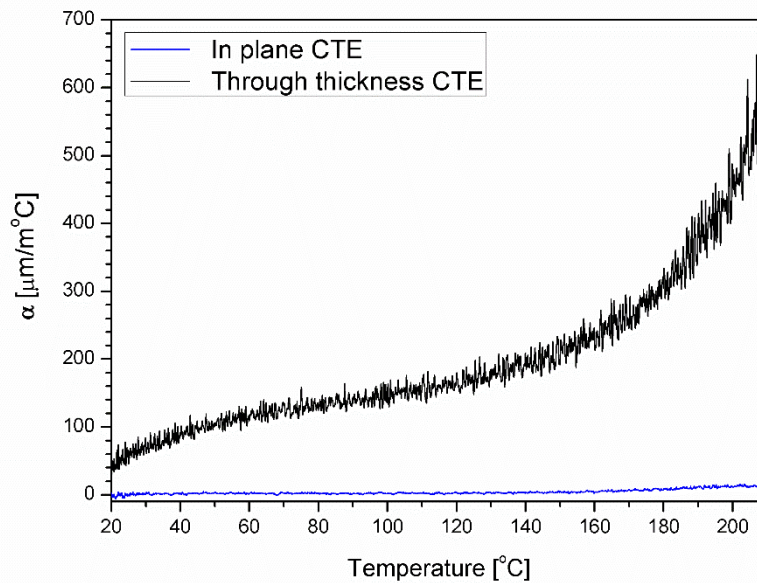


Figure 5. 7. Comparison of in-plane CTE α_{ci} and through thickness CTE α_{ct} ; $l_o = 4.0$ mm, specimen cross-section approx. 4×4 mm, applied load 0.038N, heating or cooling rate $5^\circ\text{C}/\text{min}$.

5.3 Concluding remarks

The thermo-mechanical behavior of highly concentrated CTT composite has been characterized by applying the conventional way of measurement in principal directions: in-plane and through thickness directions. CTT specimens fabricated from thin prepreg sheets present reproducibility due to the homogeneous constituents and dispersion of fibers. Reproducibility for CTT specimens has been achievable by dimensional accuracy of specimens, and test results have shown the validity of this approach. Thermal expansion coefficients of CTT specimens were assessed in the valid range of temperature of instrument used by using discretized data plots. Because of the consistent contribution of thermal expansion of fibers in radial and longitudinal directions, two expansion coefficients represent the different characteristics as a function of temperature. With the aid of data analysis tool, CTE in each direction could be assessed, and two distinctive regions were identified in TMA results of through thickness CTE: an increase of CTE with a low slope below T_g and drastic increase of CTE when the temperature gets close to T_m above T_g . Anisotropic CTEs (in-plane CTE and through thickness CTE) were also observable, which show a difference in several dozen times. The difference in order of magnitude allows to assume through thickness CTE is dominant contribution to the bulk expansion compared to in-plane CTE.

The results give valuable information of thermo-mechanical behaviors related to thermal expansion properties, which affects volumetric change during the manufacturing process of materials, in the present case compression molding. Contacting force by compression tools, molds in general cases generates a pressure difference between contacting areas and free surfaces without contacts. The volumetric change affects pressure distribution, which is driving force of flow during compression: applied pressure increases with large volumetric change. The results clearly deliver anisotropic thermal expansion properties. The difference in order of magnitude suggests that in-plane CTE is negligible compared to the through thickness CTE during the manufacturing process.

It is expected that characterization in this study will contribute to establishing Pressure-Volume-Temperature (PVT) relationship models regarding volumetric change as a change of applied temperature and pressure for process modeling applications. From this phase of CFRTP innovation, developing process model would be available despite additional characterization is required to construct the PVT models at various pressure conditions. If the study is extendable and finally inserted to numerical applications to predict flow behaviors, it would contribute to design economical CTT production system by considering the thermal expansion properties of CTT. Such consideration would allow one to establish optimal heating stage and following forming stage by compression molding in the entire processing stages, and could also be used to develop efficient production cycles for commercial applications.

Chapter 6

Conclusions of Dissertation

6.1 Scientific contributions

The research work presented in this dissertation has allowed particular contributions to the knowledge and literature on the processing knowledge of CTT composites. The major contributions are described in the following.

Chapter 2: Drawing processing window when forming complex geometry, especially applying to the ribbed tray geometry

- The formability when applying complex geometries of the molding die and direct insertion of CTT preform sheets without pre-consolidation or other preparation work was confirmed using five different types of preforms without pre-consolidation or preheating.
- The formability investigation has been performed by using preforms, from 6 mm length and 5 mm width to 30 lengths and 5 mm width in the practical range of forming conditions in terms of short molding time and effective pressure applied.
- The relationship between formability and forming parameters (strand size, pressure, molding time) was studied with varying the parameters, and the influential factors in literature were discussed.
- Forming behaviors of CTT suspensions are greatly dependent on strand size and the effective pressure in the given geometry of mold.
- Critical defects, e.g. phase separation, unfilled areas could be avoidable after molding in the molded components by adjusting forming conditions.
- Short mold filling time is achievable when complex parts are formed using CTT preforms.

: Chapter 3 > The simplified and experimental approach for evaluation of mold filling time is studied.

- The question becomes major influential factors on properties of final molded parts

: Chapter 3 > Evaluation of content fraction (fiber, polymer, void: not undesirable), optical microscopy and mechanical performance are studied.

Chapter 3: Introducing methods for observing the progression of flow front and assessing mold filling time and involved properties

- The simplified approach, uni-axial, and bi-axial squeeze flow tests were designed to identify flow behaviors during compression molding process by referring the widely accepted literature in squeeze flow theory and its valid utilization.⁵⁶
- In practical range of closing forces and corresponding pressure, mold filling time can be evaluated by tracking the visible mark on the sample surfaces
- Mold filling time from the initial position to fill the areas of mold cavity depends on the applied closing force and charge properties: preform charges and pre-consolidated charge.
- Involved properties, such as thermal stabilization in heating phase, void formation, internal structure observation and even mechanical properties were investigated using frequently used experimental methods.
- Formed samples exhibited comparable mechanical performance with samples without flow in cases fully consolidated.
- A challenging task, designing realistic and rapid process, was explored and partially obtainable by combining each stage of processing including heating, consolidation and forming stages in one molding cycle.
- The importance of rheological characterization and thermo-mechanical properties to construct the constitutive relationship (stress-strain rate relationship) and define the degree of volumetric change, which is included in governing equations (equation of motion and mass conservation) in a numerical approach in process modeling of a wide class of materials.

: Chapter 4 > Rheological characterization is performed from melt rheology of the polymer matrix to suspension rheology of the composite sample.

: Chapter 5 > Thermo-mechanical behavior is investigated by adopting the general standards for characterizing the properties.

Chapter 4: Characterization of rheological properties by applying valid theoretical considerations for shear viscosity of fiber concentrated suspensions.

- Out-of-plane shear viscosity models for CTT suspensions was established, which are treated as dominant deformation mode in cases of complex flow during compression molding; when forming complex parts the material may undergo in-plane and out-of-plane flow, however, out-of-plane shear can be dominant contribution to the bulk flow in cases using compression molding with non-slip condition and narrow gap assumption.¹²
- Various experimental setups were designed to construct the models: materials of two kinds of volume fraction, three sequential steps (shear viscosity of equivalent polymer to the matrix of the composite system without fiber fillers, the yield stress of CTT suspensions and out-of-plane shear viscosity models for CTT suspensions).
- Oscillatory shear experiments showed the validity of this approach, enabling superposition of multiple plots at various strain amplitudes.
- Three distinctive regions were identified in the viscosity results and models: a linear viscoelastic region below 3% of strain amplitude, a predominantly pseudo-solid behavior region at low effective shear rates, and a transition region combining frictional and viscous components at high effective shear rates.
- The complex flow behavior of CTT suspensions, out-of-plane shear, can be expressed in the form of the Herschel-Bulkley fluid model with a high yield stress, which applies to the commercialized numerical software.

Chapter 5: Characterization of thermal expansion behaviors of CTT composites using a thermo-mechanical analyzer.

- Coefficients of thermal expansion (CTE) in principal directions (in-plane and through thickness) were evaluated, and guaranteed reproducibility of experimental results.
- Because of the consistent contribution of thermal expansion of fibers in radial and longitudinal directions, two expansion coefficients represented the different characteristics as a function of temperature
- Anisotropic CTE clearly exhibited directional dependent expansion due to the internal structure of the composite samples: dispersion of fibers in the polymer matrix and their networking structure.

- The results give valuable information of thermo-mechanical behaviors related to thermal expansion properties, and thus a volumetric change in governing equations (equation of motion and mass conservation) can be estimated instead of incompressible assumption.

In conclusions, this dissertation contains the suggestions of essential experimental methodology related compression molding of carbon fiber-reinforced thermoplastic composite. Most of the fundamental issues for applying numerical approaches were evaluated and characterized; formability, squeeze flow behaviors, evaluation of mold filling time, defect formation in the manufacturing process, rheological properties, and thermo-mechanical properties. Much of efforts have been primarily focused on constructing the baseline for process modeling in CTT manufacturing. In the effort to characterize flow behaviors of chopped carbon fiber tape reinforced thermoplastics, there are several important issues to consider. The first is the fact that composite preform sheets are heated to above the melting temperature of the polymer matrix which behaves as a viscous fluid during the forming procedure. This consideration necessitates the development of predictive models for the viscosity of fiber-filled viscous fluids. Thus, the first effort here was to experimentally validate formability in cases of complex geometry samples and visualization of compression mold filling. In addition, the second effort here was to develop constitutive relations for fiber-filled fluids based on the imposed kinematics in shear deformation mode and valid assumptions by regarding internal geometry of the materials.

Since the sheet-forming process generally involves the deformation of multi-axial fibers and viscous matrix during the forming process, the integrated behavior is an important consideration. Results presented for the analogy to classical rheology theory and experimental methodology revealed that the mechanism of deformation is cumbersome and not easy to be predictable. However, the findings from this thesis may lead one to achieve the design of mold frames, drawing a processing window for newly developing products with a geometric feature, the deduction of optimal processing conditions, and finally the cost-effective usage of materials. These contributions have directly or indirectly led to the literature on the processing of CTT composites, in the form of conference proceedings [20, 58], published journal paper [57] and submitted journal articles [59, 60].

6.2 Expansion of this dissertation

In order to achieve accessible features of the CTT composite for wider applications to manufacturing industries, the additional investigation should be placed to explore the possibility and expand the current level of applications:

1. **An extensive study of the mold filling time evaluation could be performed.** For securing

clear advantages of the materials, an extension of parametric studies is required in a wider range of heating condition, squeezing condition and cooling condition. In this dissertation, the mold filling time was studied under a limited number of parameters, for example, fixed closing forces, charge dimension and prescribed heating conditions. Reproducibility of each test condition should be sufficiently obtained by applying various conditions. If the efforts are accumulated to draw the entire processing window in most feasible conditions, the industrial field could be easily accessed the material in various applications.

2. **An intensive study of the rheological properties considering internal structure on a smaller scale.** Yield stress and shear viscosity of one integrated system of fibers and polymer melt of CTT composite samples were investigated according to the theoretical approach. Clarifying the difference between inter-ply and Intra-ply shear of strands, above that, in-ply shear and inter-ply of preform sheet ply is an invaluable contribution to understanding flow behaviors of such unique material.
3. **Linking with applications of numerical simulation.** This dissertation basically constructed the baseline for simulation applications and it was not achievable to directly reach a connection with process modeling in CTT manufacturing process. The objective function of the simulation would be a prediction of mold filling time, which could be achievable using a commercial software for simulating compression molding process. From the experimental works presented in this thesis including rheological models and coefficients of thermal expansion could be essential governing equations, which are variables in the Navier-Stokes equations to construct physical properties during compression molding. Furthermore, squeeze flow behaviors and mold filling observation could be comparing group after establishing all the necessary set-ups in simulation tools including governing equations, boundary conditions, and mold charge setting.

If that goal is accomplished by steady efforts on on-going researches, that would be a remarkable achievement for both of researchers in a composite field and ambitious manufacturers, who intend to achieve light-weight and strong mechanical properties by exploring the unrevealed possibility.

References

1.	B. A. Davis, P. J. Gramann, T. A. Osswald and A. C. Rios, <i>Compression Molding</i> , 1st ed. München: Hanser Gardner Publications, Inc., 2003, pp. 1-110.
2.	J. miller, "Transport policy.net," South Korea: Light-duty: Fuel Economy and GHG, February 2016. [Online]. Available: http://www.transportpolicy.net/index.php?title=South_Korea:_Light-duty:_Fuel_Economy_and_GHG .
3.	J. miller, "Transport policy.net," Japan: Light-duty: Fuel Economy, January 2017. [Online]. Available: http://www.transportpolicy.net/index.php?title=Japan:_Light-duty:_Fuel_Economy .
4.	M. Smith, "Oilprice.com," July 2016. [Online]. Available: http://oilprice.com/Energy/General/Oil-Prices-Waver-As-Market-Uncertainty-Takes-A-Jump.html .
5.	B. Destler, "Huffington post," October 2012. [Online]. Available: http://www.huffingtonpost.com/bill-destler/electric-cars_b_1929481.html .
6.	Z. Tadmor and C. G. Gogos, <i>Principles of Polymer Processing</i> , 2nd ed. New Jersey: John Wiley & Sons, 2006, pp. 1-913.
7.	M. Bruderick, D. Denton, M. Shinedling and M. Kiesel, "Applications of carbon fiber SMC for the Dodge," in <i>SPE Automotive Composites Conference</i> , Troy, Michigan, September 2002.
8.	T. A. Oswald and S. -C. Tseng, "Compression molding," in S. G. Advani (ed) <i>Flow and Rheology in Polymer Composites Manufacturing</i> , 1st ed. Amsterdam: Elsevier Science, 1994, pp. 361-411.
9.	F. C. Campbell, <i>Structural Composite Materials</i> , 1st ed. Ohio: ASM International, 2010, pp. 63-100.
10.	C. M. O' Brádaigh, "Sheet forming of composite materials," in S. G. Advani (ed) <i>Flow and Rheology in Polymer Composites Manufacturing</i> , 1st ed. Amsterdam: Elsevier Science, 1994, pp. 517-569.
11.	F. N. Cogswell, "Continuous-fiber systems," in S. G. Advani, (ed) <i>Flow and Rheology in Polymer Composites Manufacturing</i> , 1st ed. Amsterdam, Elsevier Science, 1994, pp. 127-141.
12.	S. G. Advani and E. M. Sozer, <i>Process Modeling in Composites Manufacturing</i> , 2nd ed. Boca Ranton, Florida: Taylor & Francis Group, 2011, pp 263-390.
13.	G. W. Ehrenstein, G. Reidel and P. Trawiel, <i>Thermal Analysis of Plastics</i> , 1st ed. Cincinnati, Ohio: Hanser Gardner Publications, Inc., 2004, pp. 172-358.
14.	A. Vicari, "Scaling up carbon fiber: Roadmap to automotive adoption," Lux market report, 2014.
15.	M. M. Schwartz, <i>Composite Materials: Processing, Fabrication, and Applications</i> , 1st ed. NJ: Prentice Hall, 1997, pp. 437-488.
16.	R. B. Pipes, D. W. Coffin, P. Simacek, S. F. Shuler and R. K. Okine, "Rheological behavior of collimated fiber thermoplastic composite materials," in S. G. Advani (ed) <i>Flow and Rheology in Polymer Composites Manufacturing</i> , 1st ed. Amsterdam, Elsevier Science, 1994, pp. 86-125.

17.	Y. Wan and J. Takahashi, "Tensile and compressive properties of chopped carbon fiber tapes reinforced thermoplastics with different fiber lengths and molding pressures," <i>Composites Part A: Applied Science and Manufacturing</i> , vol. 87, 2016, pp. 271-281.
18.	S. Yamashita, K. Hashimoto, H. Suganuma and J. Takahashi, "Experimental characterization of the tensile failure mode of ultra-thin chopped carbon fiber tape-reinforced thermoplastics," <i>Journal of Reinforced Plastics and Composites</i> , vol. 35, 2016, pp. 1342-1352.
19.	H. Suganuma, S. Yamashita, X. Zhang, K. Hashimoto, I. Ohsawa and J. Takahashi, "Influence of dispersion method to dispersibility and mechanical properties of ultra-thin carbon fiber tape reinforced thermoplastics," in <i>Proceeding of ICCM-20</i> , P201-10, Copenhagen, Denmark, July 2015.
20.	S. Tang, T. Hayashi, H. Lee, W. Nagatsuka, I. Ohsawa and Jun Takahashi, "Flowability of discontinuous carbon fiber reinforced thermoplastics," in <i>Proceeding of ICCM-20</i> , P201-11, Copenhagen, Denmark, July 2015.
21.	G.-P. Picher-Martel, A. Levy and P. Hubert, "Compression molding of Carbon/Polyether ether ketone composites: Squeeze flow behavior of unidirectional and randomly oriented strands," <i>Polymer Composites</i> , 2015, DOI: 10.1002/pc.23753.
22.	G.-P. Picher-Martel, A. Levy and P. Hubert, "Compression moulding of Carbon/PEEK Randomly-Oriented Strands composites: A 2D Finite Element model to predict the squeeze flow behaviour," <i>Composites Part A: Applied Science and Manufacturing</i> , vol. 81, 2016, pp. 69-77.
23.	S. Yamashita, "Effect of thin-ply on the material properties of chopped carbon fiber tape reinforced thermoplastics (CTT)," (Doctoral Dissertation), The University of Tokyo, Tokyo, Japan, 2016.
24.	Y. Wan and J. Takahashi, "Tensile properties and aspect ratio simulation of transversely isotropic discontinuous carbon fiber reinforced thermoplastics," <i>Composites Science and Technology</i> , vol. 137, 2016, pp. 167-176.
25.	A. Ionita and Y. J. Weitsman, "Randomly reinforced composites: properties, failure and aspects of material design," <i>Probabilistic Engineering Mechanics</i> , vol. 21, no. 1, 2006, pp. 64-72.
26.	Y. Pan and A. A. Pelegri, "Progressive damage analysis of random chopped fiber composite using finite elements," <i>Journal of Engineering Materials and Technology</i> , vol. 133, no. 1, 2011, doi:10.1115/1.4002652.
27.	B. Landry and P. Hubert, "Experimental study of defect formation during processing of randomly-oriented strand carbon/PEEK composites," <i>Composites Part A: Applied Science and Manufacturing</i> , vol. 77, 2015, pp. 301-309.
28.	S. Shin, R. Y. Kim, K. Kawabe and S. W. Tsai, "Experimental studies of thin-ply laminated composites," <i>Composites Science and Technology</i> , vol. 67, no. 6, 2007, pp. 996-1008.
29.	J. Schuster, D. Heider, K. Sharp and M. Glowania, "Thermal conductivities of three-dimensionally woven fabric composites," <i>Composites Science and Technology</i> , vol. 68, no. 9, 2008, pp. 2085-2091.
30.	G.-P. Picher-Martel, A. Levy and P. Hubert, "Squeeze flow of randomly oriented-oriented strands

	thermoplastic composites," in <i>Proceeding of ICCM-19</i> , eProceedings part1, pp.1872-1864, Montréal, Canada, August 2013.
31.	H. C. Stadtfeld, M. Erninger, S. Bickerton and S. G. Advani, "An experimental method to continuously measure permeability of fiber preforms as a function of fiber volume fraction," <i>Journal of reinforced plastics and composites</i> , vol. 21, no. 10, 2002, pp. 879-899.
32.	C.-Y. Chang, L.-W. Hourng and C.-S. Yu, "Analysis of flow phenomena during the filling stage of CTM," <i>Journal of reinforced plastics and composites</i> , vol. 23, no. 14, 2004, pp. 1561-1570.
33.	P. Brookbank, L. Savage and K. E. Evans, "Economical carbon and cellulosic sheet moulding compounds for semi-and non-structural applications," <i>Journal of reinforced plastics and composites</i> , vol. 34, no. 6, 2015, pp. 437-453.
34.	ASTM D3039/D3039M: Tensile properties of polymer matrix composite materials, 2002.
35.	H. H. Lin, S. Ranganathan and S. G. Advani, "Consolidation of continuous fiber systems," in S. G. Advani (ed) <i>Flow and Rheology in Polymer Composites Manufacturing</i> , 1st ed. Amsterdam, Elsevier Science, 1994, pp. 326-358.
36.	R. Törnqvist, P. Sunderland and J.-A. E. Månson, "Non-isothermal process rheology of thermoplastic composites for compression flow moulding," <i>Composites Part A: Applied Science and Manufacturing</i> , vol. 31, no. 9, 2000, pp. 917-927.
37.	P. Olivier, J. P. Cottu and B. Ferret, "Effects of cure cycle pressure and voids on some mechanical properties of carbon/epoxy laminates," <i>Composites</i> , vol. 26, no. 7, 1995, pp. 509-515.
38.	M. R. Barone and D. A. Caulk, "Kinematics of flow in sheet molding compounds," <i>Polymer Composites</i> , vol. 6, no. 2, 1985, pp. 105-109.
39.	S. F. Shuler and S. G. Advani, "Transverse squeeze flow of concentrated aligned fibers in viscous fluids," <i>Journal of Non-Newtonian Fluid Mechanics</i> , vol. 65, no. 1, 1996, pp. 47-74.
40.	R. Törnqvist, P. Sunderland and J.-A. E. Månson, "Determination of the rheological properties of thermoplastic composites for compression flow molding," <i>Polymer Composites</i> , vol. 21, no. 5, 2000, pp. 770-788.
41.	J. Thomasset, P. J. Carreau, B. Sanschagrín and G. Ausias, "Rheological properties of long glass fiber filled polypropylene," <i>Journal of Non-Newtonian Fluid Mechanics</i> , vol. 125, no. 1, 2005, pp. 25-34.
42.	T. S. R. Al-Hadithi, H. A. Barnes and K. Walters, "The relationship between the linear (oscillatory) and nonlinear (steady-state) flow properties of a series of polymer and colloidal systems," <i>Colloid and Polymer Science</i> , vol. 270, no. 1, pp. 40-46, 1992, pp. 40-16.
43.	C. Servais and J.-A. E. Månson, "Fiber-fiber interaction in concentrated suspensions: disperse fibers," <i>Journal of Rheology</i> , vol. 43, no. 4, 1999, pp. 991-1004.
44.	C. Servais, A. Luciani and J.-A. E. Månson, "Fiber-fiber interaction in concentrated suspensions: dispersed fiber bundles," <i>Journal of Rheology</i> , vol. 43, no. 4, 1999, pp. 1005-1018.
45.	C. Servais and J.-A. E. Månson, "The relationship between steady-state and oscillatory shear viscosity

	in planar randomly oriented concentrated fiber suspensions," <i>Journal of Rheology</i> , vol. 43, no. 4, 1999, pp. 1019-1031.
46.	L. C. F. Andrade, J. A. Petronílio, C. E. d. A. Maneschy and D. O. A. Cruz, "The Carreau-Yasuda fluids: A skin friction equation for turbulent flow in pipes and Kolmogorov dissipative scales," <i>Journal of the Brazilian Society of Mechanical Sciences and Engineering</i> , vol. 29, no. 2, 2007, pp. 162-167.
47.	D. Doraiswamy, A. N. Mujumdar, I. Tsao, A. N. Beris, S. C. Danforth and A. B. Metzner, "The Cox-Merz rule extended: a rheological model for concentrated suspensions and other materials with a yield stress," <i>Journal of Rheology</i> , vol. 35, no. 4, 1991, pp. 647-685.
48.	R. Mas and A. Magnin, "Experimental validation of steady shear and dynamic viscosity relation for yield stress fluids," <i>Rheologica acta</i> , vol. 36, no. 1, 1997, pp. 49-55.
49.	Y. Wan, T. Otori and J. Takahashi, "Mechanical properties and modeling of discontinuous carbon fiber reinforced thermoplastics," in <i>Proceeding of ICCM-20</i> , 3222-4, Copenhagen, Denmark, 2015.
50.	S. Toll, "Note: on the tube model for fiber suspensions," <i>Journal of Rheology</i> , vol. 37, no. 1, 1993, pp. 123-125.
51.	M. I. Worldwide, "Understanding Yield Stress Measurements," Malvern Instruments Limited, 2012.
52.	E. Siderdis, "Thermal expansion coefficients of fiber composites defined by the concept of the interphase," <i>Composites science and technology</i> , vol. 51, no. 3, 1994, pp. 301-317.
53.	V. K. Ganesh and N. K. Naik, "Thermal expansion coefficients of plain-weave fabric laminates." <i>Composites Science and Technology</i> , <i>Composites Science and Technology</i> , vol. 51, no. 3, 1994, pp. 387-408.
54.	A. Ahmed, B. Tavakol, R. Das, R. Joven, P. Roozbehjavan and B. Minaie, "Study of thermal expansion in carbon fiber-reinforced polymer composites," in <i>SAMPE International Symposium</i> , Baltimore, USA, May 2012.
55.	ISO 11359-2: Plastics Thermomechanical analysis (TMA) Part 2: Determination of coefficient of linear thermal expansion and glass transition temperature, 1999.
56.	J. Engmann, C. Servais and A. S. Burbidge, "Squeeze flow theory and applications to rheometry: a review." <i>Journal of non-newtonian fluid mechanics</i> vol. 132. no.1, 2005, pp. 1-27.
57.	T. Otori, H. Lee, I. Ohsawa and J. Takahashi, "Optimal structural design of discontinuous carbon fiber reinforced thermoplastics plate subjected to bending load", <i>Journal of Japan Society for Composite Materials</i> , vol. 43 no. 2, 2017, pp. 65-73.
58.	H. Lee, S. Tang, T. Otori, T. Hayashi, Y. Wan, J. Takahashi, I. Ohsawa, K. Kawabe and T. Murakami, "Applicability of FEM to Complex Parts Made by Ultra-thin Chopped Carbon Fiber Tape Reinforced Thermoplastics", in <i>Proceeding of JISSE14</i> , Kanazawa, Japan, December 2015.
59.	H. Lee, G. Cai, S. Yamashita, I. Ohsawa and J. Takahashi, "Rheological properties of carbon/polyamide 6 randomly oriented strand composites under oscillatory shear", <i>Polymer</i>

	<i>Composites</i> , under review.
60.	H. Lee, C. Bi, S. Tang, T. Hayashi and J. Takahashi, "Formability and flow front observation of carbon/polyamide 6 randomly oriented strand composites during compression molding", <i>Journal of Reinforced Plastics and Composites</i> , under review.

Appendix A – Nomenclature

A. 1. List of acronyms

Acronyms	Full form
B	
BMC	Bulk molding compound
C	
CFRP	Carbon fiber reinforced plastics
CFRTP	Carbon fiber reinforced thermoplastics
CFRTS	Carbon fiber reinforced thermosets
CO ₂	Carbon dioxide
CTE	Coefficient of thermal expansions
CTT	Chopped carbon fiber tape reinforced thermoplastics
CV	Coefficient of variation
G	
GHG	Greenhouse gas
GMT	Glass mat thermoplastic
GNF model	Generalized Newtonian fluid model
L	
LFT	Long fiber thermoplastic
LVE	Linear viscoelastic
LVR	Linear-viscoelastic region
M	
MPa	Mega Pascal
P	
PAN	Polyacrylonitrile
PA6	Polyamide 6
PEEK	Polyether ether ketone
PEKK	Polyether ketone ketone

PI	Polyimide
PI	Proportional integral
PP	Polypropylene
PPS	Polyphenylene sulfide
PTFE	Polytetrafluoroethylene
PVT	Pressure-Volume-Temperature
R	
ROS	Randomly oriented strands
S	
SMC	Sheet molding compound
T	
TMA	Thermo-mechanical analysis
U	
UD	Unidirectional
V	
VE models	Viscoelastic models

A. 2. List of symbols

Symbol	Definition
L	Particle length
D	Diameter of particle
h	Height
h_i	Initial height
h_f	Final height
ε_f	Final strain
ρ	Density
W	Weight
V	Volume
f	Fiber
m	Matrix
c	Composite
M_w	Molecular weight
p_{eff}	Effective pressure
C_p	Heat capacity

K	Thermal conductivity
t_c	Characteristic time
f	
V_f	Fiber volume fraction
\emptyset	
$^{\circ}C$	Degree Celsius
T_m	Melting temperature
T_g	Glass transition temperature
σ	Bulk stress
$\sigma^{(l)}$	Liquid stress
$\sigma^{(p)}$	Particle stress
P	Packing stress
f_n	Normal force
f_f	Tangential friction force
f_h	Hydrodynamic lubrication force
k_h	Hydrodynamic lubrication coefficient
k_f	Friction coefficient
η	Steady-state viscosity
$ \eta^* $	Complex viscosity
$ \eta_{sp}^* $	Complex viscosity of suspensions
η_0	Zero shear rate viscosity
η_{∞}	Infinite shear rate viscosity
λ	Relaxation time
τ^*	Critical stress
n	Power Law Index
$\dot{\gamma}$	Steady-state shear rate
γ_m	Strain amplitude in oscillatory test
w	Angular frequency
τ_y	Yield stress
d	Fiber diameter
l	Fiber length
α	Shear gap around contact point
f	Distribution function of in-plane orientation
G'	Storage modulus
G''	Loss modulus

α_{fl}	CTE of carbon fiber in longitudinal direction
α_{fr}	CTE of fiber in radial direction
$\alpha(T)$	Differential coefficient of linear thermal expansion
$\bar{\alpha}(\Delta T)$	Mean coefficient of linear thermal expansion
ΔT	Temperature difference
α_{ci}	In-plane CTE of composite specimen
α_{ct}	Through thickness CTE of composite specimen
P_i	Cartesian coordinate system at point
$f'(x)$	Derivative function of x

Appendix B – List of Publications

(1) 学術雑誌等に発表した論文、著書：

〔 査読有り 掲載済 〕

- 1) **H. Lee**, J. W. Lee, I-K. Hong and S. Lee, “Optimal two-stage single-screw design for PMMA extrusion by Taguchi technique”, *Journal of Industrial and Engineering Chemistry*, vol. 20, no. 1, 2014, pp. 1119-1125.
- 2) T. Ohori, **H. Lee**, I. Ohsawa and J. Takahashi, “Optimal structural design of discontinuous carbon fiber reinforced thermoplastics plate subjected to bending load”, *Journal of Japan Society for Composite Materials*, vol. 43 no. 2, 2017, pp. 65-73.

〔 査読有り 投稿中 〕

- 1) **H. Lee**, G. Cai, S. Yamashita, I. Ohsawa and J. Takahashi, “Rheological properties of carbon/polyamide 6 randomly oriented strand composites under oscillatory shear”, *Polymer Composites*, under review.
- 2) **H. Lee**, C. Bi, S. Tang, T. Hayashi and J. Takahashi, “Formability and flow front observation of carbon/polyamide 6 randomly oriented strand composites during compression molding”, *Journal of Reinforced Plastics and Composites*, under review.
- 3) S. Tang, **H. Lee**, T. Hayashi and J. Takahashi, “Investigation on the flowability of ultra-thin chopped carbon fiber tape reinforced thermoplastics with rib structure”, *Journal of Thermoplastic Composite Materials*, under review.

〔 斜体準備中 〕

- 1) **H. Lee**, I. Ohsawa and J. Takahashi, “Anisotropic thermal expansion of carbon/polyamide 6 randomly oriented strand composites”.

(2) 学術会議における発表：

〔 査読有り ○：発表者 〕

- 1) ○ S. M. Kim, **H. Lee**, Y. Ahn and J. W. Lee, “Fabrication of Polyethylene Naphthalate/C₁₂-PPH Mica Nanocomposite”, *Autumn Conference of the Polymer Society of Korea*, Changwon, Republic of Korea, (2012-10).
- 2) S. M. Kim, ○ **H. Lee**, S. Lee and J. W. Lee, “Properties of Ultrasound-assisted Blend Composites of PC / SAN / CNT”, *28th International Conference of the Polymer Processing Society (PPS-28)*, Pattaya, Thailand, (2012-12).
- 3) ○ **H. Lee**, J. Park, S. Lee and J. W. Lee, “Flow Behavior Analysis of PMMA in Coat Hanger Dies”, *Spring Conference of the Polymer Society of Korea*, Daejeon, Republic of Korea, (2013-4).
- 4) ○ **H. Lee**, J. Park, S. Lee and J. W. Lee, “Rheological Properties of PMMA in Coat Hanger Dies”, *Spring Conference of the Korean Society of Rheology*, Seoul, Republic of Korea, (2013-5).
- 5) ○ J. H. Choi, **H. Lee**, J. Park, J. S. Yoo, S. Lee, S. K. Han, H. S. Kim, K. D. Lee, J. S. Shim and J. W. Lee, “Characterization for Plastic Bonded Explosive Simulants”, *Spring Conference of the Korean Society of Rheology*, Seoul, Republic of Korea, (2013-5).
- 6) **H. Lee**, J. Park, S. Lee and ○ J. W. Lee, “Optimization of the Coat-hanger Manifold via Computer Simulation of PMMA Film”, *29th International Conference of the Polymer Processing Society (PPS-29)*, Nuremberg, Germany, (2013-7).
- 7) ○ S. Tang, T. Hayashi, **H. Lee**, W. Nagatsuka, I. Ohsawa and J. Takahashi, “Flowability of Discontinuous Carbon Fiber Reinforced Thermoplastics”, *20th International Conference on Composite Materials (ICCM20)*, P201-11, Copenhagen, Denmark, (2015-11).
- 8) ○ **H. Lee**, S. Tang, T. Hayashi, J. Takahashi, I. Ohsawa, K. Kawabe and T. Murakami, “Flow Behavior of the Tapes during Compression Molding of Ultra-thin Chopped Carbon Fiber Tape

- Reinforced Thermoplastics”, *1st International Symposium on Emerging Functional Materials*, Daejeon, Republic of Korea, (2015-11).
- 9) ○ **H. Lee**, S. Tang, T. Ohori, T. Hayashi, Y. Wan, J. Takahashi, I. Ohsawa, K. Kawabe and T. Murakami, “Applicability of FEM to Complex Parts Made by Ultra-thin Chopped Carbon Fiber Tape Reinforced Thermoplastics”, *14th Japan International SAMPE Symposium and Exhibition (JISSE14)*, Kanazawa, Japan, (2015-12).
- 10) ○ D. Kobayashi, Y. Wan, **H. Lee**, T. Nakamura, H. Wei, J. Takahashi and I. Ohsawa, “Flow Behavior of Complex Shaped Hybrid Carbon Fiber Reinforced Thermoplastics during Compression Molding”, *17th European Conference on Composite Materials (ECCM17)*, Munich, Germany, (2016-6).
- 11) ○ C. Bi, **H. Lee**, I. Ohsawa and J. Takahashi, “Temperature dependent rheological properties of ultra-thin chopped carbon fiber tape reinforced thermoplastics”, *21st International Conference on Composite Materials (ICCM21)*, Xi’an, China, (2017-8).

以上